Gergely Zaránd

Quantum Impurity Problems

Work presented to obtain the title
'Doctor of the Hungarian Academy of Sciences'

Budapest University of Technology and Economics
Budapest, 2005

Contents

1 Introduction

Quantum impurity models have continuously been in the focus of intense research in the past 50 years. While the expression designating this class of models indicates that these models were originally constructed to describe the quantum mechanical properties of an impurity or imperfection such as a magnetic atom, dislocation, or a substitutional ion in a lattice, in reality, the history of these models dates back to the very early days of quantum mechanics, when the quantum mechanics of the electron spin and magnetic ions in an external magnetic field and the tunneling of a particle in a double well potential (two level system) have been worked out.

The behavior of an isolated spin or two level system is, of course, trivial. However, their physics becomes extremely complex once one considers them as 'impurities', *i.e.*, once one takes into account that they couple to excitations in the environment. In fact, quantum impurity models represent the simplest non-trivial quantum field theories which, despite of their simplicity, provide the simplest examples of exciting phenomena such as quantum criticality, dynamical mass generation, asymptotic freedom, duality, or universality. Besides being interesting on their own, quantum impurity models also serve as a test ground for more complicated strongly correlated lattice systems that occur in nature. As an introduction to this thesis, let me give here a short overview of some of the most important milestones in the theory of quantum impurity problems to introduce the reader into this exciting field.

1.1 The Kondo effect

The complexity of the problem of coupling a quantum mechanical degree of freedom to a dissipative environment has been probably first realized by Kondo, who proposed to describe the interaction of a magnetic impurity and the conduction electrons by the following simple Hamiltonian [1]

$$H_{\rm int} = \frac{J}{2} \sum_{\mathbf{k},\mathbf{k}',\sigma,\sigma'} \vec{S}\, c^\dagger_{\mathbf{k}\sigma} \vec{\sigma}_{\sigma\sigma'} c_{\mathbf{k}'\sigma'} \ , \tag{1}$$

where $J > 0$ denotes the antiferromagnetic coupling between the impurity spin $\vec{S}$ and the conduction electron spin density at the origin, and the operator $c^\dagger_{\mathbf{k}\sigma}$ creates a conduction electron with momentum $\mathbf{k}$ and spin σ. Kondo discovered that the simple Hamiltonian Eq. (7) - called the Kondo model after Kondo - gives rise to a

logarithmic increase in the resistivity at low temperatures. However, while the theory of Kondo successfully explained the low-temperature resistivity anomaly observed in various magnetic alloys, it also alerted physicists: the seemingly innocent and simple Kondo model contains *infrared singularities* which make it impossible to understand the low-temperature properties of this model by simple perturbation theory, that breaks down at the so-called Kondo temperature,

$$T_K \approx E_F \; e^{-1/J\varrho_0} \; . \tag{2}$$

In the above expression E_F denotes the Fermi energy, and ϱ_0 is the density of states of the conduction electrons at the Fermi level for a given spin direction.

One of the major steps in understanding the Kondo model was made by Anderson and his coworkers [3, 4]. First Anderson, Yuval, and Hamann used renormalization group (RG) techniques to study the strongly anisotropic version of Eq. (7)

$$H_{\rm int} = \frac{J_\perp}{2} \sum_{kk'} (c^\dagger_{k\uparrow} c_{k'\downarrow} S^- + \text{h.c.}) + \frac{J_\parallel}{2} \sum_{kk'} (c^\dagger_{k\uparrow} c_{k'\uparrow} - c^\dagger_{k\downarrow} c_{k'\downarrow}) S^z \; , \tag{3}$$

where the coupling in the z-direction is much larger than the one in the x, y directions, $J_\parallel \gg J_\perp$. Anderson, Yuval and Hamann expanded the free energy functional of this model as an imaginary time path integral by treating $J_\perp$ as a perturbation, and mapping it to the one-dimensional Coulomb gas: spin flips behave as charged particles after the mapping and interact through a logarithmic interaction in time. The scaling analysis of Anderson *et al.* showed that the amplitude of spin-flip processes increases as one lowers the temperature, and ultimately dominate the low temperature physics [3].

Later Anderson proposed a much simpler version of renormalization group analysis, the so-called 'poor man's scaling method', where the elimination of high-energy conduction electrons has been compensated by changing the value of the dimensionless coupling, $\varrho_0 J$, while keeping matrix elements of the T-matrix in the vicinity of the Fermi surface invariant [4]. Anderson's scaling approach can be shown to sum up the most singular diagrams in the perturbation series, first identified by Abrikosov [5], and it breaks down at the Kondo scale (2), where the effective coupling obtained diverges. Anderson believed that this is an artifact of the approach, and conjectured that the effective coupling diverges only in the $T \to 0$ limit. The divergence of the effective coupling could be formally cured by extending Anderson's method to sum up

subleading diagrams and casting in the form of multiplicative renormalization group, though the results of these perturbative renormalization group calculations remained consistent only above (a somewhat reduced) T_K, where the effective coupling was much less than unity [6, 7, 8]

The real break-through in understanding the low-temperature behavior of the Kondo problem came from Nozières [9], who took the divergence of the effective coupling seriously, and showed by an expansion in $1/J$ that the $J = \infty$ fixed point is indeed stable. He also identified the leading corrections around the $J \to \infty$ limit, and showed that at low temperatures the Kondo model becomes a 'local Fermi liquid', with weakly interacting quasiparticles at the impurity site, and derived the behavior of resistivity and thermodynamic quantities. In other words, the impurity spin forms a singlet state with the conduction electrons at low temperatures, and completely disappears from the problem. A quantitative understanding of the Kondo problem has been finally achieved by Wilson who - in the spirit of renormalization group - proposed a numerical scheme (discussed in Section 2.3 of this thesis) to diagonalize the Kondo Hamiltonian iteratively [10]. With this method, he was able to compute thermodynamic quantities at all temperatures, and he has also been able to deduce the renormalization group flow of the effective coupling, and confirm Anderson's conjecture and Nozières Fermi liquid picture.

The solution of the Kondo problem, however, did not end with the work of Wilson: five years after Wilson's work a complete Bethe ansatz solution of the Kondo problem was constructed [11, 12, 13], but one had to wait another fifteen years until it became also possible to compute dynamical correlation functions and the resistivity numerically with a high accuracy [14, 15].

Parallel to the efforts to understand the Kondo model, the problem of magnetic impurities has been attacked from another direction as well. In 1961 Anderson proposed a more detailed model to describe the formation of magnetic moments on the d-level of rare earth metals [16]. Anderson showed that if the interaction energy U of the d-electrons is strong enough compared to the hybridization energy Γ then, in general, a magnetic moment will be formed on the d-level. Later, Schrieffer and Wolff constructed a unitary transformation and showed that, for small values of Γ/U and small enough energy scales, the physics of Anderson's model is practically equivalent to that of the Kondo model in the local moment regime [17]. A year after Nozières' Fermi liquid theory, Yamada and Yosida published a series of papers [18],

where they showed that perturbation theory in the Anderson model is convergent, and the low temperature properties are that of a Fermi liquid. In a way, the results of Yamada and Yosida were the logical extensions of the general theory of Luttinger [19, 20].

Based on the above results, we now understand the Kondo effect as follows (see Fig. 1): Due to the strong coulomb interaction, a local moment is formed on the deep d or f-levels of rare earth and actinide materials. This local moment is essentially free at temperatures $T > T_K$, and its susceptibility - apart from small logarithmic corrections - increases as $\chi_{\rm imp} \sim 1/T$ for $T > T_K$. However, as we lower the temperature, the system tries to get rid of the high temperature entropy of the spin, $S = k_B \ln(2S+1)$, and a conduction electron spin is bound to the impurity antiferromagnetically to screen the impurity spin and form a local singlet. The energy of this many-body state is given by the Kondo energy T_K. Since a finite energy $\sim T_K$ is needed to break up this singlet, conduction electrons at the Fermi energy are not allowed to enter the impurity site and correspondingly, scatter off elastically with a phase shift $\pi/2$, and the impurity contribution to the susceptibility is finite at low temperatures, $\chi_{\rm imp} \sim 1/T_K$.

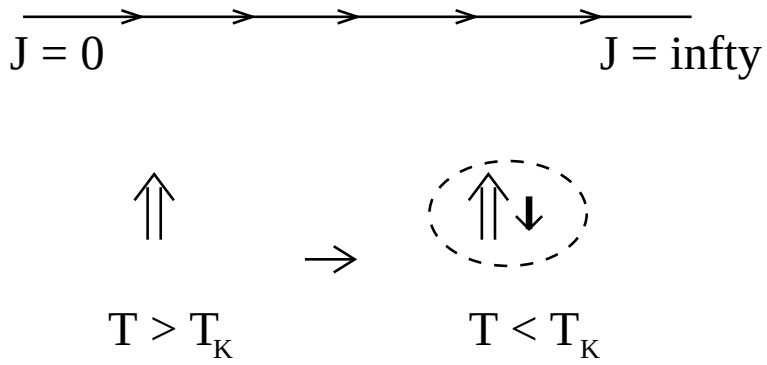

Figure 1: renormalization group flow of the effective coupling and the the formation of the corresponding local singlet in the single channel Kondo model.

1.2 Dissipative two level systems

One of the most important and most interesting quantum impurity problems is that of a dissipative two level system (TLS). This model has been maybe first proposed by Leggett in the context of macroscopic quantum tunneling [21, 22], who studied how coupling to a dissipative environment destroys the quantum-coherent motion of

a two state system. Leggett proposed to study the simplest non-trivial model one can envision, a tunneling system coupled to a bath of harmonic oscillators:

$$H_{\rm SB} = -\frac{1}{2}\Delta\tau_x + \frac{1}{2}\varepsilon\tau_z + \sum_i \omega_i(a_i^\dagger a_i + \frac{1}{2}) + \frac{1}{2}\tau_z \sum_i \frac{C_i}{\sqrt{2m_i\omega_i}}(a_i + a_i^\dagger). \qquad (4)$$

Here $\tau_i, i = x, y, z$ are Pauli spin matrices, the two states of the system correspond to $\tau_z = \pm$, Δ is the bare tunneling matrix element and ε is a bias.[1] The harmonic oscillators are labeled by the index i, have masses m_i and frequencies ω_i, and couple linearly to the coordinate $Q = \frac{1}{2}\tau_z$ of the two level system with couplings C_i. Eq. (4) being quadratic in the oscillator coordinates, one can integrate out the bosonic degrees of freedom, and finds that the dynamics of the spin operators is uniquely determined by the oscillators' spectral function $J(\omega) = \frac{\pi}{2}\sum_i(\frac{C_i^2}{m_i\omega_i})\delta(\omega - \omega_i)$.

Maybe the most interesting case is that of an Ohmic heat bath, where $J(\omega)$ is linear below a high frequency cut-off ω_c, $J(\omega) = 2\pi\alpha\omega$. In this case, as we shall discuss in Section 3.1.3, increasing dissipation strength α first makes the motion of the tunneling particle incoherent, and for $\alpha > 1$ dissipation can even completely suppress tunneling and localize the tunneling particle [22]. Remarkably, there is an exact mapping outlined in Section 3.1.2, which maps the above basic model of dissipation on the anisotropic Kondo model, Eq. (3) [22, 23]. This mapping connects the parameters of the two models as

$$\frac{\Delta}{\omega_c} = \varrho_0 J_\perp \equiv j_\perp \qquad (5)$$

$$\alpha = (1 - \frac{2\delta}{\pi})^2, \qquad (6)$$

where $\delta = \arctan\frac{\pi\rho J_\parallel}{4}$ is the scattering phase shift for conduction electrons generated by the potential $J_\parallel/4$, and the bias ε in Eq. (4) corresponds to a local magnetic field in the Kondo problem. This surprising result implies that many dynamical properties of the two models and their thermodynamics are completely equivalent, and essentially all dissipative physics is contained in the anisotropic Kondo problem.

[1] Throughout this dissertation we use units $\hbar = k_B = \mu_B = 1$. In many cases we also set the Fermi velocity to $v_F = 1$.

1.3 Non-Fermi liquid models

In the eighties another new class of fascinating quantum impurity problems challenged theoretical physicists. In 1980 Noziéres and Blandin attempted to construct realistic models for magnetic impurities, *i.e.*, to take into account crystal field effects properly [24]. Under special circumstances they found that the coupling between the magnetic moment and the conduction electrons is described by a multichannel version of Eq. (7)

$$H_{\rm int} = \frac{J}{2} \sum_{\sigma,\sigma',a} \vec{S}\, \psi^\dagger_{\sigma a} \vec{\sigma}_{\sigma\sigma'} \psi_{\sigma' a} \ , \tag{7}$$

where the channel quantum number $a = 1, .., f$ is *conserved* in course of the scattering process. The variant of this model with spin $S = 1/2$ and $f = 2$ is the so-called two-channel Kondo model.

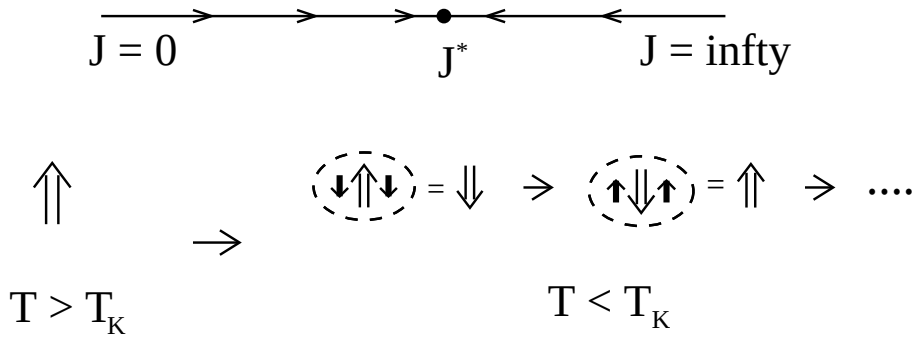

Figure 2: Renormalization group flow of the effective coupling in the two-channel Kondo model. No singlet can be formed because of the symmetry of the two channels, and an intermediate coupling fixed point governs the $T \to 0$ physics.

Nozières and Blandin realized that this model must have properties very different from the usual spin $S = 1/2$ Kondo problem, as can be understood by simple renormalization group arguments: similar to the Kondo problem, for small values of $j = \varrho_0 J$ the effective coupling increases under the renormalization group transformation, suggestive of a strong coupling fixed point. However, the $j \to \infty$ fixed point of the RG is unstable: For $j = \infty$ the impurity spin would bind a conduction electron from each channel, thus giving a local residual spin $\tilde{S} = 1/2$. This residual spin couples to the rest of the system through an antiferromagnetic exchange coupling of size $\tilde{j} \sim 1/j$. This coupling is again relevant, implying that for very large values of j, $\tilde{j}$ must increase and thus j must *decrease* under the RG (see Fig. 2). These arguments imply that the effective low energy theory has a finite exchange

coupling j^*, and is not trivial. As a consequence, the model has a residual entropy at $T = 0$ temperature, the susceptibility and the linear specific heat coefficient diverge as $T \to 0$ [25, 26], and the resistivity shows a power-law anomaly [27]. Furthermore, Maldacena and Ludwig showed that quasiparticles at the Fermi energy are orthogonal to conduction electrons [28], and an incoming electron at the Fermi surface 'evaporates' and scatters to infinitely many electron-hole excitations.

Nozières and Blandin realized that non-Fermi liquid states are extremely fragile, and therefore they did not really believe in the existence of realizations of these exotic models [29]. It came therefore as a surprise when D.L. Cox suggested that many of the logarithmic anomalies in Uranium and Cerium based heavy fermion compounds can be explained in terms of the two-channel Kondo model, and showed that the two-channel Kondo model naturally shows up as a consequence of the crystal field structure of these materials [30, 31]. The most important ingredient of these models is the strong spin-orbit coupling at the deep f-levels of Uranium and Cerium, originally not considered by Nozières and Blandin.

Since then, a few other realizations of non-Fermi liquid systems have been proposed such as non-commutative two level systems [32, 33, 34], quantum dots in the vicinity of their degeneracy point [35], and multi-dot systems [36], some of which will be also discussed in this thesis.

1.4 New Directions

To close this Introduction, let us discuss a few more recent applications of quantum impurity models.

1.4.1 Heavy Fermion physics, strongly correlated systems, and quantum critical points

One of the major challenges of today's solid state physics is to understand strongly correlated heavy fermion systems and strongly correlated systems such as high temperature superconductors or manganites. Heavy fermion compounds are usually (seemingly) complicated Cerium or Uranium-based alloys, where much of the physical properties is governed by the f-electrons on the Ce and U ions. These ions usually form a dense lattice, and provide local moments at high temperature which are screened by the conduction electrons as one lowers temperatures. At these low temperatures, the f electrons form a narrow resonance (Kondo resonance) at the

Fermi level which gives the dominant contribution to the specific heat and the susceptibility, corresponding to an effective mass $100 - 1000$-times larger than the free electron mass m_e.[2, 34] It is for this reason that we call these systems heavy Fermion systems or heavy Fermi liquids.

Surprisingly, many of the thermodynamic properties of these systems could be qualitatively understood in terms of single impurity physics [34]. To obtain a better understanding, however, more elaborate methods are needed. One of the most efficient methods is the so-called dynamical mean field theory in which one keeps local time-dependent correlations, but spatial correlations are treated only at the mean field level [37, 38]. This theory becomes exact in the limit of infinite coordination number, and entails solving a quantum impurity problem, where the conduction electrons' spectral function is determined self-consistently. Therefore, having a deep understanding of quantum impurity problems is essential in understanding phenomena such as the Mott metal-insulator transition. There is currently a major effort in combining dynamical mean field theory with usual band theoretical methods to keep track of correlations, however, efficient impurity solvers still need be developed to achieve this goal.

As mentioned before, in heavy Fermion compounds the conduction electrons screen out the magnetic moments at low temperatures. This is, however, not the only way to get rid of the residual entropy of the local moments: the conventional way to get rid of the residual entropy in a magnetic material is through the formation of a magnetically ordered state. In fact, in most heavy Fermion systems these two mechanisms compete with each other, and depending on the ratio of exchange coupling between neighboring ions and the Kondo temperature one or the other prevails. The before-mentioned ratio can be fine-tuned by pressure, impurity concentration, or magnetic field to lead to a transition from a non-magnetic metal state to a magnetically ordered metal [39, 40, 41, 42, 43, 44, 45]. In many cases this $T = 0$ temperature transition is of second order, and the corresponding transition is a quantum phase transition governed by quantum fluctuations [46]. In some systems neutron scattering data are suggestive of a quantum critical point that can be described in terms of *local* quantum fluctuations, *i.e.*, some quantum impurity models [41]. One of the most prominent candidates to describe these locally quantum critical systems is the Bose-Fermi Kondo model, and shall be analyzed in Section 3.3 of this dissertation.

Finally, another open question to answer is the origin of heavy Fermion superconductivity. In many heavy Fermion systems the heavy electrons become superconducting at low temperature and usually form a non-conventional superconducting condensate with gapless nodes or lines at the Fermi level [34]. The mechanism to form this superconducting state is almost certainly provided by local quantum fluctuation-generated correlations, which probably also determine the symmetry of the superconducting state. This is a fascinating possibility that has never been carefully studied before, probably because of the difficulty of the problem. With the fast development of numerical methods, however, it appears to be possible to study these phenomena in the near future by combining dynamical mean field theory with other approaches.

1.4.2 Mesoscopic systems: Building artificial atoms from electrical circuits

With the recent development of lithography it became possible to design and build electronic circuits in a controlled way with sizes down to the μ range and below. The energy needed to put an electron to such a small island is roughly $E_C \sim e^2/d \sim 10^{-3}\text{eV} \sim 10K$, *i.e.* it can be larger than the temperature of the device. Under these conditions the island operates as an 'artificial atom' [47]. One can also build 'artificial molecules' by joining several 'artificial atom', attach them to leads to measure transport properties and the effect of quantum fluctuations and change the number of electrons on them by simply varying gate voltages.

One can also engineer narrow constrictions (point contacts or nano-wires), allowing one to measure the dynamical properties of individual atoms [71]. Similar to single electron transistors, these point contacts can also be used as voltage probes or amplifiers in nanoscale circuits.

Quantum impurity models proved extremely useful in mesoscopic physics, since much of these systems including single electron transistors, metallic islands, or Josephson qubits (being maybe the most promising candidates for quantum computing) can be described in terms of them.

Mesoscopic technology also makes it possible to study out of equilibrium transport properties of these 'artificial' atoms in an unprecedented way, and many unexpected strongly correlated states have been observed in this way [48, 49, 50, 51, 135]. More recently, it became also possible to contact real molecules, and perform ex-

periments on them [118]. The experiments are performed in many cases out of equilibrium. The complete understanding of these mesoscopic and nanoscopic circuits with strong correlation effects represents therefore a major challenge for todays' theoretical physicists, and represents an unsolved problem of this field [54, 56, 55]. In this effort quantum impurity problems serve as a test ground, but combining quantum field theoretical techniques to study transport through molecules is still a dream.

1.5 Structure and subject of the dissertation

The purpose of this dissertation is to review some of the results obtained by the author in the field of quantum impurity problems. First, in Chapter 2 I give a short review of the theory of Kondo effect and introduce some of the methods I shall use to study quantum impurity models later, such as multiplicative renormalization group, numerical renormalization group, and Bethe ansatz.

In Chapter 3 I study dissipation effects. First I introduce and analyze using various methods the most basic Ohmic dissipative two level system model in Section 3.1. Then in Section 3.2 I study the same system by numerical renormalization group methods in the case when the tunneling particle has a spin. The last section of this chapter is devoted to the ϵ-expansion study of the Bose-Fermi Kondo problem, where both dissipative bosonic fields and conduction electrons couple to an impurity spin.

Chapter 4 is devoted to various non-Fermi liquid models and the discussion of their physical realizations. First in Section 4.1.1 I show using $1/f$ expansion methods how the physics of fast two level systems maps on the two-channel Kondo problem. Then in Sections 4.1.2 and 4.1.3 I study the anisotropic Kondo model using Abelian bosonization and Bethe ansatz methods. In the last two sections of the chapter, Sections 4.2.1 and 4.2.2, I generalize the mapping discussed in Section 4.1.1 to the case of M-state systems, and then solve the corresponding Coqblin-Schrieffer model by Bethe ansatz techniques.

Finally, in Chapter 5 I study mesoscopic systems. After giving a short introduction to the theory of single electron transistors, in this chapter I analyze phenomena such as the singlet-triplet transition, the $SU(4)$ Kondo effect, quantum fluctuations of a ferromagnetic grain, and study magnetic impurities in point contacts.

Section 3.1.4, Section 3.2, Section 3.3, Section 4.1.1, the second part of Section 4.1.2, Section 4.1.3, Section 4.2, Section 5.1.3, Section 5.1.4, and Section 5.2

contain mostly or exclusively my own results.

2 The single channel Kondo problem

The Kondo model given by Eq. (7) is one of the most elementary quantum impurity problems, and much of our understanding of other quantum impurity problems relies on our experience with it and the methodology that has been used to study it. We shall therefore start by reviewing part of the theory of Kondo model in this chapter.

2.1 Renormalization group analysis

2.1.1 Poor man's scaling

As mentioned in the introduction, the Kondo model contains infrared singularities. This can be seen most easily if one computes the on-shell matrix elements of the many-body T-matrix at $T = 0$ temperature between single electron states, $|\text{in}\rangle = c^\dagger_{\mathbf{k}'\sigma'}|s'\rangle$ and $|\text{out}\rangle = c^\dagger_{\mathbf{k}\sigma}|s\rangle$ doing perturbation theory in Eq. (7). Here $|s\rangle$ denotes the filled Fermi see (vacuum) with the impurity spin in state $S^z = s$. Straightforward second order perturbation theory yields [1]

$$\langle \text{out}|\hat{T}|\text{in}\rangle \approx \frac{J}{2}\vec{S}_{ss'}\vec{\sigma}_{\sigma\sigma'}(1 + J\varrho_0 \ln\frac{D}{\omega} + \ldots) \,, \tag{8}$$

where ω is the energy of the incoming electron (or hole) measured from the Fermi energy, and D is a bandwidth cut-off of the order of Fermi energy. Clearly, the second order term diverges as ω approaches the Fermi energy. This infrared divergence is due to intermediate electron states with arbitrarily small energies, and is characteristic of almost all quantum impurity problems where an impurity is coupled to the Fermi sea.

Higher order contributions can be most easily computed using Feynman diagrams, and can be classified according to their leading singularity [5]. In general, the most singular order n corrections to the T-matrix diverge as $\sim J^{n+1}\ln^n\frac{D}{\omega}$, and correspond to a special subset of diagrams, the so-called parquet diagrams. These diagrams can be explicitly summed up and give the following result,

$$\langle \text{out}|\varrho_0\hat{T}|\text{in}\rangle_{\text{leading}} = \frac{1}{2}\vec{S}_{ss'}\vec{\sigma}_{\sigma\sigma'}t(\omega) \,, \qquad t(\omega) = \frac{\varrho_0 J}{1 - J\varrho_0\ln\frac{D}{\omega}} = \frac{1}{\ln\frac{T_K}{\omega}} \,, \tag{9}$$

where the Kondo temperature defined by Eq. (2) has been introduced and $t(\omega)$ is the dimensionless T-matrix. Most disturbingly, the sum of the leading logarithmic

diagrams diverges at T_K.

Anderson provided a much simpler way to sum up these most divergent contributions [4]. One only has to assume that the physical properties of the Kondo model are not sensitive to the high-energy cut-off D, and the only energy scale that enters is the dynamically generated scale T_K, as also suggested by Eq. (9). In other words, one can reduce the cut-off D in Eq. (9) and compensate it by rescaling the exchange coupling J such that all physical (measurable) quantities remain constant. In the language of particle physics, this simply means that the theory is renormalizable, *i.e.* that one can remove the cut-off from the problem through a renormalization procedure [57]. With this assumption one can immediately derive solely from Eq. (8) the dimensionless T-matrix $t(\omega)$ as follows: Clearly, to keep the dimensionless quantity $\langle \mathrm{out}|\varrho_0 \hat{T}|\mathrm{in}\rangle$ constant, one must change the value of J in the following way to compensate the reduction of the cut-off, $D \to D'$,

$$D \to D' \,, \qquad J \to J' = J + J^2 \varrho_0 \ln \frac{D}{D'} + \ldots \quad . \tag{10}$$

For infinitesimal transformations this equation can be cast in the form of a differential (or scaling) equation, originally constructed by Gell-Mann and Low

$$\frac{\partial j}{\partial l} = \beta(j) \,, \tag{11}$$

where $\beta(j) = j^2 + \ldots$ is the beta function, $j(l) = \varrho_0 J(D)$ the renormalized dimensionless coupling, D_0 is the original cut-off, and we introduced the logarithmic energy scale $l = \ln \frac{D_0}{D}$.

To obtain the effective coupling for an equivalent model with band-width D one has to integrate Eq. (11) up to $l = \ln \frac{D_0}{D}$ with the initial condition $j(l = 0) = j_0$. This invariance can be used to determine physical quantities in a very efficient way if we observe that in a theory with cut-off $D \equiv \omega$ the logarithmic terms identically vanish, and physical quantities are thus given by the leading order (non-logarithmic) diagrams. The dimensionless T-matrix, *e.g.* can be immediately obtained from Eq. (11) using $t(\omega) = j(l = \ln D_0/\omega)$ in this way. Leading singularities of thermodynamic quantities and the resistivity can be obtained in a similar way, by exploiting the fact that all physical (measurable) quantities are invariant under the renormalization group (RG) transformation.

2.1.2 Multiplicative Renormalization Group

Although possible, it is not very easy to generalize the method of Anderson to sum up subleading singularities, which correspond to higher order terms in the beta function on the r.h.s of Eq. (11) [6]. A more efficient way to do this was invented independently by Fowler and Zawadowski and Abrikosov and Migdal [7, 8], who used field theoretical renormalization group methods to derive the scaling equations. The essence of this technique is to represent spin states by pseudofermions as $|S_z = s\rangle \leftrightarrow b_s^\dagger|0\rangle$ and the spin operator as [5]

$$\vec{S} \to \sum_{s,s'} b_s^\dagger \vec{S}_{ss'} b_{s'} \ , \qquad \sum_s b_s^\dagger b_s \equiv 1 \ . \tag{12}$$

The latter constraint can be enforced by introducing a chemical potential λ for the pseudofermions and then collecting leading contributions $\sim e^{-\beta\lambda}$ as $\lambda \to \infty$.

The theory is then formulated in terms of the electronic Green function, $G(\omega, \xi(\mathbf{k}))$, the pseudofermion Green function, $\mathcal{G}(i\omega, \xi(\mathbf{k}))$, and the pseudofermion-conduction electron vertex function $\Gamma(\{\omega_i\})$, where $\{\omega_i\}$ denote the external Matsubara frequencies of the pseudofermions and the electrons, respectively. Implicitly, all these functions depend on the high energy cut-off D and the dimensionless coupling j. Similar to poor man's scaling, the multiplicative renormalization group scheme provides connection between equivalent physical systems with different parameters but the equivalence is formulated as an internal symmetry of the Green's functions. The main assumption of of the multiplicative renormalization group is that the Green's functions and vertex functions of the original and the renormalized problem have the same functional form, apart from overall multiplicative factors Z_e and Z, which are independent of ω [7, 8]

$$G(\omega, D', j') = Z_e(D'/D, j)\, G(\omega, D, j) \ , \tag{13}$$

$$\mathcal{G}(\omega, D', j') = Z(D'/D, j)\, \mathcal{G}(\omega, D, j) \ , \tag{14}$$

$$\Gamma(\omega, D', V') = Z_e(D'/D, j)^{-1} Z(D'/D, j)^{-1} \Gamma(\omega, D, j) \ , \tag{15}$$

where the primed parameters are those of the renormalized system, and the renormalized electron- and pseudofermion Greens functions are given by

$$G = (i\omega - \epsilon - \Sigma_e(\omega))^{-1} \ , \tag{16}$$

$$\mathcal{G} = \left(i\omega - \lambda - \Sigma(\omega)\right)^{-1} , \tag{17}$$

with $\Sigma_e(\omega)$ and $\Sigma(\omega)$ the electrons' and the pseudofermion's self-energy. Note that the multiplicative prefactors do not contain the dynamical variables ω, and that the prefactor of the vertex function and the two Green's functions are related (see Eq. (15)). This latter relation is necessary to ensure that the singular part of the free energy remain invariant. Again, the connection between j and j' is given by the scaling equation (11), where the β function can be determined order by order by computing logarithmic corrections to the pseudofermion self energy and the vertex function. For quantum impurity problems the above equations greatly simplify as $Z_e = 1$ in all orders. The vertex and self-energy corrections needed to compute β to third order in j are given in Fig. 3, and the corresponding pseudofermion Green's function and vertex function read

$$\mathcal{G}^{-1}(\omega) = \omega\left(1 + S(S+1)\, j^2 \, \ln\frac{D}{-\omega} + \ldots\right) , \tag{18}$$

$$\Gamma(\omega) = \frac{j}{2}\vec{\sigma}\cdot\vec{S}\left(1 + \ln\frac{D}{-\omega}\left(j + [S(S+1)-1]\, j^2 + \ldots\right) + \ldots\right) , \tag{19}$$

where $i\omega - \lambda \to \omega$ measures the energy with respect to the chemical potential of the pseudofermions. Replacing these expressions into Eqs. (14) and (15) we obtain the following scaling equations,

$$\frac{\partial j}{\partial l} \approx j^2 - j^3 . \tag{20}$$

As is obvious, the third order term in this expression cuts off the divergence of the effective coupling, which approaches 1 for electrons with energies at the Fermi level, $\omega \to 0$ (corresponding to $l \to \infty$). This result should, however, not be taken too seriously, since for $j \sim 1$ higher order terms in the β function cannot be neglected. The third order term in Eq. (20) also results in a suppression of the Kondo temperature Eq. (2) by a factor $\sim \sqrt{j}$.

The next to leading logarithmic scaling equations and the multiplicative RG do not give qualitatively new information for the Kondo model, although they formally solve the problem of infrared singularities and accidentally they happen to give back even the $\sim T^2$ Fermi liquid property of the impurity contribution to the resistivity. However, as we shall see in Sections 3.3 and 4.1.1, the multiplicative renormalization group proves to be an extremely useful technique for non-Fermi liquid models, where

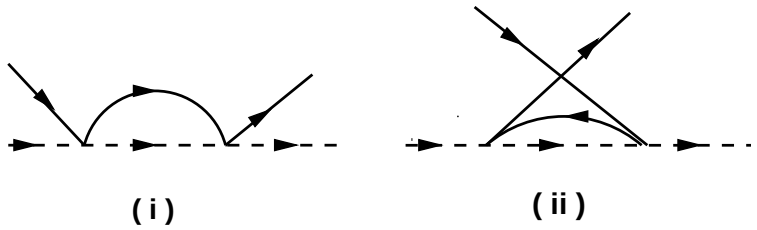

Fig. a

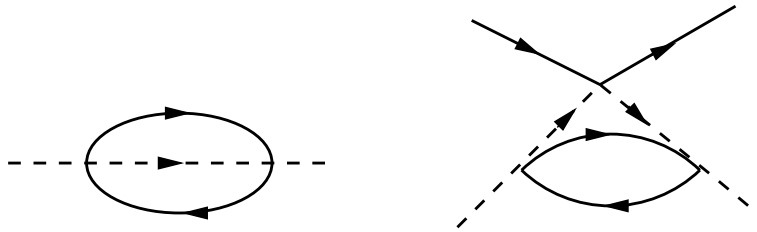

Fig. b

Figure 3: Diagrams generating the leading and next to leading logarithmic contributions to the scaling equations. Dashed lines denote unperturbed pseudofermion propagators, continuous lines stand for unperturbed conduction electron propagators.

it can be used to generate systematic and controlled expansions in some parameter.

2.2 The Bethe ansatz solution

To obtain an analytical solution of the Kondo problem, we first observe that the coupling to conduction electrons in Eq. (7) is local. This implies that only s-electrons with angular momentum $l = 0$ scatter off the impurity spin, and we thus have to keep only the s-wave part of the Hamiltonian:

$$H \to H = \sum_{\sigma} \int dk\ k\ a^{\dagger}_{\sigma}(k) a_{\sigma}(k) + \sum_{\sigma,\sigma'} \frac{j}{2}\ \vec{S}\ \int dk \int dk' a^{\dagger}_{\sigma}(k) \vec{\sigma}_{\sigma\sigma'} a_{\sigma'}(k')\ , \qquad (21)$$

where $a^{\dagger}_{\sigma}(k)$ creates a conduction electron in the s-wave channel with radial momentum $p = k + k_F$, and is normalized as $\{a^{\dagger}_{\sigma}(k), a_{\sigma'}(k')\} = \delta_{\sigma\sigma'}\delta(k - k')$. In Eq. (21) we linearized the dispersion relation around the Fermi energy, $\xi(k) \approx v_F k \equiv k$, and the coupling $j = \varrho_0 J$ is just the dimensionless coupling defined earlier.

It is useful to introduce the left-going fields $\psi_{\sigma} \equiv \int dk\ e^{-ikx} a_{\sigma}(k)$, and rewrite this Hamiltonian in real space as

$$H = \sum_{\sigma=\pm} \int \frac{dx}{2\pi}\ \psi^{\dagger}_{\sigma}(x)\ i\partial_x \psi_{\sigma}(x) + \frac{j}{2}\ \vec{S}\ (\psi^{\dagger}(0) \vec{\sigma} \psi(0))\ , \qquad (22)$$

The field $\psi_\sigma(x)$ above is related to the s-wave part of the three-dimensional field operator as $\psi_\sigma^{(s)}(\mathbf{r}) = \psi_\sigma(r) \sim (e^{-ik_F r}\psi_\sigma(r) - e^{ik_F r}\psi_\sigma(-r))/r$, *i.e.* the $x > 0$ and $x < 0$ pieces of $\psi_\sigma(x)$ represent incoming and outgoing s-electrons, respectively.

The Bethe ansatz method provides a way find directly the eigenfunctions Φ of Eq. (22) in a first quantized form as [58]

$$\Big[\sum_{i=1}^{N} i\frac{\partial}{\partial x_i} + \frac{j}{2}\sum_{i=1}^{N}\vec{S}\,\vec{\sigma}_i\delta(x_i)\Big]\,\Phi = E\,\Phi \tag{23}$$

$$\Phi_{\{\sigma_i\},s}(\{x_i\}) \;=\; \mathcal{A}\sum_Q A^Q_{\sigma_1,..,\sigma_N,s}\; e^{-i\sum_i x_i k_i}\;\Theta^Q(\{x_i\})\;, \qquad E = \sum_i k_i\;. \tag{24}$$

Here the permutation Q specifies the order of the impurity spin $x_0 = 0$ and the conduction electrons x_i $(i = 1, .., N)$, and the function $\Theta^Q(\{x_i\})$ is one if $x_{Q0} < x_{Q1} < \ldots < x_{QN_e}$ and vanishes for other permutations. Of course, the wave function must be fully antisymmetric with respect to the electronic coordinates, which is assured by the operator $\mathcal{A}$ in front that antisymmetrizes the wave function. To obtain a well-defined spectrum, one further assumes a finite system size L and imposes periodic boundary conditions.

In principle, Eq. (23) determines only the impurity-conduction electron S-matrix,

$$R^{s'\sigma'}_{s\sigma} = [e^{i\,j\,\vec{\sigma}\vec{S}/2}]^{s'\sigma'}_{s\sigma}\;, \tag{25}$$

which connects amplitude of the wave function with one electron on the right, $A(x > 0)_{s\sigma}$, to the amplitude $A_{s'\sigma'}(0 < x)$ corresponding to having the electron on the left. In a similar way, for N electrons the scattering matrix between electron i and the impurity can be defined as

$$[S^{0i}]^{\{\sigma_i\},s}_{\{\sigma'_i\},s'} = (\prod_{j\neq i}\delta^{\sigma_j}_{\sigma'_j})R^{s'\sigma'_i}_{s\sigma_i}\;. \tag{26}$$

However, as a consequence of the linearized dispersion, we are free to choose *any* scattering matrix between two conduction electrons,

$$\begin{aligned} A(\ldots < x_j < x_i < \ldots)_{\{\sigma_i\},s} &\equiv \sum_{\{\sigma'_i\},s'}[S^{ij}]^{\{\sigma_i\},s}_{\{\sigma'_i\},s'}A(\ldots < x_i < x_j < \ldots)_{\{\sigma'_i,s'} \\ &= \sum_{\sigma'_i,\sigma'_j}[\tilde{R}]^{\sigma'_i\sigma'_j}_{\sigma_i\sigma_j}A(\ldots < x_i < x_j < \ldots)_{\sigma_1,..,\sigma'_i,\ldots,\sigma'_j,\ldots,s}\;. \end{aligned} \tag{27}$$

This freedom in the choice of $\tilde{R}$ can be used to solve the model exactly as we discuss below.

Two regions corresponding to two different permutations Q and Q' can be usually related in many independent ways in the configuration space. As shown in Fig. 4, from the region $x_0 < x_1 < x_2$, *e.g.*, we can reach region $x_0 > x_1 > x_2$, in two different ways. Of course, the wave function amplitude A should be independent of the way we proceed, and in general, the ansatz Eq. (24) can only provide a consistent solution of the Schrödinger equation if the two-body scattering matrices satisfy the so-called Yang-Baxter or triangle equations:

$$S^{jk} S^{ik} S^{ij} = S^{ij} S^{ik} S^{jk} \,, \tag{28}$$

where in our case $i, j, k = \{0, 1, \ldots, N\}$. For the single channel Kondo model this can be achieved by choosing $\tilde{R}$ to be the *exchange operator*. This choice corresponds to selecting a particular basis in the space of many-body wave functions, dictated by the impurity-conduction electron interaction.

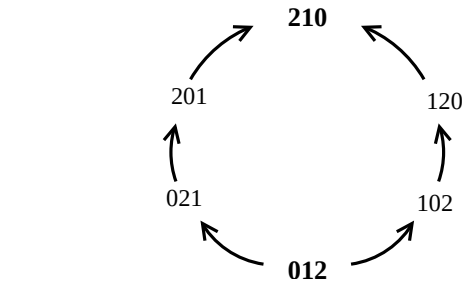

Fig. a

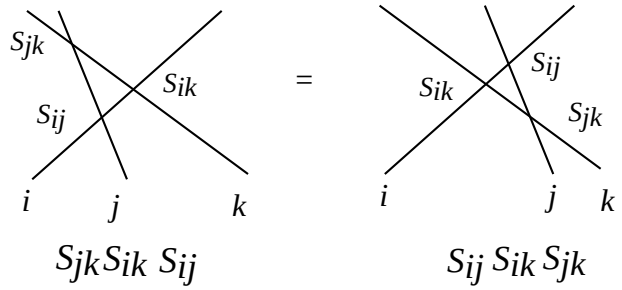

Fig. b

Figure 4: Graphical representation of the Yang-Baxter relations assuring integrability. (a) There are two ways to connect region 012 with region 210 in the parameter space. (b) The scattering matrices connecting the wave function in neighboring regions of the parameter space must satisfy the 'triangle equation' for consistency.

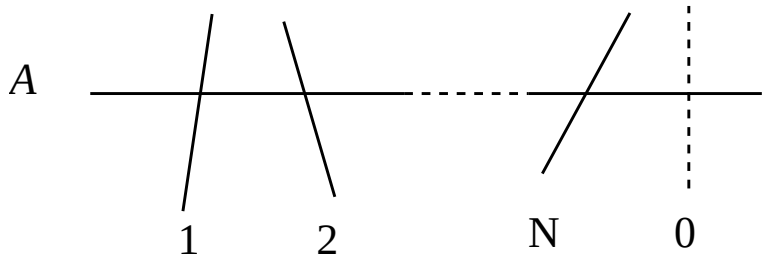

Figure 5: Graphical representation of the monodromy matrix. $T(\alpha)$ is a 2×2 matrix in the auxiliary space A, and each element of it acts on the spin part of the wave function, $A_{\{\sigma_i\},s}$. The auxiliary particle is denoted by A. The last dashed line corresponds to the impurity scattering matrix.

2.2.1 The algebraic Bethe ansatz

Relation (28) ensures consistency. However, to determine the eigenstates and the spectrum of the Hamiltonian one has to construct amplitudes A such that the many-body wave function satisfies *periodic boundary conditions* in all electronic coordinates. This is a difficult task that we shall complete using the algebraic Bethe ansatz [58].

Instead of attempting to give a detailed description of the method here, we shall rather outline its main ingredients. The spectrum can be constructed in an algebraic way if the scattering matrices can be written in the following form,

$$S^{ij} = S^{ij}(\alpha_i - \alpha_j) \ , \tag{29}$$

where $S^{ij}(\alpha)$ acts only on particles i and j, and the spectral parameter (rapidity) α_i characterizes particle i. Usually, in most other Bethe ansatz problems α is related to the momentum of the particles. In our case the S-matrices can be simply parametrized as

$$S^{ij}(\alpha_i - \alpha_j) = \frac{\alpha_i - \alpha_j + icP^{ij}}{\alpha_i - \alpha_j + ic} \ , \tag{30}$$

with the parameter c related to the exchange coupling j,[2] $\alpha_0 = -1$ and $\alpha_i = 0$ for $i = 1, .., N$. As a next step, one defines the monodromy matrix $T(\alpha)$, depicted in Fig. 5

$$T(\alpha) \equiv \begin{pmatrix} A(\alpha) & B(\alpha) \\ C(\alpha) & D(\alpha) \end{pmatrix} = S^{0A}(\alpha_0 - \alpha) S^{1A}(\alpha_1 - \alpha) \dots S^{NA}(\alpha_N - \alpha) \ , \tag{31}$$

[2]The relation between c and j is non-universal, but for small j-s $c \sim j$.

where A refers to an auxiliary particle. The monodromy matrix is a 2×2 matrix in the subspace of the auxiliary particle. Its matrix element $B(\alpha)$ lowers the spin of the spin part of the wave function $A_{\{\sigma_i\},s}$ by one, and its trace over the auxiliary particle, $\mathrm{tr}_A T(\alpha) = A(\alpha) + B(\alpha)$ is related to the operator which takes one particle and commutes it through all other particles. In other words, periodic boundary conditions can be rewritten as

$$T(\alpha_i)A = e^{-iLk_i}A \; . \tag{32}$$

This equation determines the spin structure A of the wave function, and can be diagonalized in a simple algebraic way using the Yang-Baxter relations. The basic idea is to produce states from the fully polarized state, $\Omega^{(0)}$ by multiple application of the operator B as

$$A(\Lambda_1, .., \Lambda_M) \equiv B(\Lambda_1)B(\Lambda_2)\ldots B(\Lambda_M)\Omega^{(0)} \; . \tag{33}$$

This state is an eigenstate of $T(\alpha_i = 0)$ with an eigenvalue z_i provided that $\lambda_\gamma \equiv \Lambda/c - i/2$ satisfy the so-called Bethe ansatz equations, that read in our case:

$$\prod_{\delta=1}^{M} \frac{\lambda_\delta - \lambda_\gamma + i}{\lambda_\delta - \lambda_\gamma - i} = -\left(\frac{\lambda_\gamma - \frac{i}{2}}{\lambda_\gamma + \frac{i}{2}}\right)^N \frac{\lambda_\gamma + \frac{1}{c} - \frac{i}{2}}{\lambda_\gamma + \frac{1}{c} + \frac{i}{2}} \; , \qquad \gamma = 1, \ldots, M \; , \tag{34}$$

$$e^{-ik_jL} = z_j = \prod_{\delta=1}^{M} \frac{\lambda_\delta + \frac{i}{2}}{\lambda_\delta - \frac{i}{2}} \; , \qquad j = 1, \ldots, N \; . \tag{35}$$

The logarithm of the second equation determines the eigenvalues k_j and thus the energy,

$$E = \sum_{j=1}^{N} \frac{2\pi}{L} n_j + \frac{N}{L} \sum_{\gamma=1}^{M} (\Theta(2\lambda_\gamma) - \pi) \; , \tag{36}$$

where the integers n_j denote the 'holon' quantum numbers of the ground state, $\Theta(\lambda) = -2\tan^{-1}(\lambda)$, and the spin rapidities λ_δ must be determined from Eq. (34). One of the most important features of Eq. (36) is that - as a manifestation of spin-charge separation - the contributions from the spin and charge sectors to the energy separate. This is characteristic of impurity models with a linear dispersion.

2.2.2 The $T = 0$ temperature limit

Equations (34) and (35) are not particularly useful. To make some progress, one usually takes the thermodynamic limit, $N \to \infty$ $L \to \infty$, while keeping the energy cut-off $D = N/L$ fixed. As we have seen before, each eigenstate of the Hamiltonian is characterized by a set of holon quantum numbers $\{n_j\}$ and possibly complex rapidities $\{\lambda_\delta\}$. More precisely, one can show [13, 59] that in the thermodynamic limit the solutions λ_δ of Eq. (34) are organized into *strings* on the complex plane, *i.e.*, consist of sets containing n complex rapidities $\lambda_j^{(n)} = \tilde{\lambda} + i[j - (n+1)/2]$, with $\tilde{\lambda}$ the center of the string ($j = 1, \ldots, n$).

In general, all these string solutions should be considered. One can show, however, that for the ground state of the single channel Kondo problem all λ_δ's are real, and taking the logarithm of Eq. (34) we obtain

$$-N\Theta(2\lambda_\gamma) - \Theta(2\lambda_\gamma + 2/c) + \sum_{\delta=1}^{M} \Theta(\lambda_\gamma - \lambda_\delta) = 2\pi I_\gamma \ , \tag{37}$$

with $\{I_\gamma\}$ a set of integers (or half-integers). This equation can be rewritten in terms of the *density* of solutions, $\varrho(\lambda)$ and the density of 'holes', $\tilde{\varrho}(\lambda)$ as

$$a(\lambda) - \int K(\lambda - \lambda')\varrho(\lambda')d\lambda' = \varrho(\lambda) + \tilde{\varrho}(\lambda) \ , \tag{38}$$

where the kernel K and the driving term a are defined as

$$K(\lambda) = -\frac{1}{2\pi}\frac{\partial}{\partial\lambda}\Theta(\lambda) = \frac{1}{\pi}\frac{1}{1+\lambda^2} \ , \tag{39}$$

$$a(\lambda) = \frac{2}{\pi}\left(\frac{N}{1+4\lambda^2} + \frac{1}{1+4(\lambda+1/c)^2}\right) \ . \tag{40}$$

The spin part of the energy can be expressed as

$$E_{\rm spin} = D\int d\lambda[\Theta(2\lambda_\gamma) - \pi]\ \varrho(\lambda) \ . \tag{41}$$

In the ground state there is no hole in the series of rapidities, $\tilde{\varrho}_o \equiv 0$, and the ground state density of solutions, $\varrho_o(\lambda)$, can thus be determined by simply solving the inhomogeneous integral equation (38). The corresponding ground state energy can be computed from (41). The contribution of the impurity can be separated and is of order $\sim T_K$.

The simplest excitations of the ground state turn out to be spin 1/2 *spinons*, where one creates a hole in the series of λ_δ, *i.e.* $\tilde{\varrho}(\lambda) = \delta(\lambda - \lambda_h)$. Note, that in reality -for a nonlinear dispersion - this spinon is always glued together with a holon, thus forming a spin 1/2 charge 1 quasiparticle. In the Bethe ansatz solution, however, spinons and holons are independent quasiparticles.

2.2.3 The thermodynamic Bethe ansatz equations

While at $T = 0$ temperature it was sufficient to consider only real λ_δ's, at finite temperatures all kinds of string excitations must be considered. However, the previous considerations can easily be generalized to this case. One has to introduce string quantum numbers $I_\gamma^{(n)}$ and corresponding densities ϱ_n and $\tilde{\varrho}_n$. These densities are then related to each other by integral equations similar to Eq. (38),

$$\varrho_n(\lambda) = a_n(\lambda) - \sum_{n'} \int d\lambda' K_{nn'}(\lambda - \lambda')\varrho_{n'}(\lambda') \; , \tag{42}$$

and the expression of the energy takes also a similar form,

$$E^{\rm spin} = \sum_n \int d\lambda E_n(\lambda)\varrho_n(\lambda) \; , \tag{43}$$

where the a_n's, E_n's and $K_{nn'}$'s denote appropriately defined driving terms, string energies, and kernels, whose specific form is not very important for the discussion here.

At finite temperature, microscopic rapidity distributions (*i.e.*, the $\lambda_\delta^{(n)}$'s of a given state) fluctuates, and a state characterized by a given set of ϱ_n's corresponds to many such 'microscopic' state. These internal degrees of freedom can be taken into account through the entropy defined as

$$S^{\rm spin} = k_B \sum_n \int d\lambda [\varrho_n \ln(1 + \frac{\tilde{\varrho}_n}{\varrho_n}) + \tilde{\varrho}_n \ln(1 + \frac{\varrho_n}{\tilde{\varrho}_n})] \; . \tag{44}$$

Minimizing the free energy, $F^{\rm spin}[\varrho_n] = E^{\rm spin} - TS^{\rm spin}$ with respect to the ϱ_n's with the constraint (42) yields then the famous thermodynamic Bethe ansatz equations for $\eta_n \equiv \tilde{\varrho}_n/\varrho_n$,

$$\ln \eta_n = G * [\ln(1 + \eta_{n+1}) + \ln(1 + \eta_{n-1})] \; , \tag{45}$$

$$\ln \eta_1 = -\frac{2D}{T}\tan^{-1} e^{\pi\lambda} + G * \ln(1+\eta_2) \ , \tag{46}$$

with the integral operator G defined as

$$[G * f](\lambda) \equiv \frac{1}{2}\int_{-\infty}^{\infty} d\lambda' \frac{f(\lambda')}{\cosh\left(\pi(\lambda-\lambda')\right)}. \tag{47}$$

Together with the expression of the spin contribution to the free energy,

$$F^{\rm spin} = -T\int d\lambda \frac{1}{2}\left[\frac{N}{\cosh\pi\lambda} + \frac{1}{\cosh\pi(\lambda+1/c)}\right]\ln(1+\eta_1(\lambda)) \ , \tag{48}$$

the above equations constitute the full thermodynamic 'solution' of the Kondo problem. Of course, one still has to solve a set of coupled integral equations, but this can be relatively easily done numerically, and one can also obtain asymptotic expansions from them in the limit $T \gg T_K$ and $T \ll T_K$, respectively [11, 12, 13].

It is remarkable, that the integral equations (46) are totally independent of the magnetic impurity, which finally only enters in Eq. (48) as an additive term to the free energy, which is uniquely determined by the distribution of one-strings.

The manipulations above can also be carried out in the presence of an external magnetic field, H which enters through the expression of the string energies as $E_n \to E_n + 2Hn$, and modifies the asymptotic values of the η_n's. At $T = 0$ the thermodynamic Bethe ansatz equations simplify to a single integral equation, analogous to Eq. (38), and can be solved analytically.

Instead of a rather demanding detailed analysis of these integral equations, let us just list the main results that can be obtained from them:

- *Universality:* In the limit, $T, h \ll D$ the bandwidth cut-off D can be scaled out of the thermodynamic Bethe ansatz equations, and the impurity contribution to the free energy can be written in a scaling form:

$$F^{\rm imp} = T f\left(\frac{T}{T_K}, \frac{h}{T}\right) \ , \tag{49}$$

  where the Kondo scale is defined as $T_K \equiv 2De^{-\pi/c}$.

- *High temperature expansion:* A high temperature expansion of the free energy

yields

$$F^{\rm imp} = -T\left[\ln(2\cosh\frac{h}{T}) - \frac{1}{2}\frac{h}{T}\tanh\frac{h}{T}\left(\frac{1}{\ln(T/T_K)} + \frac{1}{2}\frac{\ln\ln(T/T_K)}{\ln^2(T/T_K)}\right)\right] \ , \quad (50)$$

implying a a logarithmic suppression of the Curie susceptibility.

- *Fermi liquid regime:* For $T \ll T_K$ the susceptibility and the linear specific heat coefficient become finite corresponding a the Fermi liquid behavior,

$$C^{\rm imp} = \frac{\pi}{6T_K}T \ , \qquad \chi^{\rm imp} = \frac{\mu_B^2}{\pi T_K} \ . \quad (51)$$

  These results also imply that the so-called Wilson ratio, $T\chi^{\rm imp}/C^{\rm imp}$ is a factor of two larger than that of a free electron gas [10]. This surprising result is simply the consequence of spin-charge separation: For a free electron gas the specific heat comes from both the spin and the charge sectors, $C^{\rm el} = C^{\rm charge} + C^{\rm spin} = 2C^{\rm spin}$, while the susceptibility only comes from the spin sector, $\chi^{\rm el} = \chi^{\rm spin}$. The impurity spin, however, only gives quasiparticle excitations in the spin sector, implying $\chi^{\rm imp}/c^{\rm imp} = \chi^{\rm spin}/c^{\rm spin} = 2\chi^{\rm el}/c^{\rm el}$.

- $T = 0$ *magnetization:* The impurity contribution to the zero temperature magnetization is a universal function of h/T_K, $M^{\rm imp} = M^{\rm imp}(h/T_K)$. In the $h \gg T_K$ limit

$$M^{\rm imp} = 1 - \frac{1}{2\ln\frac{h}{T_1}} + \frac{\ln 2}{\ln^2\frac{h}{T_1}} - \frac{\ln\frac{h}{T_1}+}{2\ln^2\frac{h}{T_1}} + \ldots \quad (52)$$

  with $T_1 = (e\pi/2)^{1/2}T_K$.

These results of the exact solution fully justify Nozières' Fermi liquid picture and the existence of a single, dynamically generated energy scale T_K, as suggested by the renormalization group method.

2.3 Numerical renormalization group (NRG)

While the Bethe ansatz provides a solution of the full thermodynamics of a quantum impurity problem, it is not possible to obtain *dynamical* correlation functions with it.

To this purpose, it is much more convenient to use Wilson's numerical renormalization group (NRG) method [10, 14], which is a powerful technique to study almost any quantum impurity problem, and actually preceded five years the Bethe ansatz solution of the Kondo problem. Since we shall use Wilson's numerical renormalization group method later on, let us shortly review this technique here.

2.3.1 Discretization

There are two crucial observations that naturally lead to Wilson's numerical solution of the Kondo problem:
(a) Perturbation theory results in logarithmic singularities. This implies that all electrons in the conduction band contribute to the formation of the Kondo state, and a *logarithmic discretization procedure* is needed to perform an accurate numerical calculation. To this end, one first divides the conduction band onto logarithmic 'subbands', and discretizes the kinetic part of Eq. (21) as

$$H_{\rm band} \approx \sum_{\sigma} \sum_{n=1}^{\infty} \epsilon_n (b_{n\sigma}^{\dagger} b_{n\sigma} - d_{n\sigma}^{\dagger} d_{n\sigma}) \ , \tag{53}$$

where $b_n \sim \int_{\Lambda^{-n}}^{\Lambda^{1-n}} a(k)$, $d_n \sim \int_{-\Lambda^{1-n}}^{-\Lambda^{-n}} a(k)$, ϵ_n is the average energy $\epsilon_n \approx (\Lambda^{-n} + \Lambda^{1-n})/2$, and the cut-off energy has been taken to be unity $D_0 \equiv 1$. The constant $\Lambda > 1$ here is a discretization parameter. In the limit $\Lambda \to 1$ the discrete levels introduced represent the conduction electron band faithfully, but numerically a very good accuracy can be reached even with $\Lambda \approx 3$.
(b) Second, we want to be able to capture the strong coupling limit $J \gg D_0 = 1$ too. In this limit, the exchange coupling to the magnetic moment dominates. This interaction part of the Hamiltonian can be simply written as

$$H^{\rm int} = j D_0 \ \vec{S} \ (f_0^{\dagger} \vec{\sigma} f_0), \tag{54}$$

where $f_{0,\sigma}^{\dagger} = (\int dk a_{\sigma}^{\dagger}(k))/\sqrt{2D_0}$ creates an electron at the impurity site. Clearly, to solve the Kondo problem with sufficient accuracy, one only has to capture the time-dependence of f_0 with a logarithmic accuracy. To this end, one first writes $f_{0,\sigma}$ as a sum of the operators $b_{n\sigma}$ and $d_{n\sigma}$, computes the commutator $[H_{\rm band}, f_0]$ using Eq. (53), and identifies the piece f_1 in this expression, which is orthogonal to f_0. This procedure can be repeated recursively to yield the following approximation for

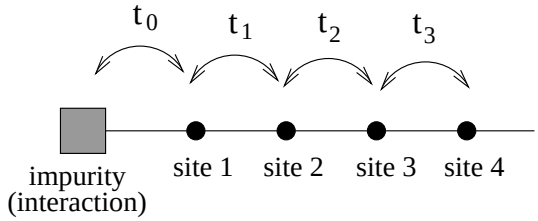

Figure 6: Structure of the effective Hamiltonian of Wilson.

$H_{\rm band}$

$$H_{\rm band} = \sum_\sigma \sum_{i=0}^{\infty} t_i \left(f^\dagger_{i,\sigma} f^\dagger_{i+1,\sigma} + h.c. \right) \ . \tag{55}$$

where the hopping matrix elements decay exponentially, $t_i \approx \frac{1+\Lambda^{-1}}{2}\Lambda^{-i/2}$, with Λ the NRG discretization parameter defined earlier. The structure of this Hamiltonian is shown in Fig. 6: the impurity is sitting at the end of this semi-infinite chain. Taking longer and longer segments of the chain corresponds to taking electron-hole excitations with lower and lower energy into account. One can also show that the operators $f^\dagger_{i\sigma}$ above create states of larger and larger spatial extension, $R_i \sim \Lambda^{i/2}$.

2.3.2 Numerical procedure

To solve $H = H^{\rm imp} + H^{\rm band}$ numerically, we shall first rewrite the Hamiltonian in a more inspiring way as

$$\tilde{H}_{N+1} = \Lambda^{1/2}\, \tilde{H}_N + \sum_\sigma \left(f^\dagger_{N\sigma} f^\dagger_{N+1\,\sigma} + h.c. \right) \tag{56}$$

$$H = \lim_{N\to\infty} \frac{1+\Lambda^{-1}}{2} \Lambda^{-(N-1)/2} \tilde{H}_N \ , \tag{57}$$

where we have introduced the rescaled Hamiltonians

$$\tilde{H}_N \equiv \frac{2}{1+\Lambda^{-1}} \Lambda^{(N-1)/2} H_N \ , \tag{58}$$

$$H_N \equiv H_{\rm imp} + \sum_\sigma \sum_{i=0}^{N-1} t_i \left(f^\dagger_{i,\sigma} f_{i+1,\sigma} + h.c. \right) \ . \tag{59}$$

Note that H_0 in this series just represents the impurity Hamiltonian and contains only f_0.

To compute the physical properties of the Kondo model, one diagonalize the Hamiltonians $\tilde{H}_N$ iteratively: Knowing the eigenstates $|E\rangle_N$ of a chain of length N

and the matrix elements of the operators $f^\dagger_{N\sigma}$ between these states, one can construct new basis states for a chain of length $N+1$ from them by simply adding the site $N+1$. Clearly, one can also compute the matrix elements of the hopping term $\sim \sum_\sigma (f^\dagger_{N,\sigma} f_{N+1,\sigma} + \text{h.c.})$, and of the operator $f^\dagger_{N+1,\sigma}$ in this new basis, construct the eigenstates $|E\rangle_{N+1}$ of $\tilde{H}_{N+1}$, and determine the matrix elements of $f^\dagger_{N+1,\sigma}$ between these states. Of course, this procedure cannot be repeated too many times without making further approximations, since the Hilbert space increases exponentially fast. Therefore, after a few iterations, one truncates the spectrum of $\tilde{H}_N$, and keeps only a finite number of eigenstates $|E\rangle_N$ to build the new basis set.

To increase the accuracy and speed of the calculation, one usually exploits symmetries too. This is a rather complex task, especially if more complex symmetries with non-Abelian generators such as spin SU(2) symmetry, pseudospin symmetries *etc.* are considered. The difficulty arises, because $f^\dagger_\sigma$ being a spin 1/2 charge one operator (which may also have additional quantum numbers in more complicated models) connects states corresponding to different irreducible representations in a non-trivial way. To keep track of these matrix elements one has to use irreducible tensor operators and the Wigner-Eckhart theorem [60].

A typical spectrum of $\tilde{H}_N$ for the Kondo model is shown in Fig. 7 as a function of iteration number. The spectrum of $\tilde{H}_N$ is practically the finite size spectrum of the Hamiltonian, Eq. (22), where the iteration number controls the system size. To understand this, we recall that the $f^\dagger_N$ creates a conduction electron state of spatial extent $L \sim \Lambda^{N/2}$. Thus H_N is the Hamiltonian of a Kondo impurity put into a box of finite size, $L \sim \Lambda^{N/2}$. On the other hand, the energy scale $\Delta_L \equiv 2\pi/L \sim \Lambda^{-N/2}$ occurring in the definition of $\tilde{H}_N$ in Eq. (58) is nothing, but the single particle level spacing of a system of size L. In other words, apart from a constant, the spectrum of $\tilde{H}_N$ is just the spectrum of a system of size L divided by the level spacing $\Delta_L = 2\pi/L$, *i.e.* the finite size spectrum.

This finite size spectrum contains already a lot of information: For large iteration numbers N the spectrum simplifies and becomes usually invariant under the iteration. Thus $\tilde{H}_N$ becomes universal and independent of N (see Fig. 7). The Hamiltonian corresponding to this spectrum is called the *fixed point* Hamiltonian, and the spacing, quantum numbers, and degeneracy of the states is characteristic of the universal fixed point Hamiltonian of the renormalization group as $l \to \infty$. From the relaxation of the levels to their fixed point value one can determine the

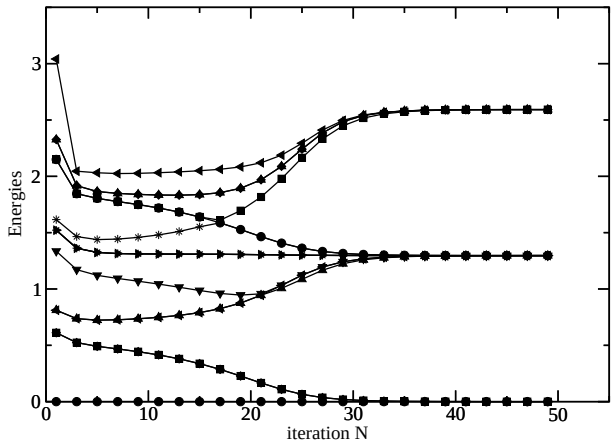

Figure 7: Spectrum of the operators $\tilde{H}_N$ as a function of iteration number for the Kondo problem.

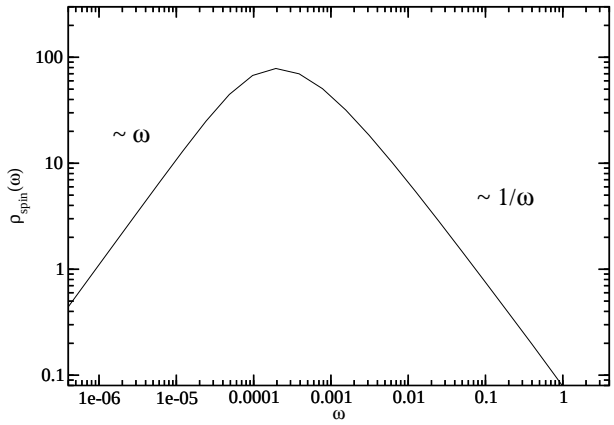

Figure 8: Spectral function of the local spin-spin correlation function.

scaling dimensions of the irrelevant operators around the fixed point, which are directly related to the low temperature exponents of the free energy, and other physical quantities. As we shall discuss in Chapter 5, the finite size spectrum can also be directly used to compute physical quantities such as magneto-conductance [50, 61] .

Having the many-body eigenstates and eigenenergies of H_N at hand, one can calculate thermodynamic quantities at an energy scale $T, \omega \sim \omega_N \sim \Lambda^{-(N+1)/2}$, by simply computing the partition function and numerically differentiating it. More interestingly, however, it is possible to compute local *dynamical* correlation functions too. More precisely, one can calculate the spectral function of any local correlation function. To compute, *e.g.*, the $T = 0$ temperature spectral function of the spin-spin

autocorrelation function, we express it as

$$\varrho^{\rm spin}(\omega) = 2\pi \sum_E \delta(E_n - E_G - \omega) |\langle n|S_z|G\rangle| \ , \tag{60}$$

where $|G\rangle$ denotes the exact ground state and $|n\rangle$ are the exact eigenstates of Eq. (21). Replacing the Dirac delta above by some average over a finite window, we can then use the finite size spectrum $\tilde{H}_N$ with $\omega_N \sim \omega$ to obtain the spectral function at frequency ω with a very high accuracy. As a typical example, we show the spin spectral function of the single channel Kondo model in Fig. 8. The peak in the spectral function is around $\omega \sim T_K$. Below that scale the spectral function scales as $\varrho^{\rm spin} \sim \omega/T_K^2$. This behavior is characteristic of a Fermi liquid and corresponds to a finite susceptibility

$$\chi \sim \int d\omega \ \frac{\varrho^{\rm spin}(\omega)}{\omega} \sim \frac{1}{T_K} \ , \tag{61}$$

by the Kramers-Kronig relation, in agreement with the Bethe ansatz results [12, 13].

3 Dissipation effects in quantum impurity models

Dissipation effects are present whenever we couple some degree of freedom to a macroscopic heat bath: This coupling opens up relaxation channels and is ultimately responsible for irreversibility. Dissipation is thus implicitly present in practically any quantum impurity problem, whether it includes bosonic or fermionic degrees of freedom.

Dissipative models are usually constructed to study how dissipation destroys the quantum coherent motion of some microscopic degree of freedom. However, the distinction between 'dissipative' models and 'non-dissipative' models is somewhat academic. As we already mentioned in Chapter 1, the Ohmic dissipative two level system (TLS) - the most studied model of dissipation - is equivalent to an anisotropic Kondo problem, and thus the Kondo model could also be considered as a model with 'dissipation'.

In the present chapter we shall study dissipative models in the above loose sense. First, we shall review the physics of the Ohmic dissipative two state system and compute its full thermodynamics with Bethe ansatz techniques. Then we shall study how dissipation is generated by the spin of a tunneling particle. Finally, we shall analyze a very general dissipation model, the so-called Bose-Fermi Kondo model, where a spin is coupled to bosonic and fermionic degrees of freedom at the same time.

3.1 The Ohmic dissipative two state system

The Ohmic spin-boson (or dissipative two state) model is defined by Eq. (4) and the spectral function $J(\omega) = 2\pi\alpha\omega$ below a high frequency cut-off, ω_c, and is one of the most frequently used models of dissipation. The reason we call this model 'Ohmic' is that the linear spectral function $J(\omega) \sim \omega$ naturally arises whenever we consider the motion of a particle in a metal.

3.1.1 Microscopic model

To show this more explicitly, let us study the motion of an atom (that we shall sometimes call heavy particle) with a mass M moving in a double well potential $U(\mathbf{R})$ and coupled to free conduction electrons through an interaction $V(\mathbf{R} - \mathbf{r})$, with $\mathbf{R}$ and $\mathbf{r}$ the coordinates of the atom and the conduction electrons, respectively

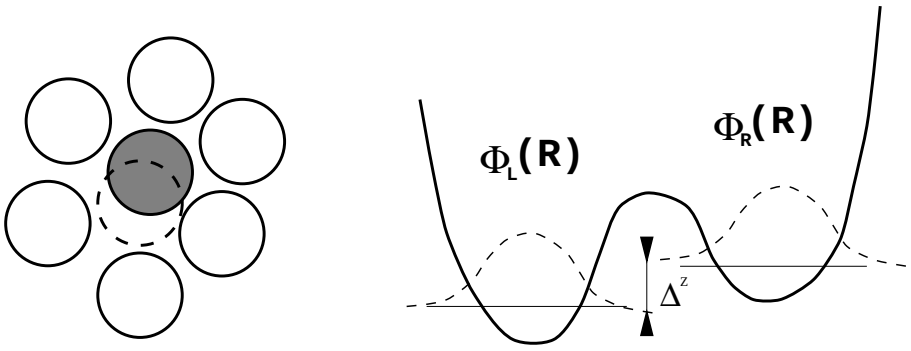

Fig. a **Fig. b**

Figure 9: TLS formed in a disordered region and the effective potential $U(\mathbf{R})$ describing its motion.

(see Fig. 9). Such a tunneling center can form in amorphous metals or disordered regions of a metal. The potential $U(\mathbf{R})$ is the effective potential produced by all other atoms and conduction electrons. At low temperatures the wave function of the heavy particle is localized around the right/left minimum $\mathbf{R}_{L/R}$ of the double well potential. For typical parameters the extension of the wave function around the minima is in the range of $\sim 0.01\mathring{A}$, and for a separation between the minima, $d = |\mathbf{R}_R - \mathbf{R}_L| \sim 0.1\mathring{A}$, the particle moves with tunneling from one minimum to the other. Therefore, at low temperatures we can describe the heavy particle by the tunneling Hamiltonian

$$H_{\rm TLS} = -\frac{1}{2}\Delta\tau_x - \frac{1}{2}\varepsilon\tau_z \ , \tag{62}$$

where the τ_i's denote Pauli matrices, $\Delta \equiv \Delta_x$ is the tunneling amplitude, and $\varepsilon \equiv \Delta_z$ denotes the asymmetry of the double well potential, and $\tau_z = \pm 1$ correspond to the two tunneling positions.

For the sake of simplicity, let us consider a symmetrical tunneling system. To take the effect of conduction electrons into account, we introduce operators $a^\dagger_{s,\sigma}(k)$ and $a^\dagger_{p,\sigma}(k)$ creating spherical waves in the s and p-channels around the impurity

$$a^\dagger_{s,\sigma}(k) \sim \int \frac{d\hat{\mathbf{p}}}{4\pi} c^\dagger_{\mathbf{p},\sigma} \ , \qquad a^\dagger_{p,\sigma}(k) \sim \int \frac{d\hat{\mathbf{p}}}{4\pi} \hat{\mathbf{p}}\hat{z}\ c^\dagger_{\mathbf{p},\sigma} \ . \tag{63}$$

Here the direction $\hat{z}$ is oriented along the axis of the two level system, $c^\dagger_{\mathbf{p},\sigma}$ creates a free electron with momentum $\mathbf{p}$ and spin σ, and we average over all directions $\hat{\mathbf{p}}$ while fixing $|\mathbf{p}| = k_F + k$. For a symmetrical two state system we can construct the

leading interaction term by simple symmetry considerations and express it as

$$H_{\rm int}^{\rm TLS} = v_z \sum_\sigma (\psi^\dagger_{p,\sigma}\psi_{s,\sigma} + {\rm h.c})\ \tau_z + v_x \sum_\sigma (\psi^\dagger_{s,\sigma}\psi_{s,\sigma} - \psi^\dagger_{p,\sigma}\psi_{p,\sigma})\ \tau_x + \dots\ . \tag{64}$$

where $\psi^\dagger_{s/p,\sigma} = \int dk\ a^\dagger_{s/p,\sigma}(k)$ creates a local fermion state with s or p-wave symmetry around the two state system. One can simply estimate the dimensionless couplings above, and one finds that $v_z \sim k_F d$ while $v_x \sim (k_F d)^2 e^{-\gamma} \ll v_z$ with γ the Gamow factor [32]. For the time being, we shall drop the latter - usually rather small - coupling, which describes 'electron assisted tunneling' and shall keep only the dissipative term v_z, that hinders the tunneling process. To make the structure of (64) more transparent, it is worth making a unitary transformation and introducing the 'right' and 'left' fields $\psi_{s/p} \to \psi_\pm \equiv (\psi_s \pm \psi_p)/\sqrt{2}$. In this basis, the dissipative part of (64) reads

$$H_z^{\rm TLS} = v_z \sum_\sigma (\psi^\dagger_{+,\sigma}\psi_{+,\sigma} - \psi^\dagger_{-,\sigma}\psi_{-,\sigma})\tau_z\ . \tag{65}$$

The conduction electrons can be described in terms of chiral fermions, $\psi_{\mu,\sigma}(x) \equiv \int dk\ e^{-ikx}\ a^\dagger_{s/p,\sigma}(k)$, just as in Section 2.2,

$$H_{\rm band} = \sum_{\sigma=\pm}\sum_{\mu=\pm}\int \frac{dx}{2\pi}\ \psi^\dagger_{\mu,\sigma}(x)\ i\partial_x\psi_{\mu,\sigma}(x)\ . \tag{66}$$

From Eq. (65) it is clear why the coupling v_z suppresses dissipation. For $\tau_z = -$ the fermions $\psi_{+,\sigma}$ experience an attractive potential at the origin. Accordingly, they try to *screen* this potential by accumulating charge at the origin. If the particle tunnels to the state $\tau_z = +$, then the potential scattering changes sign, and accordingly, the previously accumulated charge in channel $\psi_{+,\sigma}$ has to be removed and piled up in channel $\psi_{-,\sigma}$. In other words, the tunneling particle has to carry along its screening cloud, and thereby its tunneling amplitude is reduced.

The simplest way to show the equivalence of this model with Eq. (4) is to use bosonization techniques (see Appendix A for more details). With this method, we can rewrite $H_z^{\rm TLS}$ as

$$H_z = \sqrt{\frac{\alpha}{2}}\ \partial_x\phi(0)\ \tau_z\ , \qquad \phi(x) = -\sum_{q\neq 0}\left(\frac{2\pi}{|q|L}\right)^{1/2} e^{-iqx}e^{-|q|a/2}\ b_q\ , \tag{67}$$

where the dissipation strength α is related to v_z as

$$\alpha = 2\Big(\frac{2\delta_{TLS}}{\pi}\Big)^2 , \qquad \delta_{TLS} = \arctan(\pi v_z) . \tag{68}$$

The operators $b^\dagger_{q>0} = b_{-q} \sim \sum_{\mu,\sigma}\sum_k \mu\; a^\dagger_{\mu,\sigma}(k+q)a_{\mu,\sigma}(k)$ satisfy canonical anticommutation relations, and create a density wave with energy q: $H_{\rm band} \to \sum_{q>0} q\; b^\dagger_q b_q$. The factor 2 in the expression of α is due to the spin of the electrons. It is easy to show that the bosonic spectral function indeed takes the form $J(\omega) = 2\pi\alpha\omega e^{-\omega/\omega_c}$, where the cut-off ω_c can be identified as the inverse of the cut-off length a that appears in the bosonization procedure.

3.1.2 Equivalence with the anisotropic Kondo problem

The simplest way to prove the equivalence of the Kondo problem and the spin-boson model is by using the bosonization techniques presented in Appendix A. We can, however, understand the mapping between these two models quite easily from a simple scattering point of view.

Let us first write the anisotropic Kondo model as

$$H_{\rm AK} = \sum_{\sigma=\pm}\int \frac{dx}{2\pi}\; \psi^\dagger_\sigma(x)\; i\partial_x\psi_\sigma(x) + \frac{1}{2}j_z S_z \psi^\dagger(0)\sigma_z\psi(0) + \frac{1}{2}j_\perp(S^+\psi_\downarrow(0)\psi_\uparrow(0) + \text{h.c.}) , \tag{69}$$

where, as in Eq. (22), the left-moving fermionic fields with $x > 0$ and $x < 0$ represent incoming and outgoing conduction electrons in the s-wave scattering channel. For $j_\perp \equiv 0$ this model can be solved exactly, and it is a simple matter to show that the fields ψ_σ get a phase shift $\delta_z = \arctan(\pi j_z/4)$ as they pass from the right to the left:

$$\psi_\sigma(x<0) = e^{\mp 2i\delta_z}\psi_\sigma(x>0) , \tag{70}$$

where the sign of the phase depends on the orientation of the impurity spin.

To prove the equivalence of Eqs. (69) and (4), one constructs a unitary transformation U that transforms Eq. (69) into Eq. (4) (see Appendix A.2 for details). This transformation simply consists of tying a conduction electron antiferromagnetically to the impurity spin and considering the states:

$$|+\rangle \equiv \frac{1}{\sqrt{a}}\psi_\downarrow|S_z = 1/2\rangle , \qquad |-\rangle \equiv \frac{1}{\sqrt{a}}\psi_\uparrow|S_z = -1/2\rangle , \tag{71}$$

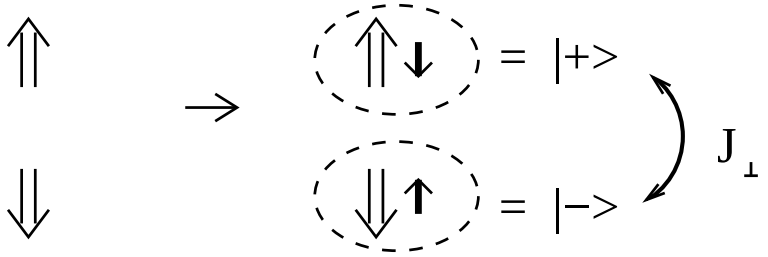

Figure 10: Sketch of the mapping between the dissipative Ohmic two state system and the anisotropic Kondo problem.

as shown in Fig. 10. The prefactor $1/\sqrt{a} = (\langle 0|\psi(0)\psi^\dagger(0)|0\rangle)^{1/2}$ above is needed to normalize the states $|\pm\rangle$, where $1/a$ is of the order of the bandwidth. Clearly, the effect of $j_\perp$ is simply to flip the states $|\pm\rangle$. However, the scattering properties of the conduction electrons are also changed in this new basis: Since there is a fermion tied to the impurity at the origin, they pick up an *additional phase* $\pi/2$ as they pass the impurity, due to the fermionic anticommutation relations. In other words, the part $\sim j_z$ of the Hamiltonian becomes after this unitary transformation:

$$\tilde{H}_K = \frac{1}{2a} j_\perp \tau_x + \lambda_z \tau_z (\psi_\uparrow^\dagger \psi_\uparrow - \psi_\downarrow^\dagger \psi_\downarrow) \; , \tag{72}$$

where the τ_i's act in the subspace of the states $|\pm\rangle$, and λ_z is a coupling producing a phase shift $\delta_{\rm eff} = \delta_z - \pi/2$ for the conduction electrons in the transformed Hamiltonian. Clearly, this Hamiltonian is just the spinless version of Eq. (65), and thus maps on the dissipative two level system with

$$\Delta = j_\perp / a \; , \tag{73}$$

and the effective dissipation strength given by the spinless version of Eq. (68),

$$\alpha = \left(\frac{2\delta_{\rm eff}}{\pi} \right)^2 = \left(1 - \frac{2\delta_z}{\pi} \right)^2 \; . \tag{74}$$

Evidently, a local field hS^z in the Kondo problem maps on an asymmetry $\epsilon = h$ for the tunneling system,

$$hS_z \to \frac{h}{2} \tau_z \; . \tag{75}$$

3.1.3 Renormalization Group analysis and phase diagram

To construct the phase diagram of the spin-boson model, we shall use a scaling analysis. The scaling equations can be directly computed for the dissipative two state system model, however, one can also exploit the previously established mapping to construct them. For the anisotropic Kondo problem the scaling equations have been constructed by Yuval and Anderson using a path integral approach for arbitrary values of j_z but small $j_\perp$ [3]. They can be written most easily in terms of the phase shifts δ_z introduced earlier as

$$\frac{d}{dl}\left(\frac{\delta_z}{\pi}\right) = \frac{1}{4}\left(1 - 2\frac{\delta_z}{\pi}\right) j_\perp^2 \qquad \frac{dj_\perp}{dl} = 4\frac{\delta_z}{\pi}\left(1 - \frac{\delta_z}{\pi}\right) j_\perp \; . \tag{76}$$

For ferromagnetic $\delta_z < 0$'s the scaling trajectories scale to fixed points with $j_\perp = 0$. Along this line of fixed points the impurity spin is essentially free. For antiferromagnetic $\delta_z > 0$, on the other hand, $j_\perp$ increases under scaling, spin flip processes ultimately win, and lead to a Kondo effect.

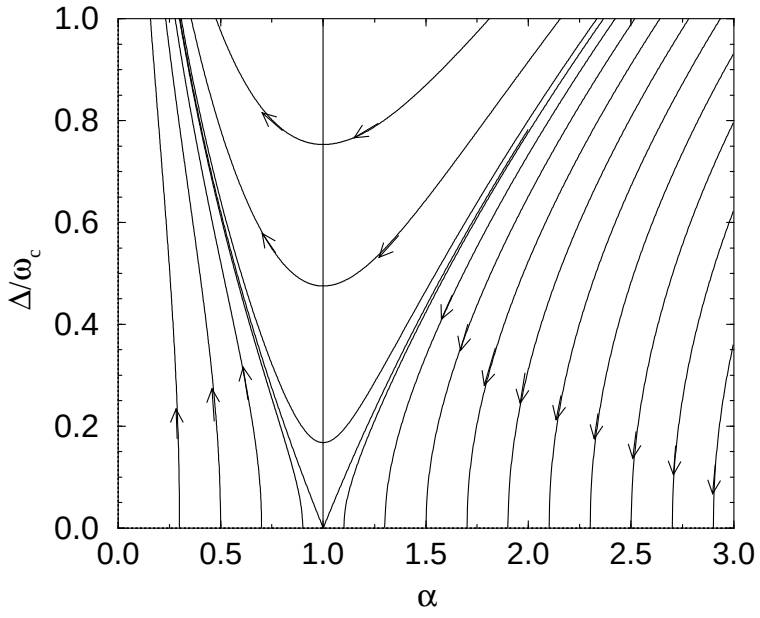

Figure 11: The scaling trajectories of the Ohmic two state system obtained from the Anderson-Yuval scaling equations for the anisotropic Kondo model. Only the region $0 < \alpha < 3$ is shown. The arrows indicate the direction of increasing l. .

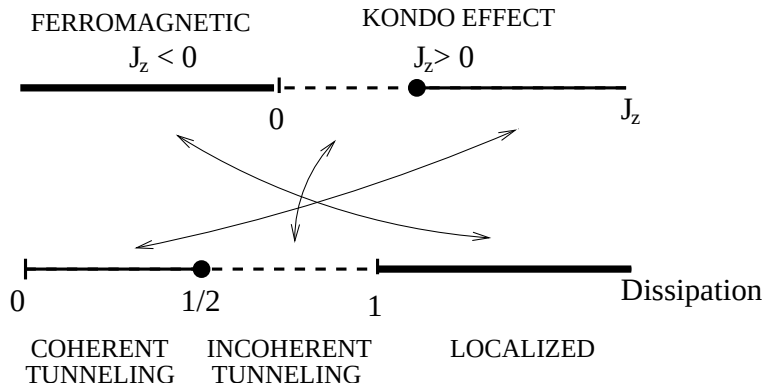

Figure 12: Sketch of the mapping between the dissipative Ohmic two state system and the anisotropic Kondo problem. The dot indicates the Toulouse point.

By equations (73) and (74) the scaling equations (76) map onto

$$\frac{d\alpha}{dl} = \alpha \left(\frac{\Delta}{\omega_c}\right)^2 + \dots \ , \qquad \frac{d(\Delta/\omega_c)}{dl} = (1-\alpha)(\frac{\Delta}{\omega_c}) + \dots \tag{77}$$

where $\omega_c \equiv 1/a$ is the cut-off energy, and $l = \ln a$. These equations can be easily integrated, and the corresponding scaling trajectories are plotted in Fig. 11.

Let us first assume that $\Delta/\omega_c \ll 1$. Then we can neglect the renormalization of α, at least initially. The antiferromagnetic ($\delta_z > 0$) and ferromagnetic ($\delta_z < 0$) regions map onto the regimes of weak ($\alpha < 1$) and strong ($\alpha > 1$) dissipations, respectively, where the physical properties of the model are qualitatively different: For very small dissipations the variable Δ/ω_c increases under scaling and dominates the low energy physics of the tunneling system. We therefore expect that the two state system oscillates, *i.e.*, the correlation function $\langle \tau_z(t)\tau_z(0)\rangle$ is a slowly decaying oscillatory function. However, the frequency of the oscillations becomes renormalized due to dissipation. From the scaling equations it is easy to obtain this renormalized oscillation frequency,

$$\Delta_r \approx \Delta_0 \left(\frac{\omega_{c,0}}{\Delta_0}\right)^{-\frac{\alpha}{1-\alpha}} \ , \tag{78}$$

where $\omega_{c,0}$ denotes the initial value of the cut-off frequency.

On the other hand, we can see that for sufficiently large α, the effective tunneling amplitude scales to zero, and Δ/ω_c is irrelevant: This can be interpreted as the dissipation-induced *localization* of the particle. In other words, at $T = 0$ temperature the two state system cannot tunnel. The correlation function $\langle \tau_z(t)\tau_z(0)\rangle$ does not go to zero for $t \to \infty$, and there is a spontaneous symmetry breaking (the ground state

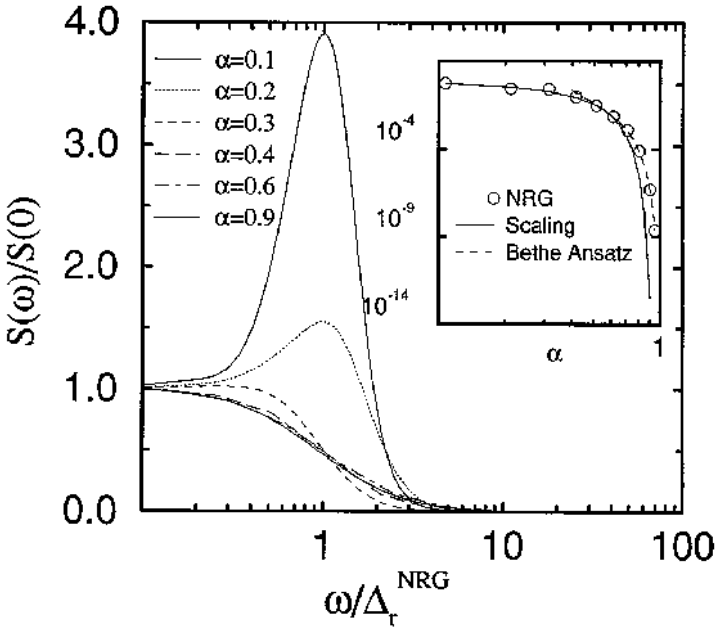

Figure 13: Spectral function of the dissipative two state system obtained by Costi and Kieffer using the numerical renormalization group method and exploiting the discussed mapping (from Ref. [62]). The inset shows the dissipation dependence of the renormalized tunneling rate.

becomes two-fold degenerate for large α's). The physics in the delocalized regime is qualitatively the same for all $\alpha < 1$, however, there is a special point, $\alpha = 1/2$, where the physical properties of the dissipative two state system change quantitatively: For $\alpha > 1/2$ the oscillations disappear from the correlation function. At this special point (Toulouse point for the Kondo problem), the model can be analytically solved using bosonization and refermionization methods. The correspondence between the anisotropic Kondo model and the dissipative tunneling system is sketched in Fig. 12.

The correspondence between the two models can be extensively used to determine the properties of the spin boson model. In Fig. 13 we show, *e.g.*, the numerically computed spectral functions of the dissipative two state system model, which have been obtained using the numerical renormalization group method for the anisotropic Kondo problem and exploiting the mapping above [62]. These results of Costi beautifully show how the finite energy peak describing coherent oscillations gradually disappears as we increase dissipation. In the next subsection, we shall use the same mapping to determine the thermodynamic properties of the spin boson model by Bethe ansatz methods.

3.1.4 Bethe ansatz results

In this subsection we shall study the thermodynamic behavior of the dissipative two state system model using Bethe ansatz methods, by exploiting the existing mapping between the anisotropic Kondo problem, and the fact that the latter is integrable.

The anisotropic Kondo problem has been solved by Melnikov and Tsvelik [63, 13]. However, these authors used their solution just to get a systematic approximation to the isotropic Kondo problem, and their study did not focus to the strongly anisotropic regime, corresponding to weak dissipations.

Similar to the isotropic single channel problem discussed in Section 2.2.1, there is a spin-charge separation and spin excitations can be characterized in terms of rapidities j_δ, which satisfy the analogues of Eqs. (34) and (35),

$$\begin{aligned} e^{ik_j L} &= \prod_{\beta=1}^{M} \frac{\sinh(\mu(\lambda_\beta + \frac{i}{2}))}{\sinh(\mu(\lambda_\beta - \frac{i}{2}))} , \qquad (79) \\ \prod_{\beta=1}^{M} \frac{\sinh(\mu(\lambda_\alpha - \lambda_\beta + i))}{\sinh(\mu(\lambda_\alpha - \lambda_\beta - i))} &= -\frac{\sinh(\mu(\lambda_\alpha + \frac{\theta}{\mu} + \frac{i}{2}))}{\sinh(\mu(\lambda_\alpha + \frac{\theta}{\mu} - \frac{i}{2}))} \left[\frac{\sinh(\mu(\lambda_\alpha + \frac{i}{2}))}{\sinh(\mu(\lambda_\alpha - \frac{i}{2}))}\right]^N . \end{aligned}$$

Here the parameters μ and θ are related to the dimensionless couplings $j_\perp$ and j_z, however, the particular connection between them depends on the regularization scheme used. Therefore, in the Bethe ansatz solution, it is rather μ and θ that should be viewed as independent microscopic couplings. The coupling μ is usually called *anisotropy*, $\mu = \pi/2$ corresponding to the fully isotropic case. As we have proven in [64], μ it is directly related to the dissipation through:

$$\frac{\mu}{\pi} = 1 - \alpha . \qquad (80)$$

The coupling θ determines a universal low temperature scale in the Kondo problem, which we can call the Kondo temperature, and can identify essentially as the renormalized tunneling rate Δ_r defined in the previous subsection,

$$\Delta_r = \alpha T_K = \left(1 - \frac{\mu}{\pi}\right) 2D \exp\left(-\frac{\pi\theta}{\mu}\right) . \qquad (81)$$

The thermodynamic Bethe ansatz equations can be constructed along similar lines as in Section 2.2.1. Similar to Eqs. (34), i the thermodynamic limit, Eqs. (79), admit string solutions. However, in this case strings can have different *parities* and

only strings of certain lengths are allowed. The allowed string solutions can be classified in terms of an infinite fraction expansion of μ/π [65] Furthermore, the thermodynamic Bethe ansatz equations reduce to a finite set of integral equations if μ/π can be written as a *finite* fraction.

We have deduced many of the thermodynamic properties of the Ohmic spin-boson model by analyzing this set of integral equations for $\mu/\pi = 1/\nu$ and $\mu/\pi = (\nu-1)/\nu$. There is, however, two important things that should be kept in mind when analyzing the dependence on the asymmetry energy ε:
(a) Firstly, to make the model integrable, one has to introduce an artificial interaction between the conduction electrons. As already emphasized by Tsvelik and P. B. Wiegmann [13], interaction renormalizes the g-factor of the electrons, and one has to take this renormalization into account.
(b) Secondly, the Bethe ansatz solution can only take into account the effect of a *global* magnetic field. As a consequence, the external field $h = \varepsilon$ acts on the conduction electrons too.
We have shown using an exact result due to Wiegmann and Finkelstein [66], that these two mechanisms exactly compensate each-other, and therefore the Bethe ansatz computations give directly the free energy of the spin boson model (dissipative two state system model).

In the high temperature limit, $T \gg \Delta_r, \epsilon$ we find

$$F(T \gg \Delta_r, \varepsilon) \approx -T\Big\{\ln \frac{\sinh(\varepsilon/T)}{\sinh(\varepsilon/2T)} - (\frac{\Delta_r}{T})^{2-2\alpha}\Big(A + B(\frac{\varepsilon}{T})^2\Big)\Big\} \,, \tag{82}$$

$$\chi(T \gg \Delta_r;\ \varepsilon = 0) = -\frac{\partial^2 F}{\partial \epsilon^2} \approx \frac{1}{T}(\frac{1}{4} - 2B(\frac{\Delta_r}{T})^{2-2\alpha}) \,, \tag{83}$$

$$c(T \gg \Delta_r;\ \varepsilon = 0) \sim (\frac{\Delta_r}{T})^{2-2\alpha} \,, \tag{84}$$

where the constants A and B depend only on α. The power law corrections are characteristic of the spin-boson model. In the low temperature limit we find:

$$F(\varepsilon \ll T \ll \Delta_r) \approx -\frac{T^2}{\Delta_r}\Big(\frac{\alpha\pi}{6} + \frac{1}{4\pi}\frac{\varepsilon^2}{T^2}\Big) \,, \tag{85}$$

$$\chi(T \ll \Delta_r;\ \varepsilon = 0) \approx \frac{1}{\Delta_r}\frac{1}{2\pi} \,, \tag{86}$$

$$c(T \ll \Delta_r;\ \varepsilon = 0) \approx \frac{\pi}{3}\frac{T\alpha}{\Delta_r} \,, \tag{87}$$

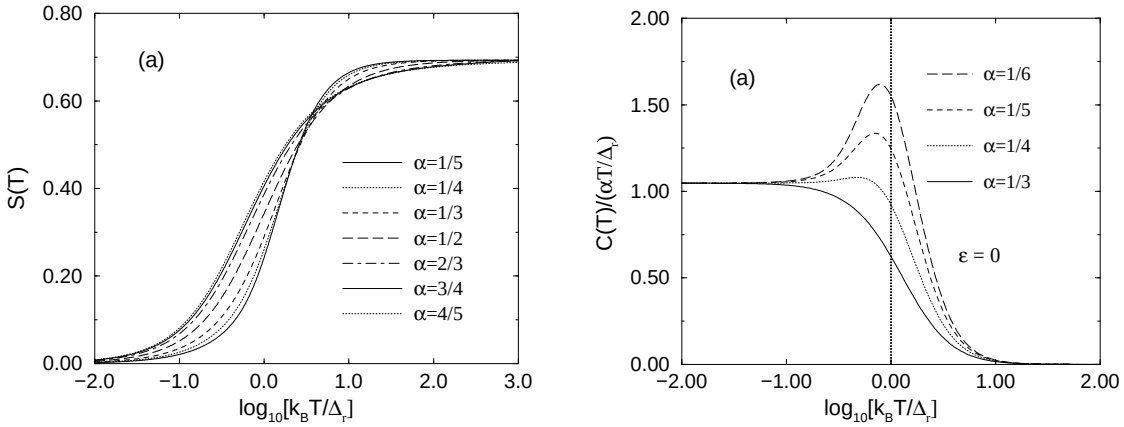

Figure 14: Left: Entropy, $S(T)$, for the symmetric two state system ($\varepsilon = 0$) for weak ($\alpha < 1/2$) and strong ($\alpha > 1/2$) dissipation cases. Right: Specific heat, $c(T)/(\alpha T/\Delta_r) = \tilde{\gamma}$, showing the development of the peak at $k_B T \approx \Delta_r$ for $\alpha \leq 1/3$ and $\varepsilon = 0$. $\tilde{\gamma}(T = 0) = \pi/3 = 1.04719755$ is recovered to 5 decimal places. The T^3 coefficient in $C(T)/T$ is negative for $\alpha > 1/3$ and positive for $\alpha < 1/3$.

where the numerical constants have been calculated following the same lines as in Ref. [13]. Thus at low temperatures the well-known Fermi liquid behavior is recovered [9, 18].

To obtain the thermodynamic quantities for all temperatures and asymmetries, one has to solve the Bethe ansatz integral equations numerically. This is particularly difficult for large values of ε, where the numerical procedure needs some care. In this regime, to compute the specific heat and susceptibility, we derived separate set of integral equations, similar to Eqs. (46) [64].

Here we shall just discuss the few most important results. The entropy of the symmetric two state system is shown in Fig. 14.a as a function of temperature for several values of the dimensionless dissipation strength, α, ranging from weak to strong dissipation. The correct value of the entropy, $S = \ln 2$, is recovered at high temperature for all α.

At low temperature the specific heat is given by $c(T) = \frac{\alpha\pi}{3}(T/\Delta_r) + b(\alpha)(T/\Delta_r)^3 + \ldots$. The coefficient $b(\alpha)$ of the T^3 term is negative for $\alpha \geq 1/3$, a special point in the parameter space of the dissipative two state system. For small dissipations, the linear specific heat coefficient develops a peak at $\sim \Delta_r$, which is reminiscent to the resonance in the spectral function in Fig. 13.

Fig. 15.a shows that the dielectric susceptibility of the dissipative two state system remains finite down to $T = 0$ for all dissipation strengths $\alpha < 1$. In contrast to the

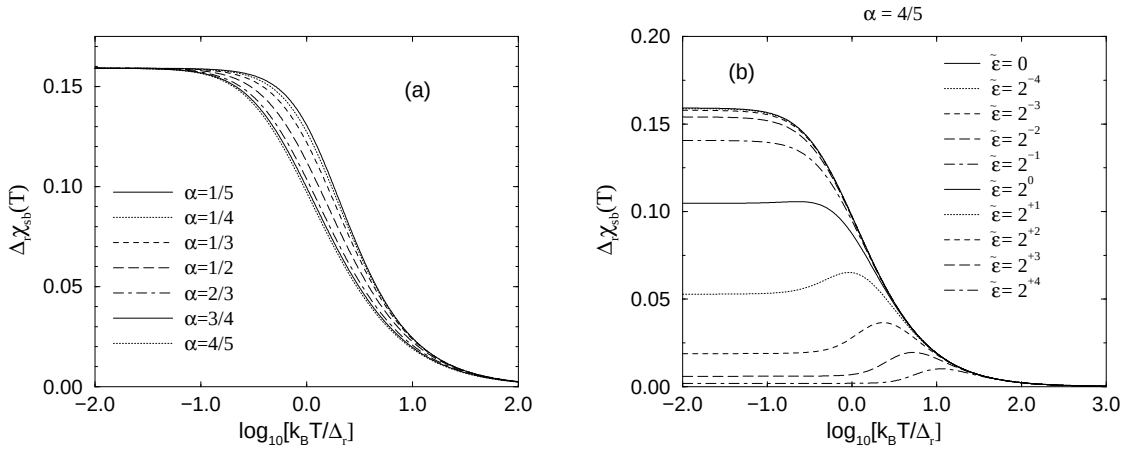

Figure 15: Left: Dielectric susceptibility, $\chi(T)$, for the symmetric two state system ($\varepsilon = 0$) for weak ($\alpha < 1/2$) and strong ($\alpha > 1/2$) dissipation cases. The susceptibility is finite at $T = 0$ with $\Delta_r(\alpha)\chi(T = 0) = 1/2\pi$ in all cases as seen in (a) and attains its free-spin value of $1/4T$ at high temperatures. Right: Dielectric susceptibility, $\chi_{sb}(T)$, for the special case of strong dissipation, $\alpha = 4/5$.

specific heat, $c(T)/T$, the susceptibility is a monotonically decreasing function of temperature for all dissipation strengths, and there is no signature of the onset of activated behavior in the susceptibility as there was for $\alpha < 1/3$ in $c(T)/T$. As shown in Fig. 15.b, the finite temperature peak in χ only arises when there is a finite level asymmetry ϵ.

3.2 Dynamics of a tunneling particle with spin

In the previous two subsections we studied the dynamics of a tunneling impurity coupled to an Ohmic bath. In particular, we have shown that the problem of a tunneling impurity in a metal can be mapped to the spin-boson model and worked out the correspondence between the dissipation strength α and the coupling v_z for short tunneling distances, Eq. (68). It has been shown by Yoshida for arbitrary separations d that for a simple s-wave scatterer in a free electron gas the dissipation can be expressed as

$$\alpha_< \equiv \Big(\frac{2}{\pi}\,\mathrm{atan}\,\frac{\tan\delta_s\,\sqrt{1-F^2}}{\sqrt{1+F^2\,\tan^2\delta_s}}\Big)^2\,, \qquad F=\frac{\sin(k_F d)}{k_F d}\,, \tag{88}$$

where δ_s denotes the phase shift in the s-channel, and F is an overlap parameter.

From Eq. (88) it is clear that to obtain strong dissipations one needs *resonant scattering* at the Fermi energy, *i.e.* $\delta_s \sim \pi/2$. One possible mechanism that could lead to such a resonant scattering is the Kondo effect. This motivated us to study a simple model, where the tunneling particle has a spin, tunnels between two positions, $\mathbf{R}_\pm$ and couples locally to the conduction electrons by a simple exchange interaction,

$$H_{\rm int} = J\ P_+\ \vec{S}\ (\Psi_+^\dagger \vec{\sigma} \Psi_+) + J\ P_-\ \vec{S}\ (\Psi_-^\dagger \vec{\sigma} \Psi_-) + \ , \tag{89}$$

where $P_\pm = \frac{1}{2}(1 \pm \tau_z)$ are projector operators and the fields $\psi_\pm$ create conduction electrons at positions $\mathbf{R}_\pm$,

$$\Psi_{\pm,\mu}^\dagger = \int e^{i\mathbf{k}\mathbf{R}_\pm} c_{\mathbf{k}\mu}^\dagger \frac{\mathbf{d}^3\mathbf{k}}{(2\pi)^3}\ . \tag{90}$$

Following Ref. [68], we have mapped this model to a two-channel problem and studied it using the numerical renormalization group technique. In Fig. 16 we present the obtained spin and orbital spin spectral functions for various overlap parameters F [69]. Two energy scales appear in the spectral functions: The Kondo scale T_K, which appears as a peak in the spin spectral function, and the renormalized tunneling energy, Δ^*. Quite surprisingly, we find that in the peculiar case, $F = 0$ the spin susceptibility diverges logarithmically, and a two-channel Kondo effect appears below Δ^*. This behavior is, however, not generic, and for any finite F crosses over to a Fermi liquid with $\varrho_S(\omega) \sim \omega$. Consequently, for very small values of F a third crossover occurs at an energy T^*. For generic F's, however, this crossover takes place almost simultaneously with the crossover at Δ^* and only a small kink remains from the two-channel Kondo behavior of $F = 0$.

To determine the scale Δ^* and the temperature-dependence of the tunneling rate we invoke renormalization group arguments. The Hamiltonian involves three dimensionless parameters: $j \equiv Jk_F^2/2\pi^2$, F, and Δ_0/ω_0, with ω_0 the high-energy cutoff of the order of the Debye frequency [124]. Well above Δ^*, the dimensionless effective tunneling $\tilde{\Delta}(\omega) \equiv \Delta(\omega)/\omega$ at energy scale ω is small, and therefore $\Delta(\omega)$ must satisfy the following scaling equation:

$$\frac{d \ln \Delta(\omega)}{d \ln\ \omega} = \alpha(j(\omega), F)\ , \quad (\Delta(\omega_0 = \Delta_0)). \tag{91}$$

Above Δ^* the impurity is immobile. Therefore the effective Kondo coupling $j(\omega)$

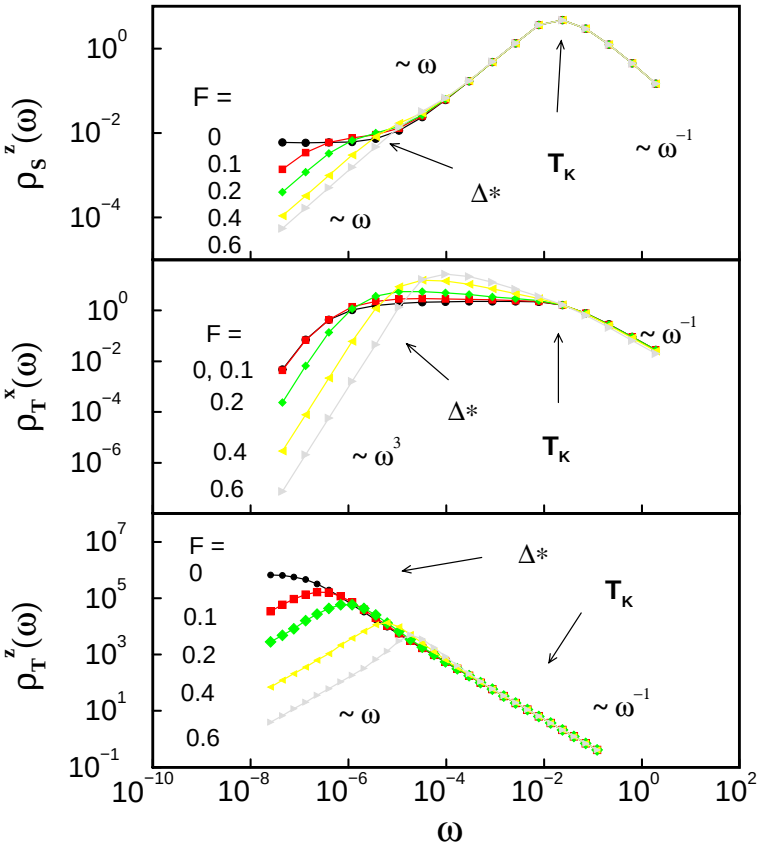

Figure 16: Logarithmic plot of the spin (ϱ_S) and orbital spin (ϱ_T) spectral functions for the tunneling spin model, computed by numerical renormalization group methods. The energy scales T_K and Δ^* are also indicated.

does not depend on the other two parameters, and is a universal function of ω/T_K. In this regime F can be completely transformed out of the Hamiltonian and is therefore constant. Thus $\alpha = \alpha(\omega/T_K, F)$ is a universal function of ω/T_K and F for $\omega \gg \Delta(\omega)$. This function is related to the time-dependent correlation function as $\langle \tau^x(t)\tau^x(0)\rangle \sim 1/t^{2\alpha(\omega)}$ ($t \sim 1/\omega$) [81]. Assuming that the retarded and the time ordered correlation functions have the same singular behavior, this immediately implies that, within logarithmic accuracy, α can be determined from the logarithmic derivative of the corresponding spectral function, ϱ_T^x as

$$\alpha(\omega) \approx \frac{1}{2}\left(\frac{d\ln\ \varrho_T^x}{d\ln\omega} + 1\right), \quad (\omega \gg \Delta^*). \tag{92}$$

We plotted this universal function in Fig. 17. For large frequencies $\alpha \approx 0$, meaning

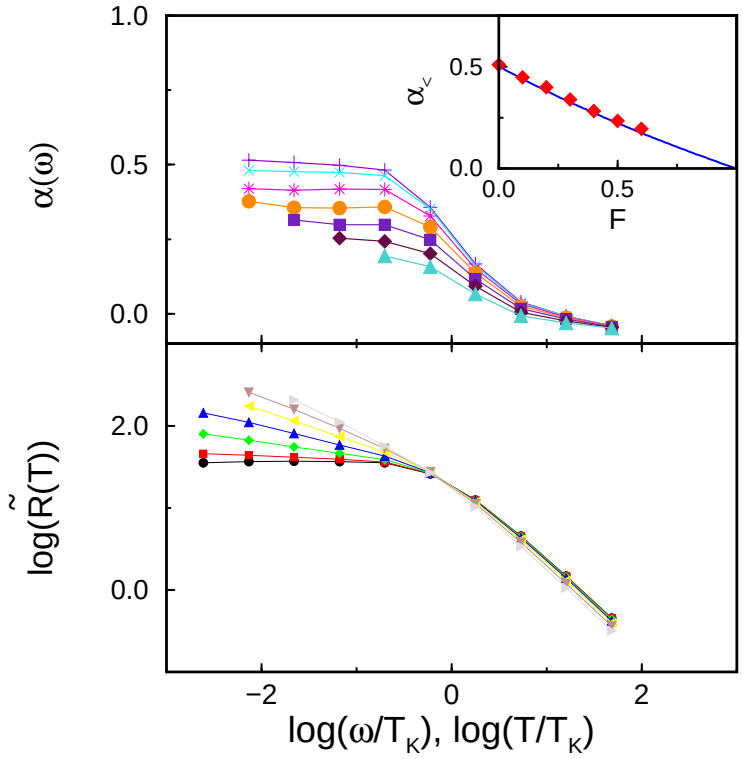

Figure 17: Top: Energy- and overlap-dependence of the anomalous dimension α of the dimensionless tunneling amplitude for $F = 0$, 0.1, 0.2 0.3, 0.4, 0.5, and 0.6 (top to bottom), as determined from the logarithmic derivative of the spectral function ϱ^x_τ. Bottom: Temperature dependence of the normalized tunneling rate, $\tilde{R}(T) = R(T)/\Delta_0^2$. F decreases from top to bottom. We used $\Lambda = 3$, $g = 0.144$, and $\Delta_0 = 2.31 \cdot 10^{-5}$ in both figures.

that the tunneling amplitude remains unrenormalized above T_K. Below T_K, on the other hand, it scales to an overlap-dependent constant, $\alpha_<(F)$. As shown in the inset, $\alpha_<$ coincides with the expression Eq. (88) for a maximally strong scatterer with a phase shift $\delta_s = \pi/2$ [67]. Thus, far below T_K (but still above Δ^*) the Kondo impurity can be replaced by maximally strong potential scatterer in agreement with Nozières' Fermi liquid picture [9]. Thus for $T < T_K$ the Kondo effect indeed leads to a strong dissipation as we expected.

We also determined the renormalized temperature dependent tunneling rate, $R(T)$, which can be experimentally determined by performing real-time measurements [71]. By dimensional analysis, we obtain [69]

$$R(T) \sim \Delta(\omega \sim T)^2/T \,, \tag{93}$$

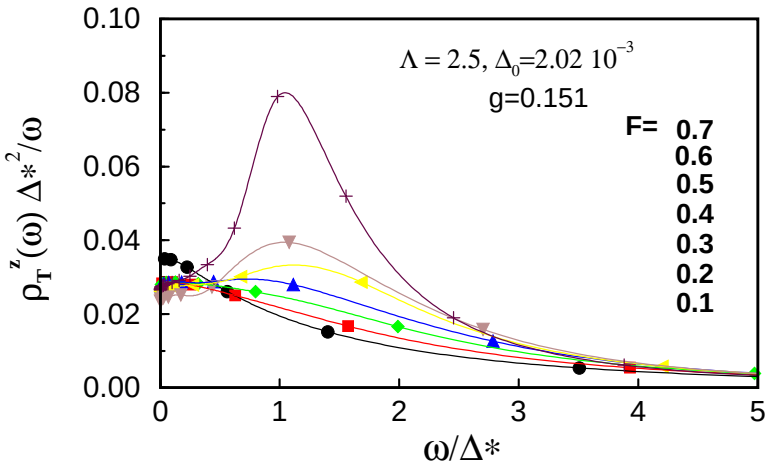

Figure 18: Rescaled spectral functions and the evolution of the coherence peak with increasing overlap.

where $\Delta(T)$ has been computed by numerically integrating Eq. (91). As the most striking consequence of the Kondo effect, the logarithmic slope of $R(T)$ changes at $T \approx T_K$ (see Fig. 17, bottom).

Finally, in Fig. 18 we show ϱ_T^z/ω, where coherent tunneling appears as a peak. Even though the exchange coupling j is small initially, below the Kondo scale it becomes large, and suppresses the coherent tunneling of the particle even for intermediate values of the overlap F.

3.3 The Bose-Fermi Kondo model

In the previous seubsections we studied the simplest possible case of a tunneling particle, where dissipation appears as a coupling to the operator τ_z only. In many cases, however, dissipative fields couple to several spin components. Moreover, in some cases fermionic degrees of freedom may also couple independently to the impurity:

(a) In case of a megnetic impurity in a three-dimensional antiferromagnet the magnetic impurity may couple to the Goldstone modes in the ordered phase [72]. These Goldstone modes give rise to *two* bosonic fields that induce Ohmic dissipation.

(b) Similar dissipative models emerge in mean field theories of quantum spin glasses [74, 73]. In these theories the dissipative field acting on a given spin is provided by the back-reaction of the other spins, and must be determined selfconsistently.

(c) It has been also argued [75] that replacing a magnetic ion in the Néel state of a two-dimensional antiferromagnet by a non-magnetic impurity leads to the formation of a local magnetic moment, which then couples to the order parameter fluctuations. The resulting interaction involves three bosonic fields corresponding to the three spin components. At the quantum critical point of the antiferromagnet these bosonic fluctuations become gapless and decay with some anomalous dimension.
(d) A 'locally quantum critical' phase transition has been observed in the alloy $CeCu_{5-x}Au_x$, where a quantum phase transition between a paramagnetic (heavy fermion) metal and an antiferromagnetic metal takes place as a function of doping [41, 76, 77]. In this material Ce ions provide a spin, which is screened by the conduction electrons in the paramagnetic phase through a Kondo effect, and this spin is responsible for the antiferromagnetism in the ordered phase. Clearly, a competition of the bosonic order parameter fluctuations and the fermionic screening mechanism gives rise to this interesting quantum critical point, where the critical fluctuations are experimentally found to be local in space but anomalous in time. To capture this competition, an extended dynamical mean field approach has been proposed, where an impurity spin is considered in the presence of both bosonic and fermionic fluctuations, the so-called Bose-Fermi Kondo problem [78, 79].

In the present subsection we shall study the *fully anisotropic* Bose-Fermi Kondo model, defined by the interaction Hamiltonian:

$$H_{\rm int} = \sum_\alpha j_\alpha S^\alpha (\psi^\dagger \frac{1}{2}\sigma^\alpha \psi) + \sum_\alpha \Lambda^{\epsilon/2} \gamma_\alpha S^\alpha \varphi^\alpha \ . \tag{94}$$

Here j_α and γ_α ($\alpha = x, y, z$) denote dimensionless coupling constants, and Λ is a high energy cutoff. We assume that the fermionic imaginary time propagator corresponds to a free degenerate Fermi gas and it therefore decays as $\sim 1/\tau$ while the bosonic field shows critical imaginary time correlations at zero temperature with an anomalous dimension $\epsilon \geq 0$ at $T = 0$:

$$\langle T\psi_\sigma(\tau)\psi^\dagger_{\sigma'}(0)\rangle = \frac{\delta_{\sigma\sigma'}}{\tau}, \qquad \langle T\varphi_\alpha(\tau)\varphi_\beta(0)\rangle = cst.\ \frac{\delta_{\alpha\beta}}{\tau^{2-\epsilon}} \ . \tag{95}$$

For $j_i = \gamma_x = \gamma_y = 0$ and $\epsilon = 0$ this model reduces to the spin boson model with a dissipation parameter $\alpha = \gamma_z^2/2$, and the field φ corresponding to $\partial_x \phi$ in Eq. (67).

The SU(2) invariant version of this model has been studied first independently by Sengupta, and Smith and Si [78, 79], who performed a leading order expansion in

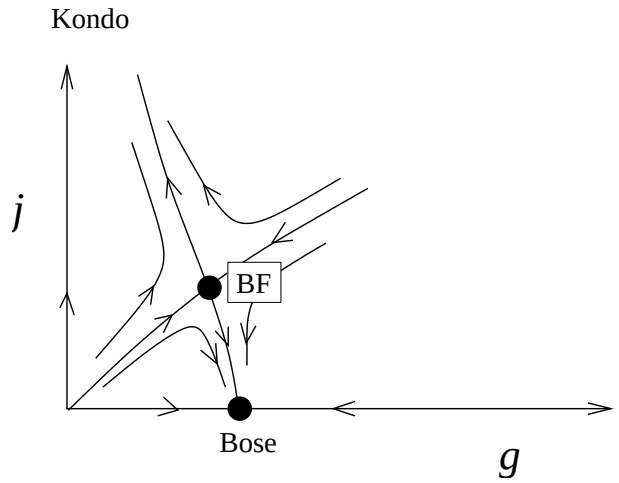

Figure 19: Renormalization group flows for the SU(2) symmetrical Bose-Fermi Kondo model. "BF" denotes the SU(2) symmetrical Bose-Fermi fixed point. Here the spin is partially screened and both the Fermi and Bose fields couple to it. At the Bose fixed point the fermionic degrees of freedom fully decouple from the spin.

the exponent ϵ. A second order expansion has been later performed for the purely bosonic and SU(2)-invariant model in Ref. [75]. In this subsection we shall present our $\sim \epsilon^2$ results for the *fully anisotropic* Bose-Fermi Kondo problem, and show that anisotropy is *relevant* in this model and cannot be neglected [80]. We shall use a scaling approach to study this problem. In most of what follows we shall assume that the magnetic field is negligible. Then the Gell-Mann-Low equations take the form

$$\frac{dj_\alpha}{dl} = \beta_\alpha^{(f)}(\{j_\gamma\},\{g_\gamma\}) \ , \qquad \frac{dg_\alpha}{dl} = \beta_\alpha^{(b)}(\{j_\gamma\},\{g_\gamma\}) \ , \tag{96}$$

where we introduced the new couplings, $g_\alpha = \gamma_\alpha^2$, since (by a Z_2 gauge invariance) only the latter can appear in any physical quantity.

3.3.1 The SU(2) symmetrical case

To start our analysis, let us first discuss the case of SU(2) symmetry with non-zero bosonic and fermionic couplings, $g, j \neq 0$. It is enough to consider the leading order scaling equations to obtain a qualitative picture of what happens in this case [78, 79],

$$\frac{dj}{dl} = j^2 - jg \ , \qquad \frac{dg}{dl} = \epsilon g - 2g^2 \ . \tag{97}$$

The sketch of the renormalization group flows is shown in Fig. 19. Eqs. (97) have three different fixed points, each of which correspond to different $T \to 0$ behaviors. Two of these fixed points are stable: At one of the stable fixed points the bosonic couplings vanish and the Kondo coupling j diverges. We can thus identify this fixed point as the 'Kondo phase', where the impurity spin is completely screened by the fermions at low temperatures. At the other stable fixed point the bosonic coupling is finite, $g \sim \epsilon$, and the Kondo coupling vanishes. This state can be identified as the *bosonic* fixed point, where the spin only interacts with the Bose field (representing the collective modes corresponding to spin fluctuations. This can be identified as a 'magnetic' phase. Finally, but very importantly, these two stable fixed points are separated by a *critical* Bose-Fermi fixed point, where both bosonic and fermionic couplings are present, $j, g \sim \epsilon$. Si and his collaborators suggested to identify this fixed point with the experimentally observed locally quantum critical behavior.

The fact that two of the fixed points are of order $\sim \epsilon$ makes us possible to carry out a systematic ϵ expansion and compute all critical exponents around these fixed points. We shall, however, not bore the reader with the rather complicated details of this calculation and the enumeration of all diagrams, which can be found in Ref. [80]. Instead, we discuss some *exact* results concerning the dynamical susceptibility.

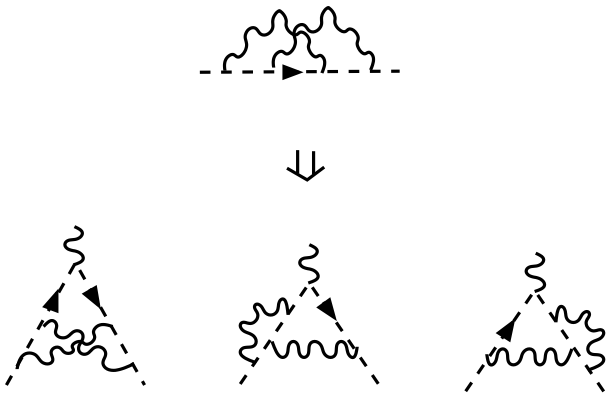

Figure 20: Diagrammatic representation of the Ward identity. Dashed lines denote spin (pseudofermion) propagators and wavy lines denote the bosonic propagators. The circles denote the local magnetic field. There is a one to one correspondence between self energies linear in $\vec{h}$ and the vertex functions.

To compute the susceptibility, we first add a local magnetic field to the Hamiltonian:

$$H \to H - \sum_{\alpha=x,y,z} h_\alpha S_\alpha \ . \tag{98}$$

In this bosonic model, there is a relation (Ward identity) between the magnetic field dependent part of the self-energy and the bosonic vertex function, demonstrated to lowest order in Fig. 20. This Ward identity ultimately results in the following exact relation:

$$\frac{1}{h_\alpha}\frac{dh_\alpha}{dl} = -\frac{\epsilon}{2} + \frac{1}{2\,g_\alpha}\beta_\alpha^{(b)}(j_\alpha, g_\alpha)\ , \tag{99}$$

where $\beta^{(b)}$ is the bosonic beta function defined earlier. At a non-trivial fixed point with finite bosonic coupling $g_\alpha^* \neq 0$, the corresponding beta function $\beta_\alpha^{(b)}$ vanishes, and the scaling dimension of the dimensionless magnetic field, $\tilde{h} \equiv h/\Lambda$ is simply $1 - \epsilon/2$. This scaling dimension is, however, known to be related to the anomalous dimension of spin-spin correlation function [81], giving

$$\chi_{\alpha\beta}^{SU(2)}(\tau) = \langle T_\tau S_\alpha(\tau) S_\beta(0)\rangle = \frac{\delta_{\alpha\beta}}{(T^*\tau)^\epsilon}\ , \qquad (T=0)\ , \tag{100}$$

where T^* is a dynamically determined energy scale (similar to the Kondo temperature, T_K), and $\langle T_\tau \ldots\rangle$ denotes imaginary time ordering.

It is easy to extend these results to finite temperature by assuming that there exists a boundary conformal field theory that corresponds to the critical dynamics of the fixed point [80, 82]. In this boundary conformal field theory the impurity lives at the $x = 0$ line of the complex plane, $z = \tau + ix$, and the theory is invariant under conformal mappings that map this boundary onto itself.

The finite temperature correlation functions can be obtained by mapping the complex plane on a strip of width $\beta = 1/T$ using *e.g.* the function $w = \frac{1}{\pi T}\mathrm{artg}\ z$. Assuming that S_α transforms as a primary field of dimension $\eta_\alpha/2 = \epsilon/2$,

$$\langle S^\alpha(w_1) S^\alpha(w_2)\rangle_T = \Big(\frac{\partial z_1}{\partial w_1}\Big)^{\epsilon/2}\Big(\frac{\partial z_2}{\partial w_2}\Big)^{\epsilon/2}\langle S^\alpha(z_1) S^\alpha(z_2)\rangle_0\ , \tag{101}$$

we obtain that at the critical point:

$$\chi_\alpha(\tau, T) = \Big(\frac{\pi T}{T_\alpha^* \sin(\pi T\tau)}\Big)^\epsilon\ . \tag{102}$$

Taking then the Fourier transform of Eq. (137) and continuing it analytically to the real axis one obtains an exact expression of the finite temperature susceptibility,

$$\chi_\alpha(\omega) = \frac{T^\epsilon}{T_\alpha^{*\epsilon}}\frac{\pi^{\epsilon-1/2}}{T}\frac{\Gamma(\frac{1}{2}-\frac{\epsilon}{2})\Gamma(\frac{\epsilon}{2}-\frac{i\omega}{2\pi T})}{\Gamma(\frac{\epsilon}{2})\Gamma(\frac{1}{2}-\frac{\epsilon}{2}-\frac{i\omega}{2\pi T})}\ . \tag{103}$$

The imaginary part of the susceptibility (measurable directly by inelastic neutron scattering) can be written in a scaling form using the asymptotic properties of the Γ function as

$$\chi_\alpha^{''} = \Big[\frac{T^*}{T}\Big]^{1-\epsilon} f(\epsilon, \frac{\omega}{T})\ \mathrm{sgn}\omega\ , \qquad f(\epsilon, x) \approx \begin{cases} C_> \ |x|^{\epsilon-1} & |\omega| \gg T, \\ C_< \ |x| & |\omega| \ll T. \end{cases} \tag{104}$$

3.3.2 Relevance of anisotropy

Until now, we have only considered the case of isotropic (SU(2) symmetric) couplings. However, as discussed in Ref. [80], anisotropy, present in most heavy fermion systems or in high temperature superconductors, is *relevant*, and completely changes the map of possible fixed points.

The fully anisotropic $\sim \epsilon^2$ scaling equations have been derived in Ref. [80], and are given by the following expressions

$$\frac{dj_x}{dl} = j_y j_z - \frac{1}{2} j_x (g_y + g_z) - \frac{1}{4} j_x (j_y^2 + j_z^2) + \frac{1}{2} j_x (g_x (g_y + g_z) - g_y g_z) + \mathcal{O}(\epsilon^4) \tag{105}$$

$$\frac{dg_x}{dl} = g_x(\epsilon - g_z - g_y) + g_x^2 (g_y + g_z) - \frac{1}{2} g_x (j_y^2 + j_z^2) + \mathcal{O}(\epsilon^4)\ . \tag{106}$$

These equations have a much richer structure than Eq. (97), and a number of new fixed points appear.

The purely bosonic case:

Let us first consider the simplest case of bosonic couplings only, when the renormalization group equations simplify to

$$\frac{dg_x}{dl} = g_x(\epsilon - g_z - g_y) + g_x^2 (g_y + g_z)\ . \tag{107}$$

This equation is rather surprising at a first sight. The second order term on the right indicates that dissipations acting in different directions *weaken* each-other. This can be understood as follows: Suppose that $g_x \ll g_z$ and $g_y = 0$. In this case, for $g_x = 0$ the spin would point upwards or downwards. Fluctuations of the field φ_x try to flip the impurity spin. However, the impurity spin also has a bosonic screening cloud since it is strongly coupled to the field φ_z. Therefore, to flip the spin, the field φ_x also has to flip this bosonic cloud, and as a result, the coupling g_x is suppressed.

This effect is the most striking in the case of Ohmic fields ($\epsilon = 0$), when strong

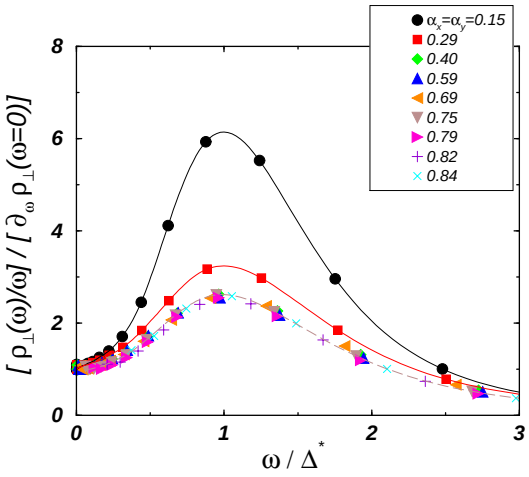

Figure 21: $\chi_\perp''(\omega,\alpha)/\omega$ as a function of ω/Δ^*. The dissipative couplings are $\alpha_x = \alpha_y = g_x/2 = g_y/2$, and Δ^* corresponds to the renormalized Weiss field, h_z. The spin rotates coherently around the z axis for any dissipation.

dissipation is typically suppressed and a flow to weak dissipation takes place. This is shown in Fig. 21, where the spectral function of an impurity spin in an anti-ferromagnet (ordered in the z-direction) is shown, as computed by the numerical renormalization group [72]. In this case the dissipative couplings appear in the x and y directions, while the Weiss field of the surrounding spins produces a local field in the z-direction, playing the role of tunneling. As shown in Fig. 21, the spectral function of spin fluctuations in the $x-y$ direction displays a beautiful coherence peak, even for extremely strong dissipations.

The situation is even more striking for $\epsilon \neq 0$. The RG flows are shown in Fig. 22. We find two non-trivial ($\sim \epsilon$) fixed points. One is the SU(2) symmetrical with $g_x = g_y = g_z = g$, while the other one has XY symmetry, $g_x = g_y \neq g_z = 0$. Both fixed points are unstable against spin anisotropy. This instability is due to the finite residual entropy associated with these fixed points: The system tries to get rid of this entropy by breaking the symmetry, and in fact, the only stable fixed point of the purely bosonic model seems to be an *infinite coupling Ising fixed point* of the form $g_x = g_y = 0 \neq g_z \to \infty$. Note that the flow to a strong Ising-type coupling is a consequence of the super-Ohmic heat bath ($\epsilon > 0$). For $\epsilon = 0$ this fixed point is replaced by a stable *line* of fixed points with Ising symmetry, g_z = finite and $g_x = g_y = 0$.

In a realistic case, a number of cross-overs may occur between SU(2)-type, XY

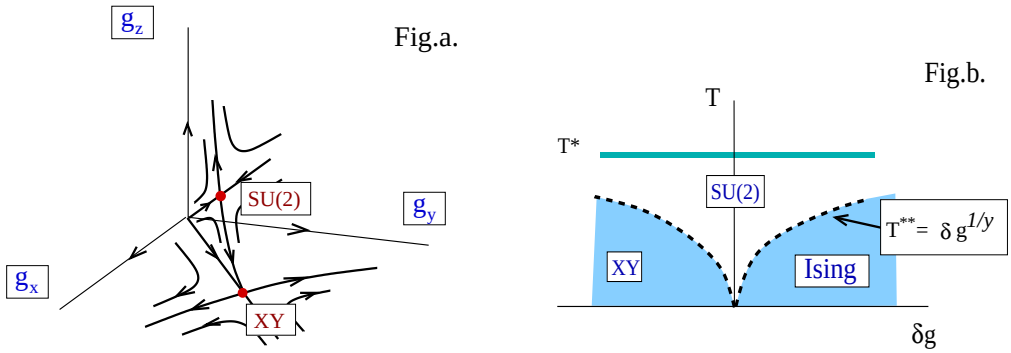

Figure 22: Fig. (a) Sketch of the renormalization flows in the purely bosonic model. We find one non-trivial SU(2)-invariant fixed point and three fixed points with XY symmetry. Both are unstable against breaking the SU(2) and XY symmetries, respectively. Fig. (b) Quantum phase transition in the purely bosonic model with XY symmetry as the anisotropy, $\delta g = g_z - g_\perp$ changes sign. The dashed lines indicate cross-over regions corresponding to T^{**}.

or Ising behaviors. In particular, for a system with XY-type symmetry, a quantum phase transition occurs between the XY-type and Ising fixed points as $\delta g \equiv g_z - g_x = g_z - g_y$ changes sign (see Fig 22). In this case, the quantum phase transition is controlled by the SU(2) type fixed point below an energy scale T^*. For small $g_\perp = g_x = g_y \approx g_z \equiv g$ one can determine T^* by integrating the scaling equations Eq. (107), and is approximately given by

$$T^* \sim \Lambda_0 \, g^{1/\epsilon} \, . \tag{108}$$

As $T \to 0$ another cross-over occurs at an energy scale

$$T^{**} \sim (\delta g)^{1/y_r} T^* \, ,$$

where $y_r = \epsilon/2 + \epsilon^2/2 + ...$ is the scaling dimension of spin-anisotropy at the SU(2) fixed point. Between T^* and T^{**} the SU(2)-invariant Bosonic model describes the behavior of the impurity, while below T^{**} the physical properties of the model are controlled by the Ising ($\delta g > 0$) or the XY-type ($\delta g < 0$) bosonic fixed points, respectively.

Although anisotropy is relevant at both $\mathcal{O}(\epsilon)$ fixed points above, in many cases the SU(2)-invariant or XY-type fixed points can be also of physical interest: In the case of high temperature superconductors, *e.g.*, spin-orbit interaction is weak and therefore the anisotropy is presumably weak. In this case the SU(2)-symmetrical fixed point

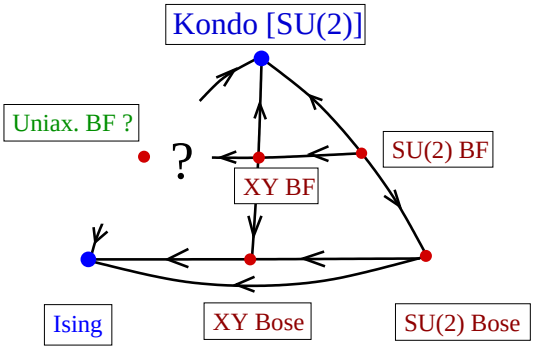

Figure 23: Summary of various fixed points and the possible flow.

may appropriately describe the physics over a wide energy range of interest. On the other hand, in most magnetic heavy Fermion compounds spin-spin interactions are generically anisotropic, and the physics is expected to be controlled by XY type or Ising fixed points.

The anisiotropic Bose-Fermi model

The analysis of the full scaling equations reveals an even richer structure, summarized in Fig. 23, and shows that the SU(2) symmetrical *critical point* is also *unstable*. Similar to the purely bosonic case, critical fixed points with XY and Ising symmetry appear, though the Ising fixed point is in this case out of the reach of our ϵ expansion.

Our previous analysis of the spin correlation functions carries over to this case. At the fixed points with XY symmetry we find, *e.g.* that only the exponents of the $T = 0$ temperature x and y correlation functions are determined by the Ward identity, while the z component of the spins decays with a non-universal exponent $\eta_z = 2\epsilon + 7\epsilon^2/4 + \ldots$.

3.3.3 Implications for the dynamical mean field theory of the locally quantum critical behavior

It has been shown in a beautiful series of neutron scattering measurements by Schröder *et al.* that the quantum critical behavior in $CeCu_{5-x}Au_x$ is entirely local within experimental accuracy [41]. This material shows a quantum phase transition from a non-magnetic heavy Fermi liquid state to a metallic antiferromagnetic state under Au doping. The Fermi liquid energy scale below which the Ce spins are screened appears to go to zero as one approaches the quantum critical point from the metallic side, indicating that at the quantum critical point (QCP) spins remain

asymptotically free at low temperature. At the quantum critical point the dynamical susceptibility is found to behave with a good accuracy as

$$\chi^{-1}(\omega, T, \mathbf{q}) \sim \text{cst.}(\chi^{-1}(\mathbf{q}) + (T - i\omega)^{\alpha}) \tag{109}$$

with an exponent $\alpha \approx 0.75$, where $\chi^{-1}(\mathbf{q})$ is an approximately frequency and temperature-independent function with minima at the ordering wave vectors. The quantum phase transition in $CeCu_{5-x}Au_x$ is clearly driven by the competition between Kondo screening and magnetic ordering.

Based on these observations, Si *et al.* proposed a self-consistent version of the Bose-Fermi Kondo model as a good candidate to describe the above quantum critical behavior within a dynamical mean field approach [77]. Our results have essential implications on this theory:
(a) Firstly, within the mean field theory, at the critical point, the correlations of the Bose field should decay with the same power law as the correlations of individual spins, since these two are basically identical. This immediately implies that the only possible non-trivial exponent is $\epsilon = 1$, leading to a logarithmic divergence of the local susceptibility

$$\chi_{\text{local}} = \int \frac{d^3\mathbf{q}}{(2\pi)^3}(\omega, T, \mathbf{q}) \sim \ln \frac{T^*}{T} \ , \tag{110}$$

Eqs. (110) and (109) are only compatible if magnetic fluctuations are strictly two-dimensional. This is indeed supported to some extent by the neutron scattering data, however, at low temperatures a cross-over to a trivial behavior would be expected based on this analysis, which has not been observed yet.
(b) Secondly, we find that for $\epsilon = 1$ the scaling dimension of the magnetic field at the critical point is 1/2. This implies an h^2/T scaling, which is clearly in contradiction with the experimental data, exhibiting h/T scaling. However, in the experiments one applies a *global* field, and we know cases where the the scaling dimension of the global field is different from that of the local field acting only on the impurity. It is therefore conceivable that the global field could give rise to a h/T scaling.
(c) Finally, but very importantly, Si and his coworkers assumed fully isotropic SU(2)-symmetrical couplings. However, magnetic interactions in $CeCu_{5-x}Au_x$ and most heavy fermion materials are strongly spin-anisotropic. As we have shown, anisotropy is relevant at the $SU(2)$-invariant Bose-Fermi Kondo fixed point, and therefore a theory with Ising symmetry must describe the quantum critical point. Luckily enough,

due to the Ward identity discussed, our most important results carry over to this case too in the easy axis direction, where our results imply a logarithmically divergent susceptibility again, $\chi'_{\mathrm{easy,local}}(\omega) \sim \ln(T^*/\omega)$, and a step-like singularity in its imaginary part, $\chi''_{\mathrm{easy,local}}(\omega) \sim \mathrm{sgn}(\omega)$. In the other directions, however, the local susceptibility should show a power law behavior, $\chi'_{\mathrm{not-easy,local}}(\omega) \sim \omega^{\alpha}$, $\chi''_{\mathrm{not-easy,local}}(\omega) \sim \omega^{\beta}$, and is likely to be dominated by analytic contributions with $\alpha = 0$ and $\beta = 1$. These predictions should be directly observable by polarized neutron scattering and NMR relaxation measurements.

4 Non-Fermi liquid models

In this Chapter, we shall study a few examples of non-Fermi liquid models. These models have rather unusual physical properties, and as their name indicates, they cannot be described in terms of Nozières' Fermi liquid theory [9]: The thermodynamic and transport properties of these models are singular at $T = 0$ temperature and electrons are not well-defined quasiparticles even at the Fermi energy. These singular properties are related to the generic *unstability* of non-Fermi liquid fixed points: all known non-Fermi liquid fixed models possess a fractional *residual entropy*, indicating the presence of some non-trivial decoupled degrees of freedom, and by a rule of thumb, all such non-zero entropy states are unstable. The low temperature behavior of these models can only be accessed by non-perturbative methods such as conformal field theory [83], numerical renormalization group [10, 29, 84], Bethe ansatz [25, 26, 85], bosonization [86, 87, 88], $1/f$ expansion [89, 90, 91], or slave particle methods [92].

Its has been believed for a long time that, due to their unstability, these exotic fixed points cannot be observed in nature [24]. However, in the early 80's a number of Uranium and Cerium alloys have been found that showed clear deviations from 'usual' heavy Fermi liquid behavior [34]. Even more interestingly, some of these materials enter a superconducting phase at low enough temperatures directly from an incoherent metal [34]. It has been proposed by Daniel Cox [30] that in these materials the interplay of local symmetry properties and strong spin-orbit interaction can generate a two-channel Kondo effect.

More recently, Dan Ralph and his co-workers also discovered a rather striking zero-bias anomaly in Cu point contacts, that showed universal V/T scaling of non-Fermi liquid character and apparently originated from some dynamical defects [33]. Ralph and his collaborators explained these anomalies in terms of non-commutative two level systems [32], discussed in Section 4.1.1. This interpretation is, however, still debated because of some difficulty with the original theoretical model proposed by Vladár and Zawadowski [124, 96]. Nevertheless, there is quite a few circumstantial evidence that most likely the original interpretation of Ralph *et al.* is correct, and these anomalies are indeed due to some so far 'unidentified dynamical impurities'.

4.1 The prototype of non-Fermi liquid models: the two-channel Kondo problem

To gain some insight into the generic structure of non-Fermi liquid systems, we shall study first the prototype of all non-Fermi liquid models, the multi-channel Kondo model [34]. In general, the f-channel Kondo model consists of a spin $S = 1/2$ magnetic impurity, that we couple to f independent and identical Fermion fields with the same exchange coupling j,

$$H = \sum_{\sigma=\pm} \sum_{a=1}^{f} \int \frac{dx}{2\pi}\, \psi^{\dagger}_{\sigma a}(x)\, i\partial_x \psi_{\sigma a}(x) + \frac{j}{2} \sum_{a=1}^{f} \sum_{\sigma,\sigma'} \vec{S}\, \psi^{\dagger}_{\sigma' a}(0) \vec{\sigma}_{\sigma\sigma'} \psi_{\sigma' a}(0)) \; . \qquad (111)$$

Here the left-moving fields $\psi_{\sigma a}(x)$ are defined in a similar way as in Section 2.2, and represent the radial part of the conduction electrons' wave function. It is crucial that all channels a couple with the *same* strength j to the spin in Eq. (111), otherwise the most strongly coupled channel screens the impurity spin and drives the system to a 'boring' Fermi liquid fixed point [34].

To motivate the study of this model we shall first discuss in Section 4.1.1 how the problem of a tunneling impurity in a metal maps onto the anisotropic two-channel Kondo model. To establish this mapping and to gain access to the non-Fermi liquid fixed point, we shall carry out a large f expansion for the two level system model [91]. Then in Section 4.1.2 we shall study the anisotropic Kondo problem by Abelian bosonization following the original work of Emery and Kivelson [86], and show how the full finite size spectrum and scattering properties of this model can be obtained through this method [88]. Finally, we shall shortly discuss the exact solution of the anisotropic two-channel Kondo problem in Section 4.1.3 [93].

4.1.1 Large f expansion for the two level system model

In Section 3.1 we constructed the minimum model to describe a tunneling system in a metal, Eq. (64). The Hamiltonian Eq. (64) already suggests that the physical properties of a tunneling system can be described by Eq. (111), although with anisotropic coupling constants: the orbital spin $\vec{\tau}$ in Eq. (64) plays the role of the impurity spin $\vec{S}$ in Eq. (111), while the angular momentum labels of the electrons (s and p) replace the electron spin in Eq. (111). The electron spin in the tunneling system problem, on the other hand, is a *conserved quantum number* and plays the

role of the channel index a with $f = 2$.

In Section 3.1 we neglected the assisted tunneling term v_x by saying that it is typically much smaller than the coupling v_z that leads to dissipation. However, as noticed by Kondo [94], the coupling v_x generates *logarithmic corrections*. A detailed renormalization group analysis by Zawadowski and Vladár revealed that v_x is indeed relevant, and generates a Kondo effect [32]. The perturbative treatment of Vladár and Zawadowski also showed that two of the angular momentum channels dominate the scattering processes at low temperature, and coupling between these two channels and the orbital degrees of freedom of the tunneling impurity leads to an *orbital Kondo effect*.

Unfortunately, the perturbative renormalization group analysis of Vladár and Zawadowski broke down at the orbital Kondo energy, T_K, and did not allow for the analysis of the low-energy fixed point of the renormalization group. Therefore Vladár and Zawadowski did not know if other angular momentum channels are important below the Kondo temperature, and originally they believed that the low temperature fixed point is a Fermi liquid [32]. In this problem, however, the *spin* of the conduction electron plays a crucial role. As noticed first probably by Nozières and Blandin [24], the presence of the additional channel index destabilizes the infinite coupling Fermi liquid fixed point, and leads to singular behavior at low temperatures.

In the present Subsection we shall show how one can access this non-Fermi liquid fixed point by replacing the spin by a flavor index in the two level system problem, $\sigma = \pm \rightarrow \sigma = 1, \ldots, f$, and performing an expansion in $1/f$ [91]. The basic idea of this approach is very similar to that of the ϵ expansion: for large values of f a non-trivial fixed point appears in the weak coupling regime [90]. Therefore, all contributions to the β function can be organized according to powers of $1/f$, and a systematic expansion can be performed to compute critical exponents and determine the fixed point structure. This analysis will show that the conjecture of Vladár and Zawadowski is indeed correct, and at the only stable fixed point two conduction electron channels dominate the physics. Moreover, we shall be able to determine the relevant and leading irrelevant operators and their dimensions at the non-Fermi liquid fixed point systematically. These operators are responsible for the singularities of various physical quantities at the non-Fermi liquid fixed point and determine the cross-over scales to other simple Fermi liquid fixed points.

To start our analysis, we generalize the simple interaction Hamiltonian Eq. (64)

to the case of any number of angular momentum channels and for non-symmetrical tunneling centers as [32]

$$H^{\rm int} = \sum_{\sigma=1}^{f} \sum_{\mu,\mu'=s,p,...} \sum_{i=x,y,z} \tau_i \; v^i_{\mu,\mu'} \psi^\dagger_{\mu\sigma} \psi_{\mu'\sigma} \tag{112}$$

where now $\psi^\dagger_{\mu\sigma} = \int d\epsilon \; a^\dagger_{\mu\sigma}(\epsilon)$ creates a local fermion state with angular momentum μ. The operator $a^\dagger_{\mu\sigma}(\epsilon)$ in the expression of $\psi^\dagger_{\mu\sigma}$ creates a conduction electron with angular momentum μ and energy ϵ around the impurity and is normalized to satisfy the anticommutation relation $\{a_{\mu\sigma}(\epsilon), a^\dagger_{\mu\sigma}(\epsilon')\} = \delta_{\mu\mu'} \; \delta_{\sigma\sigma'} \; \delta(\epsilon - \epsilon')$. The couplings $v^i_{\mu,\mu'} \to \underline{v}^i$ are now infinite-dimensional matrices, but in general only their first few columns/rows are non-negligible, because conduction electrons with large angular momenta couple only very weakly to the impurity. We also included another coupling $\underline{v}^y$ in Eq. (112). While $\underline{v}^y$ can be chosen to be zero initially, it is generated under the renormalization group transformation.

To simplify our analysis, we rewrite Eq. (62) as

$$H^{\rm TLS} = -\frac{1}{2} \sum_i \Delta^i \; \tau_i \; , \tag{113}$$

where $\Delta^x = \Delta_0$ denotes the tunneling amplitude, and $\Delta^z = \varepsilon$ is the asymmetry of the tunneling system.

The next to leading logarithmic order scaling equations for this model have been derived by Vladár and Zawadowski (for $f = 2$), and read

$$\frac{d\underline{v}^i}{dl} = -2i\varepsilon^{ijk} \underline{v}^j \underline{v}^k - 2 \; f \; [\underline{v}^i {\rm Tr}(\underline{v}^j \underline{v}^j) - \underline{v}^j {\rm Tr}(\underline{v}^j \underline{v}^i)] \; , \tag{114}$$

$$\frac{d\,\Delta^i}{dl} = -2 \; f \; [\Delta^i {\rm Tr}(\underline{v}^j \underline{v}^j) - \Delta^j {\rm Tr}(\underline{v}^i \underline{v}^j)] \; , \tag{115}$$

where we used Einstein's convention, and ${\rm Tr}\{\ldots\}$ indicates a trace over all angular momentum indices μ. The derivation of these equations follows similar lines as the one outlined for the Kondo problem in Chapter 2, the only complication being that now we have infinitely many couplings. The scaling variable l above is defined as $l = \ln D_0/D$, with D and D_0 the high energy cut-off and its initial value.

Let us first ignore Eq. (115) that describes the renormalization of the tunneling rate. To have some feeling about the solution of these equations, it is instructive to

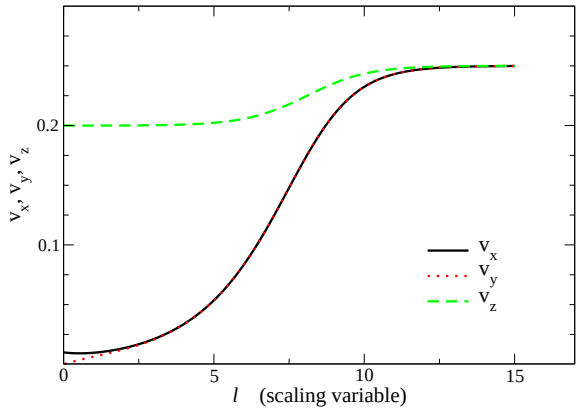

Figure 24: Scaling of the three couplings v_x, v_y, and v_z.

study the case where we keep only s-wave scattering and p-wave scattering in the p_z-channel (with the tunneling system moving along the z-direction). In this case the Hamiltonian simplifies to Eq. (64), and the matrices $\underline{v}^i$ are simply proportional to Pauli matrices, $\underline{v}^z = v_z \cdot \sigma^x$, $\underline{v}^x = v^x \cdot \sigma^z$, and $\underline{v}^y = v_y \cdot (-\sigma^y)$. Then the scaling equations simplify to those of the anisotropic Kondo problem [95],

$$\frac{dv_x}{dl} = 4v_y v_z - 4f\ v_x(v_y^2 + v_z^2)\ , \tag{116}$$

$$\frac{dv_y}{dl} = 4v_z v_x - 4f\ v_y(v_x^2 + v_z^2)\ , \tag{117}$$

$$\frac{dv_x}{dl} = 4v_x v_y - 4f\ v_z(v_y^2 + v_x^2)\ . \tag{118}$$

The solution of these equations is shown in Fig. 24. In the very initial stage of the scaling v_y is generated, and the two couplings v_x and v_y soon become equal, $v_x \approx v_y \ll v_z$. In the next stage the two couplings $v_x \approx v_y$ gradually approach v_z, and all three couplings become of the order of unity at the Kondo temperature, T_K. This Kondo scale is usually called orbital Kondo temperature to emphasize that it is generated by purely orbital fluctuations. In the vicinity of the Kondo temperature all three couplings are approximately equal, implying that the system acquires an SU(2) symmetry in orbital space.

The solutions of the more complicated Eq. (114) behave quite similarly: the second order terms in Eq. (114) tend to increase the couplings and thus generate a Kondo effect. The third order terms, on the other hand, tend to decrease the couplings $\underline{v}^i$. As we shall discuss later, while Eq. (114) admits an infinite number of

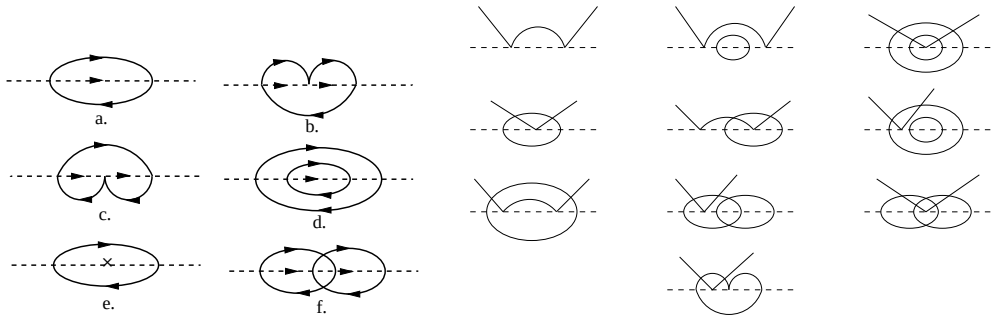

Figure 25: Pseudofermion self-energy corrections (left) and vertex corrections (right) up to the order $\sim 1/f^2$. Dashed and the continuous lines denote pseudofermion (spin) and conduction electron propagators, respectively. The cross indicates the contribution of the counterterm, which must be calculated up to the order $\sim 1/f$. For the sake of simplicity only vertex diagrams without counterterm correction are shown, and vertex diagrams that can be generated by reversing the pseudofermion and the electron lines have been also omitted.

non-trivial (finite coupling) fixed points, only the one discussed before turns out to dominate the physics at low temperatures. All non-trivial fixed points of Eq. (114) are of order $\underline{v}^i \sim 1/f$, *i.e.*, for large values of f they remain in the reach of perturbation theory. This simple observation makes it possible to carry out a systematic $1/f$ expansion [90, 91], and in fact, Eqs. (114) generate just the leading terms in such an expansion. We have to mention that while a strong coupling analysis reveals that for $f \geq 2$ the fixed point coupling is indeed finite, for $f = 1$ the presence of a finite coupling fixed point is just an artifact of the perturbative scaling approach, and in reality, the strong coupling fixed point is at infinitely large couplings.

To compute the next terms in a $1/f$ expansion we can make use of the fact that $\underline{v}^i \sim 1/f$, and accordingly, we can organize all diagrams by simply counting powers of $1/f$. In Fig. 25 we show all those self-energy and vertex diagrams that contribute in order $\sim 1/f^2$. Note that each fermion loop results in a factor $\sim f$, which partially compensates the $1/f$ factors coming from the vertices $\underline{v}^i$. There are two subtleties in these calculations: (a) Some of the diagrams shown have a leading $\sim \ln^2(D/\omega)$ behavior. For these diagrams one must determine the *subleading* contribution $\sim \ln(D/\omega)$ as well, because these subleading logarithmic contributions renormalize the vertex function. (b) Some of the diagrams contain spurious divergences. To this order, these divergences originate essentially from the first self-energy diagram, which renormalizes the pseudofermion's chemical potential. In order to get rid of these divergences one has to apply a *counterterm procedure*, which amounts in expanding

around the physical (renormalized) chemical potential of the pseudofermions.

Without going too much into details, let us just give here the expressions of the pseudofermion Green's function and the vertex function obtained this way:

$$\begin{aligned}
\mathcal{G}^{-1} &= \omega\Big\{1+(1-\ln 2)fO^{jj}+\ln\Big(\frac{D}{-\omega}\Big)\Big[fO^{jj}+12f\beta \\
&- (5-3\ln 2)f^2O^{jj}O^{kk}-(4\ln 2-6)f^2O^{jk}O^{kj}\Big]+\ldots\Big\}\,, \qquad (119)\\
\Gamma^i &= \underline{v}^i-\ln 2\, f(2O^{ij}\underline{v}^j-O^{jj}\underline{v}^i) \\
&- \ln\Big(\frac{D}{-\omega}\Big)\Big\{2i\epsilon^{ijk}\underline{v}^j\underline{v}^k-f(2O^{ij}\underline{v}^j-O^{jj}\underline{v}^i) \\
&- 4(2-\ln 2)fi\epsilon^{jkl}O^{ij}\underline{v}^k\underline{v}^l+2\ln 2\, fi\epsilon^{ijk}O^{ll}\underline{v}^j\underline{v}^k+(2+5\ln 2)f^2O^{jj}O^{kk}\underline{v}^i \\
&- (8+12\ln 2)f^2O^{kk}O^{ij}\underline{v}^j+(8+12\ln 2)f^2O^{ij}O^{jk}\underline{v}^k \\
&- (2+4\ln 2)f^2O^{jk}O^{kj}\underline{v}^i\Big\}+\ldots\,, \qquad (120)
\end{aligned}$$

where $O^{ij}=\mathrm{Tr}(\underline{v}^i\underline{v}^j)$, $\beta=-i\,\mathrm{Tr}(\underline{v}^x\underline{v}^y\underline{v}^z-\underline{v}^z\underline{v}^y\underline{v}^x)$ and a summation must be carried out over all repeated indices. The energy scale ω is measured from the (renormalized) chemical potential of the pseudofermions, and in the vertex function we have set the electrons' energy to the Fermi surface. Plugging these two expressions in the multiplicative renormalization group equations (Eqs. (14) and (15) of Section 2.1.2), we can determine the pseudofermion Z-factor and obtain the following scaling equations:

$$\begin{aligned}
\frac{d\underline{v}^i}{dl} &= 2i\epsilon^{ijk}\underline{v}^j\underline{v}^k+2f(O^{jj}\underline{v}^i-O^{ij}\underline{v}^j)-8(1-\ln 2)fi\epsilon^{jkl}O^{ij}\underline{v}^k\underline{v}^l \\
&+ 16\ln 2\, f\beta\underline{v}^i+8f^2O^{ij}O^{jk}\underline{v}^k-8f^2O^{kk}O^{ij}\underline{v}^j\,, \qquad (121)
\end{aligned}$$

It is possible to classify *all* fixed points of Eq. (121) and show that at all non-trivial fixed points the couplings are essentially just spin operators [91], $\underline{v}^i = cst\ S_e^i$, where the matrices S_e^i realize $2S_e+1$-dimensional spin representations, now acting in the angular momentum indices, $[S_e^i,S_e^j]=i\epsilon_{ijk}S_e^k$. One can also show, however, that fixed points with $S_e>1/2$ are unstable and the only stable fixed point corresponds to an $S_e=1/2$ representation, *i.e.*, to the selection of *only two orbital labels* [91]. The couplings at the stable non-Fermi liquid fixed point are thus essentially proportional

	$f > 2$	$f = 2$
$\chi^{\Delta}_{\rm imp}(\Delta, T = 0)$	$\sim \left(\frac{\Delta}{T_K}\right)^{2/f\ -1}$	$\sim \ln\left(\Delta/T_K\right)$
$\chi^{\Delta}_{\rm imp}(\Delta = 0, T)$	$\sim \left(\frac{T}{T_K}\right)^{(2-f)/(f+2)}$	$\sim \ln\left(T/T_K\right)$
$c_{\rm imp}/T$	$\sim \left(\frac{T}{T_K}\right)^{(2-f)/(f+2)}$	$\sim \ln\left(T/T_K\right)$
$\Delta R_{\rm imp}$	$\sim \left(\frac{T}{T_K}\right)^{2/(2+f)}$	$\sim \left(\frac{T}{T_K}\right)^{1/2}$

Table 1: Low temperature behavior of the impurity 'orbital susceptibility' $\chi^{\Delta}_{\rm imp} = \partial^2 F_{\rm imp}/\partial\Delta^2$, specific heat $c_{\rm imp}$ and resistivity $R_{\rm imp}$ of a two level system. All energy scales and crossover scales are assumed to be smaller than the Kondo energy T_K.

to Pauli matrices,

$$\underline{v}^i_{\rm fp} = \frac{1}{2f}\left(1 - 2\ln 2/f\right)\begin{pmatrix} \underline{\sigma}^i & 0 \\ 0 & 0 \end{pmatrix} \tag{122}$$

One can linearize Eq. (121) and the scaling equations for Δ^i to study the operator content of this fixed point [91]. We shall not bore the reader with the details of the rather straightforward but lengthy diagonalization of the corresponding infinite dimensional matrix equations. In the end of these calculations one finds that the leading irrelevant operator is simply $\sim \sum_{i,\sigma}\sum_{\mu\mu'} \tau_i\ \psi^\dagger_{\mu\sigma}\sigma^i_{\mu\mu'}\psi_{\mu'\sigma}$ and has scaling dimension

$$y = -\frac{2}{f} + \frac{4}{f^2} + \dots\ , \tag{123}$$

while the dimensionless fields $\tilde{\Delta}^i \equiv \Delta^i/D$ have scaling dimension $1 + y$. Eq. (123) gives in fact the first two terms in the expansion of the exact exponent $y = -2/(2+f)$, determined through conformal field theory [27]. Note that the physical case, $f = 2$, is marginal in the sense that the expansion in $1/f$ is strictly speaking convergent only for $f > 2$. However, the properties of the fixed point happen to be similar in the whole regime $f \geq 2$, and therefore the $1/f$ expansion gives useful information on the two-channel case $f = 2$ as well. Once the scaling dimension y at hand, we can determine the scaling properties of the impurity susceptibility, specific heat, and conductance as well by expanding the free energy. The results are summarized in Table 1.

To close this subsection, let us shortly discuss the effect of Δ^i. For the sake of simplicity, let us assume that the tunneling system is symmetrical, $\varepsilon = \Delta^z = 0$, and only the tunneling amplitude $\Delta_0 = \Delta^x$ must be considered. As we have seen,

the perturbation Δ_0 is relevant at the two-channel Kondo fixed point and has a scaling dimension $1 + y = 1/2$. Correspondingly, even if it is small, it will generate a cross-over at a temperature

$$T^* \sim \frac{\Delta_0^2(T_K)}{T_K} ,$$

where $\Delta_0^2(T_K)$ denotes the renormalized tunneling rate at temperatures T_K. This scale can be computed, *e.g.*, by solving the perturbative renormalization group equations for $D > T_K$. Below the scale T^* the tunneling dominates the physics and the tunneling system freezes into its 'symmetrical' state. For $T < T^*$ quantum fluctuations of the tunneling center are suppressed, it acts merely as a potential scatterer, and a Fermi liquid state develops. Accordingly, the interesting non-Fermi liquid behavior can be only observed in the temperature range $T^* < T < T_K$. In their original calculation, Vladár and Zawadowski assumed that the high energy cut-off D_0 is of the order of the Fermi energy [32], and showed that with this assumption one can find typically an extended non-Fermi liquid regime for fast and symmetrical tunneling systems. However, it has been pointed out recently by Aleiner *et al.* that the assumptions of Vladár and Zawadowski were incorrect, and D_0 is rather in the range of the Debye temperature, ω_D [124]: The physical reason for this is that tunneling processes take place at a time scale $\sim 1/\omega_D$. Therefore, electronic excitations with energy $\epsilon > \omega_D$ follow the tunneling particle adiabatically, and only electrons in a narrow band $\epsilon < \omega_D$ contribute to logarithmic singularities and thus the Kondo effect. As a consequence, D_0 must be replaced by ω_D, and in the weak coupling regime T^* is always larger than the Kondo temperature T_K, *i.e.*, no non-Fermi liquid regime can be observed. Fortunately, the arguments of Aleiner *et al.* stand only in the weak coupling regime [96]. It turns out that for tunneling centers with *resonant scattering* the coupling v^z can easily become sufficiently strong so that these tunneling centers are deep in the non-perturbative regime, where $T^* \ll T_K$, with T_K in the few Kelvin range [96]. Tunneling centers with resonant scattering may thus provide indeed a physical realization for the two-channel Kondo model, as originally proposed by Vladár and Zawadowski, though not in the weak coupling regime.

4.1.2 Abelian bosonization of the two-channel Kondo problem

In the present subsection we shall study the anisotropic two-channel Kondo problem through Abelian bosonization, by generalizing the work of Emery and Kivelson to finite system sizes [86, 88]. Emery and Kivelson studied the spin-anisotropic version of Eq. (111),

$$H = \sum_{\sigma=\pm} \sum_{a=1,2} \int \frac{dx}{2\pi}\, \psi^\dagger_{\sigma a}(x)\, i\partial_x \psi_{\sigma a}(x) + \sum_i \frac{j_i}{2} \sum_{a,\sigma\sigma'} S^i\, \psi^\dagger_{\sigma a}(0) \sigma^i_{\sigma\sigma'} \psi_{\sigma' a}(0)\ , \qquad (124)$$

where $i = x, y, z$ labels the three components of the spin, and for the sake of simplicity $j_x = j_y = j_\perp$. We can simplify this Hamiltonian somewhat if we bosonize Eq. (124) using the identities Eqs. (252) and (254) of Appendix A. After this transformation the Hamiltonian reads

$$\begin{aligned} H = & \sum_{\sigma,a} \frac{2\pi}{L} \frac{1}{2} \hat{N}^2_{\sigma,a} + \sum_{\sigma,a} \int_{-L/2}^{L/2} \frac{dx}{4\pi} : \left(\frac{\partial \phi_{\sigma a}}{\partial x} \right)^2 : , \qquad (125) \\ + & \sum_{\sigma,a} \frac{j_z}{2}\, S^z\, \sigma \left(\partial_x \phi_{\sigma a}(x) + \hat{N}_{\sigma a} \frac{2\pi}{L} \right) + \frac{j_\perp}{2} \sum_a \Big(S^+\, F^\dagger_{\downarrow a} F_{\uparrow a} e^{-i(\phi_{\uparrow a} - \phi_{\downarrow a})} + \text{h.c.} \Big)\ , \end{aligned}$$

where we assumed a finite system size L and assumed antiperiodic boundary conditions for the sake of simplicity. In the above equations $\hat{N}_{\sigma a}$ denote the total number of electrons with spin σ in channel a and the field $\partial_x \phi_{\sigma a}$ can be thought of as representing density fluctuations of the fermions $\psi_{\sigma a}(x)$. The Klein factors $F^\dagger_{\sigma a}$ keep track of changes in the total Fermion number and also assure that fields with different quantum numbers (σ, a) anticommute [97].

Motivated by the observation that j_z only couples to the spin density of the fermions, Emery and Kivelson made a unitary transformation by introducing charge, spin, flavor and spin-flavor quantum numbers,

$$\begin{pmatrix} \hat{\mathcal{N}}_c \\ \hat{\mathcal{N}}_s \\ \hat{\mathcal{N}}_f \\ \hat{\mathcal{N}}_x \end{pmatrix} = \frac{1}{2} \begin{pmatrix} 1 & 1 & 1 & 1 \\ 1 & -1 & 1 & -1 \\ 1 & 1 & -1 & -1 \\ 1 & -1 & -1 & 1 \end{pmatrix} \begin{pmatrix} \hat{N}_{\uparrow 1} \\ \hat{N}_{\downarrow 1} \\ \hat{N}_{\uparrow 2} \\ \hat{N}_{\downarrow 2} \end{pmatrix}\ , \qquad (126)$$

and introduced new fields φ_c, φ_s, φ_f, and φ_x in a similar way. With this notation, the charge and flavor fields φ_c and φ_f completely decouple from the impurity spin,

and the spin-dependent part of the Hamiltonian simplifies to

$$\begin{aligned} H \to H &= \sum_{y=s,x} \Big[\frac{2\pi}{L} \frac{1}{2} \hat{\mathcal{N}}_y^2 + \int_{-L/2}^{L/2} \frac{dx}{4\pi} : \left(\frac{\partial \varphi_y}{\partial x} \right)^2 : \Big] \\ &+ j_z \, S^z \left(\partial_x \varphi_s(x) + \hat{\mathcal{N}}_s \frac{2\pi}{L} \right) \\ &+ \frac{j_\perp}{2a} \left[S^- \, e^{i\varphi_s(0)} \left(F_{\uparrow 1}^\dagger F_{\downarrow 1} e^{i\varphi_x(0)} + F_{\uparrow 2}^\dagger F_{\downarrow 2} e^{-i\varphi_x(0)} \right) + \text{h.c.} \right] , \end{aligned} \tag{127}$$

To complete the transformation, we want to introduce Klein factors that correspond to the new fields, φ_y. This is, however, far from being trivial [88]. On one hand, we can convince ourself very easily that all bilinear combinations $F_{\sigma j}^\dagger F_{\sigma' j'}$ change every quantum number $\mathcal{N}_y$ by an integer. To give an example, the product $F_{\uparrow 2}^\dagger F_{\downarrow 2}$ changes the new quantum numbers as $\{\mathcal{N}_c, \mathcal{N}_s, \mathcal{N}_f, \mathcal{N}_x\} \to \{\mathcal{N}_c, \mathcal{N}_s + 1, \mathcal{N}_f, \mathcal{N}_x - 1\}$. Therefore one is tempted to replace these operators by

$$\mathcal{F}_s^\dagger \mathcal{F}_x \equiv F_{\uparrow 2}^\dagger F_{\downarrow 2} \, , \tag{128}$$

where the operators $\mathcal{F}_y$ are new Klein factors and satisfy similar commutation relations as the original Klein factors. One can also show that any bilinear combination of the original Klein factors can be expressed in terms of two new Klein factors. However, the $\mathcal{N}_y$'s are not just independent integers as the original $N_{\sigma j}$'s: Either all $\mathcal{N}_y$'s are half-integers, or all of them are integers, and moreover, they are related to each other by the following *gluing conditions*:

$$\mathcal{N}_c \pm \mathcal{N}_f = (\mathcal{N}_s \pm \mathcal{N}_x) \bmod 2 \, . \tag{129}$$

While these gluing conditions do not play an important role in the $L \to \infty$ limit, they are crucial to obtain the correct finite size spectrum. The reason is simply that the global excitations accounted for by the $\sim N_{\sigma j}^2$ terms represent only a negligible fraction of all possible bosonic excitations, and can be neglected for $L \to \infty$, but they do give a correction $\sim 1/L$ to the finite size spectrum.

The thermodynamic limit

Let us first consider the thermodynamic limit, $L \to \infty$, and rewrite the spin-

dependent part of the Hamiltonian with the above definitions as

$$\begin{aligned} H &= \int \frac{dx}{4\pi} : (\partial_x \varphi_s)^2 + (\partial_x \varphi_x)^2 : + j_z \; S^z \; \partial_x \varphi_s(x) \\ &+ \frac{j_\perp}{2a} \Big(\mathcal{F}_x e^{-i\varphi_x(0)} + \text{h.c.} \Big) \Big(S^- \mathcal{F}_s^\dagger \; e^{i\varphi_s(0)} - \text{h.c.} \Big) \; . \end{aligned} \tag{130}$$

Now the key observation of Emery and Kivelson was that one can completely eliminate the term $\sim S^z \partial_x \varphi_s(0)$ by making a unitary transformation with the operator $U \equiv e^{i \, j_z S_z \varphi_s(0)}$, which transforms $\partial_x \varphi_s(x)$ and $S^\pm$ as

$$\partial_x \varphi_s(x) \to \partial_x \varphi_s(x) - 2\pi j_z S_z \delta(x) \; , \qquad S^\pm \to S^\pm e^{\pm i \, j_z \varphi_s(0)} \; . \tag{131}$$

Moreover, the field φ_s is completely eliminated by this transformation, if $j_z = 1$. The condition $j_z \equiv 1$ defines the so-called Emery-Kivelson line [86]. At this line the transformed Hamiltonian H' reads:

$$H' = \int \frac{dx}{4\pi} : (\partial_x \varphi_x)^2 : + \frac{j_\perp}{2a} \Big(\mathcal{F}_x e^{-i\varphi_x(0)} + \text{h.c.} \Big) \Big(S^- \mathcal{F}_s^\dagger - \text{h.c.} \Big) \; , \tag{132}$$

where we dropped the decoupled parts that describe the energy of charge, flavor, and spin-wave excitations. Introducing the Fermion fields

$$c_d \equiv F_s^\dagger S^- \; , \qquad \psi_x(x) \equiv F_x \frac{1}{\sqrt{a}} e^{-i\varphi_x(x)} \; , \tag{133}$$

the above Hamiltonian becomes quadratic

$$H' = \int dx \, i \psi_x^\dagger \partial_x \psi_x + \frac{j_\perp}{2\sqrt{a}} (\psi_x^\dagger(0) + \psi_x(0))(c_d^\dagger - c_d) \; . \tag{134}$$

This Hamiltonian is almost that of a resonant level, with the important difference that the hybridization $\sim j_\perp$ only couples *half* of the field ψ_x to half of the fermion c_d. In mathematical terms, both complex fields ψ_x and c_d can be written as a sum of two real Majorana fermions, $\psi_x = (\psi_1 + i\psi_2)/\sqrt{2}$, $c_d \equiv (d_1 + i d_2)/\sqrt{2}$, and $j_\perp$ only couples one of these fields to each-other:

$$H' = \int dx \, i \, (\psi_1(x) \partial_x \psi_1(x) \; + \; \psi_2(x) \partial_x \psi_2(x)) + (-i) \frac{2 j_\perp}{\sqrt{a}} \psi_1(0) \, d_2 \; . \tag{135}$$

The structure of this coupling has a major consequence: Half of the local fermion

c_d will form a *resonance* with the conduction electrons. However, the other half of it, $d_1 \sim c_d^\dagger + c_d$, remains completely decoupled, resulting in a residual entropy [25, 27, 86],

$$S_{\rm res} = \frac{1}{2}\ln(2) \ . \tag{136}$$

It is worth mentioning, that a special line similar to the Emery-Kivelson line also exists for the single channel Kondo problem [98]: at this so-called Toulouse line the anisotropic Kondo problem can be bosonized and refermionized in a way very similar to the above procedure, and the final Hamiltonian is just a usual resonant level Hamiltonian very similar to Eq. (135), with the sole exception that there the hybridization couples *both* components of c_d to the fermion field. As a consequence, in the single channel Kondo problem both d_1 and d_2 participate in the formation of the resonance and the entropy associate with the impurity spin completely disappears.

It is instructive to see what happens if we apply a local magnetic field h on the impurity spin along the z-direction. The z-component of the spin can be easily fermionized as

$$S_z = c_d^\dagger c_d - 1/2 = i d_2 d_1 \ ,$$

and thus h results in a coupling to the other half of the local fermion, $H' \to H' - ih\ d_1 d_2$. As a consequence, in a magnetic field the other half of the fermion becomes also part of the resonance and the system is driven to a Fermi liquid state without residual entropy.

The Hamiltonian (135) is quadratic, and can be trivially solved using standard Green's function methods [86]. It is rather straightforward to compute the imaginary time correlation function of S_z

$$\langle T_\tau\, S_z(\tau) S_z(0)\rangle \begin{cases} \approx 1/4 & \text{for } \tau < 1/\Gamma \ , \\ \sim 1/\Gamma\tau & \text{for } \tau > 1/\Gamma \ , \end{cases} \tag{137}$$

where $\Gamma = j_\perp^2/4a$ denotes the width of the resonance that can be identified as the Kondo scale T_K. As a consequence, the spin susceptibility (given by the Fourier transform of Eq. (137)) diverges logarithmically at the two-channel Kondo fixed point [86],

$$\chi_{\rm spin}^{\rm imp} = \frac{1}{\pi\Gamma}\ln\frac{\Gamma}{T} \ . \tag{138}$$

There is many more information that can be extracted from this resonant level

Hamiltonian. One can, *e.g.*, determine the scaling dimensions of the magnetic field and $j_\perp$ at the Emery-Kivelson line. Requiring the invariance of the Kondo temperature implies [88],

$$\frac{dj_\perp}{dl} = \frac{1}{2} j_\perp \qquad (j_z = 1)$$

for small values of $j_\perp$, where $l = \ln a$ denotes the scaling variable. The scaling equation of the dimensionless magnetic field, $\tilde{h} \equiv a\ h$ can be determined from the scaling properties Eq. (137): As we already explained in Sec. 3.3, the standard theory of critical phenomena tells us that the scaling dimension of $\tilde{h}$ and the decay of the corresponding correlation function are related [81]. This relation implies that

$$\frac{d\tilde{h}}{dl} = \begin{cases} 1 & \text{for } a \ll 1/\Gamma\ , \\ 1/2 & \text{for } a \gg 1/\Gamma\ . \end{cases} \tag{139}$$

The latter equation also implies that a small magnetic field is a relevant perturbation at the two-channel Kondo fixed point and induces a cross-over to a Fermi liquid fixed point at an energy scale

$$T_h \sim h^2/\Gamma\ ,$$

as one can also verify it by a direct diagonalization of the Hamiltonian H' in the presence of a magnetic field h [86].

Before we proceed with the calculation of the finite size spectrum, let us discuss the scattering properties of the electrons. Constructing the scattering matrix is a rather non-trivial task, because the original fermion fields $\psi_{\sigma j}$ are related to the field ψ_x by a very complicated transformation. Nevertheless, we can determine the *asymptotic* scattering properties of the conduction electrons in the following way. We can solve analytically the Lippmann-Schwinger equation for the filed ψ_x using the quadratic Hamiltonian, Eq. (135) to determine the scattering field $\tilde{\psi}_x(x)$ [88]. The resulting formula is rather complicated, but it simplifies in the limit $|x| \to \infty$ to

$$\tilde{\psi}^\dagger_x(x) \sim \sqrt{\frac{L}{2\pi}} \int dk' e^{ik'x} [c^\dagger_{k'x}\theta(x) - c_{-k'x}\theta(-x)]\ . \tag{140}$$

where c_k is the Fourier transform of the original field $\psi_x(x)$. Clearly, since the $x > 0$ and $x < 0$ parts represent incoming and outgoing waves, respectively, this expression implies that the field ψ_x scatters as $\psi_x \to -\psi^\dagger_x$. This simple relation means that the Majorana field ψ_1 picks up a sign while the decoupled field ψ_2 remains unaffected.

In terms of Eq. (133) this also implies that the field φ_x *changes sign* in course of a scattering, while all other bosonic fields $\varphi_{c,s,f}$ remain unaffected. In the language of the original fermion fields this means that all incoming fermions $\psi_{\sigma j}$ scatter into a state which is completely orthogonal to the incoming state,

$$\langle \tilde{\psi}_{\sigma j}(x)\, \tilde{\psi}^{\dagger}_{\sigma' j'}(x')\rangle \to 0\ , \qquad (x<0<x')\ , \tag{141}$$

establishing the so-called unitarity paradox [28] Note that this formula implies that the scattering matrix identically vanishes, and an incoming electron 'evaporates' into an infinite number of electron-hole excitations during the scattering. The vanishing of the scattering matrix between single particle states implies that half of the scattering processes at the Fermi energy remain inelastic even at $T = 0$ temperature, and generate dephasing for the conduction electrons [99, 100].

Finite size spectrum

Almost all the above procedure can be generalized to the case of finite system sizes, however, special care must be exercised with the Klein factors when computing the finite size spectrum. This is because the Klein factors do not commute with the terms $\sim 2\pi\mathcal{N}_y^2/L$, and therefore affect the precise values of the energy by amounts $\sim 1/L$. It is essential to keep track of these small changes to determine the correct finite size spectrum. Furthermore, we have to keep track of the gluing conditions, Eq. (129). Our strategy to do that will be to first diagonalize the Hamiltonian for all possible states (integer and half-integer $\{\mathcal{N}_y\}$'s) and then in the end project out those states which satisfy all gluing conditions.

As a first step, we just make the Emery-Kivelson transformation again to arrive at the following Hamiltonian:

$$\begin{aligned} H' &= \frac{2\pi}{L}\sum_y \frac{\hat{\mathcal{N}}_y^2}{2} + \sum_y \int \frac{dx}{4\pi}(\partial_x\varphi_y)^2 + j_z\frac{2\pi}{L}\hat{\mathcal{N}}_s S_z \\ &+ \frac{j_\perp}{2a}\Big(\mathcal{F}_x e^{-i\varphi_x(0)} + \text{h.c.}\Big)\Big(S^-\mathcal{F}_s^\dagger - \text{h.c.}\Big)\ . \end{aligned} \tag{142}$$

This Hamiltonian can be diagonalized by introducing the fields ψ_x and c_d, however,

the definition of ψ_x must be changed as

$$\psi_x(x) \equiv F_x a^{-1/2} e^{-i(\hat{\mathcal{N}}_x - 1/2)2\pi x/L}\, e^{-i\varphi_x(x)} \equiv \sqrt{\frac{2\pi}{L}} \sum_{\bar{k}} e^{-i\bar{k}x} c_{\bar{k}x} \;, \tag{143}$$

where the last term defines the Fourier components of ψ_x. Note that for $\mathcal{N}_x$ integers the field ψ_x is anti-periodic, while for $\mathcal{N}_x$ half-integers it is periodic. Therefore the boundary conditions of this field depend on the particular sector of the Fock space we analyze. To keep track of the boundary conditions, let us introduce the label P as

$$P = \begin{cases} P = 0 & \text{for } \{\mathcal{N}_y\} \text{ integers} \\ P = 1 & \text{for } \{\mathcal{N}_y\} \text{ half-integers} \end{cases} \;. \tag{144}$$

With some algebra, one can then show that the kinetic energy of the x-fields can be refermionized, as

$$\frac{2\pi}{L}\frac{\hat{\mathcal{N}}_x^2}{2} + \int_{-L/2}^{L/2} \frac{dx}{4\pi} : (\partial_x \varphi_x)^2 := \sum_{\bar{k}} \bar{k} : c^\dagger_{\bar{k}x} c_{\bar{k}x} : + \frac{2\pi}{L}\frac{P}{8} \;. \tag{145}$$

Note that in the sectors $P = 0$ and $P = 1$ the momenta $\bar{k}$ take half-integers and integers in units of $2\pi/L$, respectively. The last term here is absolutely crucial to get the finite size spectrum correctly.

It is important to notice that the fermion $c_d = \mathcal{F}_s^\dagger S^-$ does not commute with $\hat{\mathcal{N}}_s$ either. Fortunately, this difficulty can be solved by noticing that the z-component of the total spin $S_T \equiv (\hat{\mathcal{N}}_s + S_z)$ is conserved. We can thus finally rewrite the Hamiltonian as

$$\begin{aligned} H' &= \frac{2\pi}{L}\Big(\frac{\mathcal{N}_c^2}{2} + \frac{\mathcal{N}_f^2}{2}\Big) + \sum_{q>0} q(b^\dagger_{qc} b_{qc} \; + b^\dagger_{qf} b_{qf}) \\ &+ h : c_d^\dagger c_d : + \sum_{\bar{k}} \bar{k} : c^\dagger_{\bar{k}x} c_{\bar{k}x} : + \sqrt{\frac{2\pi\Gamma}{L}} \sum_{\bar{k}} (c^\dagger_{\bar{k}x} + c_{\bar{k}x})(c_d - c_d^\dagger) \\ &+ \frac{2\pi}{L}\Big(\frac{1}{2} S_T^2 + \frac{P}{8}\Big) + h n_d^{(0)} + const \,. \end{aligned} \tag{146}$$

Here we introduced the Fourier components b_{qy} of the fields φ_y in the same way as in Appendix A.1, $: \ldots :$ denotes the normal ordering with respect to some reference state and $n_d^{(0)} = 1, 0$ is the expectation value of $c_d^\dagger c_d$ in this reference state. Clearly, the second line H_{xd} of the above Hamiltonian can be diagonalized. Introducing

Majorana fermions, performing a Bogolubov transformation for them, and finally pairing all Majorana fermions to real fermions again one obtains [88]

$$H_{xd} = \frac{h}{2} + \sum_{\varepsilon\geq 0} \varepsilon \left(\tilde{\alpha}^\dagger_\varepsilon \tilde{\alpha}_\varepsilon - \frac{1}{2} \right) + \sum_{\bar{k}>0} \bar{k} \left(\beta^\dagger_{\bar{k}} \beta_{\bar{k}} + \frac{1}{2} \right), \tag{147}$$

$$\frac{4\pi\Gamma\varepsilon}{\varepsilon^2 - h^2} = -\cot\pi\Big(\frac{L\varepsilon}{2\pi} - \frac{P}{2}\Big), \tag{148}$$

where the operators $\tilde{\alpha}^\dagger$ and $\beta^\dagger$ create quasiparticles with energy ϵ and $\bar{k}$, and the second equation determines the quasiparticle energies ϵ. In principle, the above two equations together with Eq. (146) give the full spectrum of the anisotropic Kondo model with $j_z = 1$. However, we enlarged the Hilbert space in course of the solution, and now we have to project out some of the states by applying the gluing conditions. It turns out that the gluing conditions (129) translate to a simple condition on the *parity* of total fermionic quasiparticles, $\mathcal{P}_{\tilde{E}} \equiv \left[\sum_{\varepsilon\geq 0} : \tilde{\alpha}^\dagger_\varepsilon \tilde{\alpha}_\varepsilon : + \sum_{\bar{k}>0} : \beta^\dagger_{\bar{k}} \beta_{\bar{k}} :\right] \bmod 2$,

$$\mathcal{P}_{\tilde{E}} = \begin{cases} \left(\mathcal{N}_c + \mathcal{N}_f - S_T - \frac{P+1}{2}\right) \bmod 2 & (h > 0)\,, \\ \left(\mathcal{N}_c + \mathcal{N}_f - S_T - \frac{P-1}{2}\right) \bmod 2 & (h \leq 0)\,. \end{cases} \tag{149}$$

This *generalized gluing condition* specifies which of all possible states in the extended Fock space are physical.

Having Eqs. (146), (147), and (148) and the gluing condition Eq. (149) at hand, we can easily compute the finite size spectrum along the Emery-Kivelson line, $j_z = 1$, by solving Eq. (148) numerically. The final results of this calculation are shown in Fig. 26. The first panel shows the evolution of the spectrum for $h = 0$ in the absence of the spin-flip term $j_\perp$ for $0 < j_z < 1$. As soon as we turn on the spin-flip term, the spectrum evolves to the finite size spectrum characteristic of the two-channel Kondo problem. Both the positions and degeneracies of the many-body excitation spectrum obtained are characteristic of the two-channel Kondo fixed point, and are in perfect agreement with earlier numerical renormalization group and conformal field theory results [29, 84, 27]. Note that in a Fermi liquid spectrum for any electron-like excitation with energy $E < 2\pi/L$ there is another hole-like excitation with energy $E' = 2\pi/L - E$. Clearly, the energy spectrum $\mathcal{E}_{NFL}$ does not satisfy this criterion. Note, that here we computed the finite size spectrum through a straightforward diagonalization. This is not true for the conformal field theory solution which is rather an intelligent guess for the boundary operators that describe the numerically

obtained spectrum. (Of course, one can use the predictive power of conformal field theory once the appropriate conformal boundary conditions have been identified [27].) Application of a small magnetic field deforms the non-Fermi liquid spectrum into a simple Fermi liquid spectrum characterized by phase shifts $\pm\pi/4$.

The evolution of the spectra in Fig. 26 is in some sense the analytical version of the numerical renormalization group (NRG) spectrum. As we already discussed in Section 2.3, the NRG transformation is equivalent to rescaling the size of the system and the corresponding energy unit $\Delta_L = 2\pi/L$ as $L \to \Lambda^{1/2}L$, and $\Delta_L \to \Delta_{\Lambda^{1/2}L} = \Delta_L/\Lambda^{1/2}$. In our case this corresponds to the step

$$\frac{H_x(L,\Gamma,\varepsilon_d)}{\Delta_L} \to \frac{H_x(\Lambda^{1/2}L,\Gamma,h)}{\Delta_{\Lambda^{1/2}L}} = \frac{H_x(L,\Lambda^{1/2}\Gamma,\Lambda^{1/2}h)}{\Delta_L}\,, \tag{150}$$

In other words, performing an NRG iteration is equivalent to increasing Γ and h at fixed L.

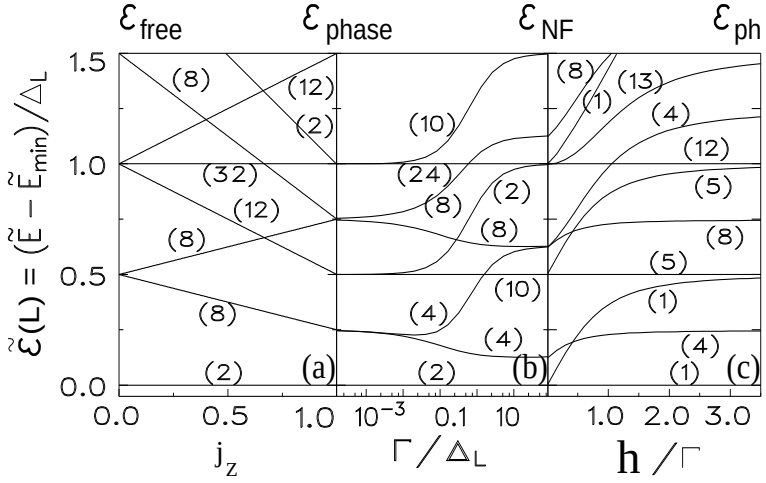

Figure 26: Finite-size spectrum of the 2CK model with antiperiodic boundary conditions. with degeneracies given in brackets. Energies are measured in units of $\Delta_L \equiv 2\pi/L$. (a) For $0 < j_z < 1$, $j_\perp = 0$ the free Fermi-liquid spectrum evolves smoothly into a simple phase-shifted spectrum, $\mathcal{E}_{\rm phase}$. (b) $j_z = 1$, $0 < j_\perp < \infty$: the spectrum crosses to the two-channel Kondo spectrum, $\mathcal{E}_{\rm NFL}$, at an energy $\Gamma = j_\perp^2/4a \sim \Delta_L$. (c) Turning on a local magnetic field h induces a further cross-over in the spectrum to a simple phase shifted spectrum with a phase shift $\pi/4$ at a field $h \sim (\Gamma 2\pi/L)^{1/2}$.

The finite size spectrum can also be used to extract a lot more information about the fixed point. In particular, it is also straightforward to implement Wilson's prescription [10] for extracting the exact scaling exponent of perturbations around the

fixed point from its effect on the finite-size spectrum [88]: In general, a perturbation causes the dimensionless energy $\tilde{\mathcal{E}}(L)$ calculated at a finite, non-zero $\Delta_L \ll \Gamma$ to differ from its universal fixed point value $\mathcal{E}_{\rm NFL}$ by an amount $\delta\tilde{\mathcal{E}}(L)$, whose leading asymptotic behavior for $L \to \infty$ is

$$\delta\tilde{\mathcal{E}}(L) \equiv \tilde{\mathcal{E}}(L) - \mathcal{E}_{\rm NFL} \sim (L^y)^n \ , \tag{151}$$

where $n \geq 1$ is some integer and y is the scaling dimension of the perturbation. Thus deviations from the universal spectrum are characteristic of the operator content of the fixed point. The scaling dimensions of these operators, on the other hand, directly determine the scaling properties of various response functions and physical observables.

Let us, *e.g.* consider deviations from the Emery-Kivelson line, $j_z \to 1 + \delta j_z$. We can do perturbation theory in δj_z to find that the first excited states (with $\mathcal{E}_{\rm NFL} = 1/8$) are shifted relative to the ground state by an amount

$$\delta\tilde{\mathcal{E}}(L) \simeq -\frac{1}{4}\delta j_z \frac{1}{\left(1 + 4\pi^2\Gamma/\Delta_L\right)^{1/2}} \sim L^{-1/2} \ . \tag{152}$$

This relation implies that the scaling dimension of δj_z is $y_z = -1/2$, and is therefore irrelevant. This is, in fact, one of the three the leading irrelevant operators, and it is responsible for the anomalous behavior of the electronic scattering rate and the resistivity, $R^{\rm imp} \sim cst - T^{1/2}$.

An analysis of the magnetic field dependence of the spectrum also reveals that for very small fields the energy levels (in units of $2\pi/L$) are shifted by an amount $\sim h^2 L$, corresponding to $n = 2$ and $y_h = 1/2$. The magnetic field is therefore a relevant perturbation of scaling dimension $1/2$, in agreement with the logarithmically divergent susceptibility discussed before.

To conclude this subsection, let us mention that the whole finite size diagonalization procedure can be also applied with some modifications to the case of the single channel Kondo model. The results are shown in Fig. 27

4.1.3 Exact solution of the anisotropic two-channel Kondo problem

In the present section we show how one can solve the anisotropic two-channel Kondo problem by the algebraic Bethe ansatz to obtain its thermodynamic properties. First

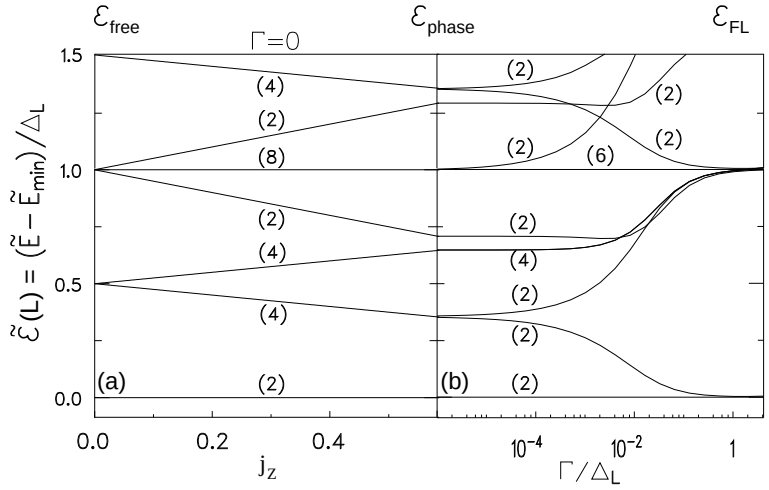

Figure 27: Evolution of the many-body finite-size spectrum of the anisotropic 1CK model for anti-periodic boundary conditions ($P_0 = 1$). (a) For $0 < j_z < j_z^* = 2 - \sqrt{2}$, $j_\perp = 0$. the spectrum is simply a phase shifted spectrum. (b) At the Toulouse line, $j_z = j_z^*$, $j_\perp \neq 0$ the spectrum smoothly evolves into the well-known Fermi liquid spectrum as a function of $\Gamma/\Delta_L = j_\perp^2/(4a\Delta_L)$ originally obtained by Wilson [10].

of all, we write the Hamiltonian in real space as

$$H = \sum_{j=1}^{N_e} \Big\{ i\frac{\partial}{\partial x_j} + \frac{1}{2} \sum_{\alpha=x,y,z} j_\alpha \, \delta(x_j) \sigma_j^\alpha S_0^\alpha \Big\} + h\Big(g \, S_0^z + g' \sum_j \frac{1}{2} \sigma_j^z \Big) \, . \tag{153}$$

The x_j denote the coordinates of the conduction electrons, $N_e = N \times f$ is the total number of electrons, and the σ_j's ($j = 0, .., N_e$) denote the spin operators of the electrons. The conserved flavor quantum numbers, $a = \{1, .., f\}$, are implicit in Eq. (153). In the following we shall discuss the case $f \geq 2$ too, though for all currently known physical realizations $f = 2$.

It is very hard to make analytical progress for the fully anisotropic case, $j_x \neq j_y \neq j_z$. We shall therefore restrict our considerations to the $j_x = j_y = j_\perp$ version of the above model, that has a $U(1)$ symmetry in spin space.

Fortunately, in view of the results of Section 4.1.1, the Hamiltonian above is enough to account for the low temperature properties of a fast (Kondo) tunneling center. For a two level system the asymmetry of the double well potential plays the role of a local magnetic field, which couples only to the impurity spin. In Eq. (153), however, we also coupled the magnetic field to the conduction electrons' spin, although with a different g-factor, g'. The Bethe ansatz allows one to treat exclusively

the case, $g = g'$, but we can also obtain results for the $g \neq g'$ case by combining the Bethe ansatz method with other non-perturbative arguments [93, 101].

The first step towards the Bethe ansatz solution of this model is to construct the scattering matrices and show that they satisfy the Yang-Baxter equations, Eq. (28). The impurity-conduction electron S-matrix, R_{0j} can be simply obtained from Eq. (153), and turns out to belong to the following $U(1)$ family of scattering matrices in the spin sector,

$$R_{0j} = U_{0j}(\alpha) = a(\alpha)P_{\uparrow\uparrow} + b(\alpha)P_{\uparrow\downarrow} + \frac{1}{2}c(\alpha)(S_0^+ S_j^- + S_0^- S_j^+) \ , \tag{154}$$

with $P_{\uparrow\uparrow}$ and $P_{\uparrow\downarrow}$ the projection operators for parallel and opposite spin directions. These scattering matrices are parametrized by the spectral parameter α, and the functions $a(\alpha)$, $b(\alpha)$ and $b(\alpha)$ satisfy

$$\frac{a(\alpha)}{c(\alpha)} = \frac{\sinh(i\mu + \alpha\theta)}{\sinh(i\mu)} \ , \quad \frac{a(\alpha)}{b(\alpha)} = \frac{\sinh(i\mu + \alpha\theta)}{\sinh(\alpha\theta)} \ , \tag{155}$$

Electrons move with the same velocity, and therefore we are free to choose their S-matrix as we wish. To maintain integrability, we choose their scattering matrix to be simply

$$R_{ij} = U_{ij}(\alpha_i - \alpha_j) \otimes F_{ij}(\alpha_i - \alpha_j) \ . \tag{156}$$

Here $U(\alpha)$ is given by Eq. (155) and F describes scattering in the flavor sector:

$$F_{ij}(\alpha_i - \alpha_j) = \frac{\alpha_i - \alpha_j + icX_{ij}}{\alpha_i - \alpha_j + ic} \ , \tag{157}$$

with X_{ij} the flavor exchange operator of particle i and j and c an arbitrary constant to be defined later. The spectral parameters α_j must be all equal, and we are free to set them all equal to $\alpha_j \equiv 0$. With this choice, the impurity-conduction electron S-matrix is simply

$$R_{0j} = U_{0j}^{(spin)}(\alpha_0 - \alpha_j)_{\sigma_0\sigma_0';\sigma_j\sigma_j'} \ , \tag{158}$$

where α_0 denotes the spectral parameter (rapidity) of the impurity, that we are free to choose $\alpha_0 = -1$. With this choice one can easily find the connection between the parameters μ and θ and the couplings $j_\perp$, and j_z. The precise connection depends somewhat on the cut-off scheme, *i.e.*, the regularization of the delta function in Eq. (153), and is of no importance. It is more appropriate to consider the parameters

μ and θ as the relevant parameters, which will turn out to be directly related to some physical observables: μ turns out to be connected to the renormalized phase shift of the conduction electrons while the ratio μ/θ determines the Kondo temperature, below which non-Fermi-liquid correlations develop:

$$T_K = (1 - f\frac{\mu}{\pi})\, 2De^{-\pi\theta/\mu}, \tag{159}$$

with $D = N/L$ a cut-off of the order of the Fermi energy, L being the system size.

Once the scattering matrices in hand, we can use the machinery of algebraic Bethe ansatz outlined in Section 2.2.1 to construct the analogues of Eqs. (34) and (34). There is, however, one complication: now the conduction electrons also possess a flavor quantum number, and therefore Bethe ansatz equations must be constructed in the flavor sector too. In fact, one has to construct a series of Bethe ansatz equations to obtain the flavor structure of the wave function, which is called the *nested Bethe ansatz* in the literature [13, 25]. The resulting Bethe ansatz equations are rather complicated: In addition to the rapidities, $\{\lambda_\alpha; \alpha = 1, .., M\}$ that characterize spin excitations from the vacuum, one must introduce $f - 1$ sets of flavor rapidities, $\{\tilde{\chi}_\mu^{(b)}\}$ $(b = 1, \ldots, f-1\ \mu = 1, \ldots, M_b)$, that keep track of excitations in the flavor sector. Fortunately, the complications coming from the flavor excitations completely disappear due to the so-called fusion [25]: it turns out, that due to the interaction introduced in the flavor sector between conduction electrons, flavor excitations become gapped once one allows for a non-linear dispersion of the electrons. As a result, conduction electrons 'fuse' to form flavor singlets, the Bethe ansatz equations simplify a lot in the spin sector, and with the choice $c \equiv \frac{\mu}{\theta}$ the spin rapidities $\{\lambda_\alpha; \alpha = 1, .., M\}$ satisfy

$$\frac{\sinh(\mu(\lambda_\alpha + \frac{i}{2}) + \theta)}{\sinh(\mu(\lambda_\alpha - \frac{i}{2}) + \theta)} \left[\frac{\sinh \mu(\lambda_\alpha + i\frac{f}{2})}{\sinh \mu(\lambda_\alpha - i\frac{f}{2})}\right]^N = -\prod_{\beta=1}^{M} \frac{\sinh \mu(\lambda_\alpha - \lambda_\beta + i)}{\sinh \mu(\lambda_\alpha - \lambda_\beta - i)}\,.$$

The momenta of the electrons and thus the total energy is determined by the periodic boundary conditions

$$e^{ik_A Lf} = \prod_{\alpha=1}^{M} \frac{\sinh \mu(\lambda_\alpha + i\frac{f}{2})}{\sinh \mu(\lambda_\alpha - i\frac{f}{2})}\,; \quad E = \sum_{A=1}^{N} f k_A\,, \tag{160}$$

where fk_A denotes the total momentum of the fused f-electron composites.

Just as in case of the single channel Kondo model, in the thermodynamic limit, $L, N \to \infty$, $N/L = D$, the 'spin rapidities' λ_α in Eq. (160) are organized into strings [13, 64] of length r and parity $v = \pm$: $\lambda \to \{\lambda_q^{(r,v)}\ ;\ \ q = 1, .., r\}$ with

$$\lambda^{(r,v)} \leftrightarrow \lambda_q^{(r,v)} = \lambda^{(r,v)} + [\tfrac{r+1}{2} - q] + i\tfrac{\pi}{4\mu}(1 - v)\ . \tag{161}$$

These strings, however, must satisfy also a *stability condition*, *i.e.*, v and r must satisfy the inequality [65, 13]

$$v \sin(\mu q) \sin(\mu(r - q)) > 0\ , \quad q = 1, .., [r/2] \tag{162}$$

for $\mu < \pi/f$. This rather non-trivial inequality has been analyzed by Takahashi and Susuki [65], who studied the anisotropic Heisenberg chain, and showed that all allowed (r, v) strings can be classified on the basis of an infinite (or finite) fraction expansion of μ/π. For simplicity, here we only discuss the most simple case $\mu = \pi/\nu$ and $f < \nu$, where only ν different stable string configurations exist: $n = (r, v) = (1, +), (2, +), .., (\nu-1, +)$ and $(1, -)$. To simplify our notation, we shall refer to these strings by the labels $n = 1, \ldots, \nu$, the last index referring to odd parity one-strings.

To derive the thermodynamic Bethe ansatz (BA) equations in the continuum limit $L, N \to \infty$ and $D \equiv N/L = cst$ one can proceed in the usual way, and defined the density of rapidities (rapidity holes), $\varrho_n(\lambda)$ ($\tilde{\varrho}_n(\lambda)$), and derive integral equations. After some algebraic manipulations one finds the following set of integral equations for the functions $\eta_n \equiv \tilde{\varrho}_n/\varrho_n$,

$$\begin{aligned}
\ln \eta_\nu &= g\ h\ \nu/2T - G * \ln(1 + \eta_{\nu-2}) + \delta_{\nu,f+1}\Theta(\lambda) \\
\ln \eta_{\nu-1} &= g\ h\ \nu/2T + G * \ln(1 + \eta_{\nu-2}) - \delta_{\nu,f+1}\Theta(\lambda) \\
\ln \eta_j &= G * \ln\Big[(1 + \eta_{j+1})(1 + \eta_{j-1})\Big] + \delta_{j,\nu-2}\ G * (1 + 1/\eta_\nu) \\
&- \delta_{j,f}\Theta(\lambda) \qquad\qquad (j < \nu - 1).
\end{aligned} \tag{163}$$

$G *$ denotes convolution with the Kernel $G(\lambda) = \frac{1}{2\cosh(\pi\lambda)}$, the driving term is given by $\Theta(\lambda) = 2D/T\ \tan^{-1}(e^{\pi\lambda})$ and $\eta_0 \equiv 0$. The impurity contribution to the free energy is given by

$$F^{\rm imp} = -T \int_{-\infty}^{\infty} d\lambda\ \frac{1}{2\cosh\Big(\pi(\lambda + \frac{\theta}{\mu})\Big)} \ln(1 + \eta_1(\lambda)))\ ,$$

and, in principle, all thermodynamic quantities can be calculated by taking the derivatives of $F^{\rm imp}$. The bandwidth can be easily eliminated from these equations by replacing the driving term by $\Theta(\lambda) \approx e^{\pi\lambda+\ln(2D/T)}$, and shifting the variable $\tilde{\lambda} \equiv \lambda + \frac{1}{\pi}\ln(2D/T)$. Then the functions $\eta_n(\tilde{\lambda})$ become universal functions of h/T, and the Free energy can be written as

$$F^{\rm imp} = -T\int_{-\infty}^{\infty} s\Big(\tilde{\lambda} - \frac{1}{\pi}\ln(2De^{-\pi\theta/\mu}/T)\Big)\ \ln(1+\eta_1(\tilde{\lambda}, \frac{h}{T}))\ d\tilde{\lambda}\ .$$

Clearly, $F^{\rm imp}/T$ is just a universal function of T/T_K and h/T with the definition Eq. (159) of the Kondo scale. Furthermore, we see that the behavior of η_1 in the $\tilde{\lambda} \to \infty$ and $\tilde{\lambda} \to -\infty$ regimes determines the low and high temperature behavior of the free energy.

We can, in fact, obtain a lot of information from the asymptotic analysis of the functions η_n. Using the ansatz $\eta_n(\lambda \to \pm\infty) \approx \eta_n^{\pm} + b_n^{\pm}\ e^{\mp\pi\ \tau_{\pm}\lambda}$ one obtains a set of algebraic equations for the $\eta_n^{\pm}$'s, $b_n^{\pm}$'s and the exponents $\tau_{\pm}$. The latter exponents govern the scaling of the free energy in the vicinity of the low- and high-energy fixed points and are given by $\tau_+ = 4/(2+f)$ and $\tau_- = 2\mu/\pi$. The crossover between the two regimes occurs at the Kondo scale Eq. (159).

Note that the exponent $\tau_+ = 4/(2+f)$ determines the asymptotic scaling of all thermodynamic quantities below the Kondo scale. For $h \ll T \ll T_K$ the impurity free energy is given by

$$-F^{\rm imp}/T \sim \begin{cases} S^{\rm imp} + \Big(a + b\left(\frac{gh}{T}\right)^2\Big)\Big(\frac{T}{T_K}\Big)^{4/(2+f)} & (f>2,\ T \ll T_K) \\ S^{\rm imp} + \Big(a + b\left(\frac{gh}{T}\right)^2\Big)\Big(\frac{T}{T_K}\ln(\frac{T}{T_K})\Big) & (f=2,\ T \ll T_K) \end{cases} \tag{164}$$

implying the divergence of the linear specific heat coefficient $c^{\rm imp}/T$ at $h=0$ and the susceptibility as $T \to 0$,

$$\chi^{\rm imp} \sim \frac{c^{\rm imp}}{T} \sim \begin{cases} \frac{1}{T_K}\Big(\frac{T}{T_K}\Big)^{\frac{2-f}{2+f}} & (f>2,\ T \ll T_K), \\ \frac{1}{T_K}\ln\Big(\frac{T}{T_K}\Big) & (f=2,\ T \ll T_K). \end{cases} \tag{165}$$

The constants a and b in Eq. (164) depend on the specific value of f and μ (but are independent of θ). The residual entropy $S^{\rm imp}$ is determined by the limiting value η_1^+,

and is the same as in the isotropic case [25],

$$S^{\rm imp} = \ln\left(\frac{\sin(\frac{f\pi}{f+2})}{\sin(\frac{\pi}{f+2})}\right) , \tag{166}$$

also in agreement with the results of conformal field theory [27] and the Abelian bosonization approach discussed in the previous Section [86].

A similar analysis can be carried out to obtain the susceptibility and the impurity contribution to the specific heat for $T \gg T_K$, and we obtain [93],

$$\chi^{\rm imp}(T \gg T_K) = \frac{1}{4T}\Big[1 - B(\frac{T_K}{T})^{2\mu/\pi}\Big] , \tag{167}$$

$$c^{\rm imp}(T \gg T_K) \sim \left(\frac{T_K}{T}\right)^{2\mu/\pi} . \tag{168}$$

The second relation allows us to determine the physical meaning of the parameter μ as well. Simple perturbation theory in $j_\perp$ shows that the leading correction to the free energy at high temperatures is proportional to $F^{\rm im} \sim T\, j_\perp^2 + \ldots$. Combining this with scaling arguments one can immediately identify μ/π as the scaling dimension of the spin flip term, $j_\perp$. This, however, can be determined exactly using a the integral approach of Yuval and Anderson [3, 102] and can be expressed as

$$\frac{\mu}{\pi} = 4\frac{\delta_z}{\pi} - 4f\frac{\delta_z^2}{\pi^2} . \tag{169}$$

where δ_z is the phase shift of the conduction electrons generated by the coupling j_z [102].

An analysis of the integral equations also reveals that for finite magnetic fields h there is a cross-over to a Fermi liquid fixed point with vanishing residual entropy at a scale $T^* \sim h^2/T_K$. Correspondingly, for small magnetic fields, the entropy of the impurity is quenched in two steps, and the logarithmic divergences are cut off below the energy scale T^*. The two steps in the entropy translate into two peaks in the specific heat at the energies T_K and T^*. Some typical curves obtained from the numerical solution of the integral equations are shown for the case $\nu = 3$ in Fig. 28. For all other values of ν we found that the low temperature part of the data almost collapsed for any value of μ. These results show that anisotropy in the couplings plays very little role around the Kondo scale and below, where the system is already essentially isotropic. At high temperatures, however, the specific heat and

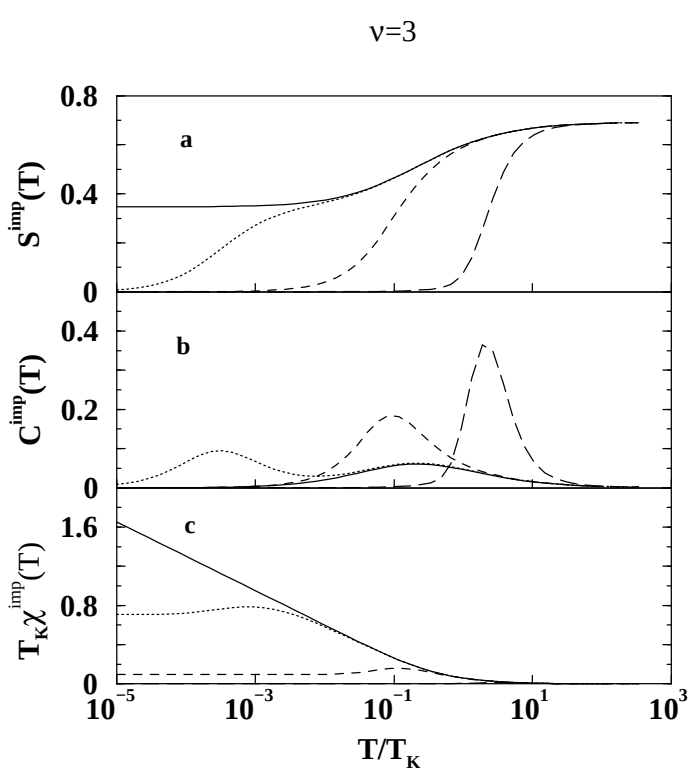

Figure 28: The impurity contribution to the entropy, $S^{\rm imp}$, specific heat, $c^{\rm imp}$, and (local) susceptibility, $\chi^{\rm imp}$, as functions of T/T_K for magnetic fields $h/T_K = 2^{-6}$ (solid), $h/T_K = 2^{-4}$ (dotted), $h/T_K = 1$ (dashed) and $h/T_K = 2^4$ (long-dashed) for the case $\nu = 3$ corresponding to the largest anisotropy studied.

the susceptibility exhibit anomalous power law behavior, that is governed by the non-universal exponent μ.

4.2 SU(N) models

In the previous section we studied the simplest non-Fermi liquid model, the multichannel Kondo problem, where a spin 1/2 impurity is coupled to f channels of conduction electrons through an antiferromagnetic exchange coupling. We have seen that for $f > 1$ this model has singular behavior at low temperatures, and displays a non-Fermi liquid behavior.

There is a number interesting generalizations of this model. First of all, one can replace the impurity spin $S = 1/2$ by a higher $SU(2)$ representation, $S > 1/2$. Already this modification gives non-trivial results. It turns out that a Fermi liquid state only appears if $S = f/2$, in which case the impurity spin is exactly screened

by the conduction electrons [25]. For $S > f/2$ the impurity spin is *underscreened* at low temperatures, and the $T \to 0$ behavior remains singular [12, 103], although in some sense it still resembles a Fermi liquid [104]. While in most cases the impurity spin is exactly screened, the underscreened state can sometimes also be realized, *e.g.*, in quantum dots having a triplet ground state [49]. For $S < f/2$, on the other hand, the impurity spin is *overscreened*, and the behavior of the specific heat is essentially identical to that of the spin $S = 1/2$ impurity model, although the residual entropy is different. Such underscreened states are most likely realized in some Uranium or Cerium based compounds and by fast tunneling enters [34]. These various possibilities are shown in Fig. 29.

Another possibility is to consider electrons with spin $S_e > 1/2$. These types of models emerged, *e.g.*, in Section 4.1.1. Fortunately, it turns out that the spin sector of the $S_e > 1/2$ f-channel models can be simply mapped to that of the multichannel spin 1/2 Kondo model with an effective channel number [105]

$$\tilde{f} = f\ \frac{2}{3} S_e(S_e+1)(2S_e+1)\ . \tag{170}$$

Therefore these models are conceptually not different from the spin $S_e = 1/2$ multichannel models.

In this section we shall focus on a more exciting family of models, where the $SU(2)$ spins of the impurity and the conduction electrons are replaced by $SU(N)$ spin operators, *i.e.*, we replace the exchange interaction as

$$\sum_{i=1}^{3} \sigma^i_{\rm imp}(\psi^\dagger \sigma^i \psi) \to \sum_{i=1}^{N^2-1} \lambda^i_{\rm imp}(\psi^\dagger \lambda^i \psi)\ , \tag{171}$$

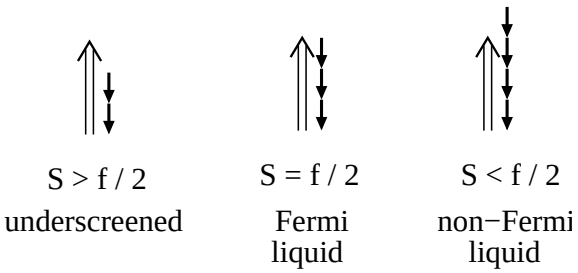

Figure 29: Simplistic, pictorial representation of the various ground states of the spin S multichannel Kondo model.

with λ^i the generators of the $SU(N)$ Lie algebra. On one hand, these models serve as interesting test grounds, because in many cases, in the limit $N \to \infty$ they have 'simple' mean field solutions, which nevertheless capture many aspects of the Kondo and the non-Fermi liquid physics [92, 106, 107]. Furthermore, $SU(N)$ spin models are sometimes also realized in nature: as we shall see in Chapter 5, double quantum dot systems or quantum dots with degenerate levels can realize an $SU(4)$ spin model. In the next subsection we first show how the low temperature physics of a fast N-state system can be described by a two-channel $SU(N)$ model [108]. Then in subsection 4.2.2 we show how this model can be solved exactly by the algebraic Bethe ansatz approach.

4.2.1 The N-state tunneling system: $1/f$ expansion

In some experimental systems like the narrow gap semiconductor $Pb_{1-x}Ge_xTe$ or the insulating system $K_{1-x}Li_xCl$, tunneling systems are formed by substitutional impurities that are sitting in the middle of a highly symmetrical 'cavity' of neighboring atoms [109, 110]. In these systems the two level system model is inappropriate since the tunneling impurity tunnels between many (three, six, or eight) equivalent positions, and forms an N-state system. In some of these systems Kondo-like anomalies have been observed that could be attributed to the presence of these tunneling centers [109].

To study how a strongly correlated state forms in these systems, we first write the Hamiltonian of the tunneling system as

$$H_{hp} = \sum_{i,j=1}^{N} \Delta^{ij} \ |i\rangle\langle j| \ , \tag{172}$$

where now $|i\rangle$ denotes the state localized at position i of the tunneling particle. The off-diagonal matrix elements of matrix Δ^{ij} describe tunneling between these states, while the diagonal ones correspond to an asymmetry of them, generated by some strain field.

The most general interaction term generated by a Coulomb interaction between the tunneling particle and the conduction electrons takes on the form

$$H_{\rm int} = \sum_{\sigma} \sum_{i,j} \sum_{\mu,\mu'=s,p,\ldots} v^{ij}_{\mu\mu'} |i\rangle\langle j| \psi^{\dagger}_{\mu\sigma} \psi_{\mu'\sigma} \ , \tag{173}$$

where similar to the two level system case, Eq. (112), the operator $\psi^\dagger_{\mu\sigma} = \int d\epsilon\, a^\dagger_{\mu\sigma}(\epsilon)$ creates a local fermion state with angular momentum μ. The off-diagonal couplings (v^{ij} with $i \neq j$) correspond to assisted tunneling processes, while diagonal terms (v^{ij} with $i = j$) generate dissipation and tend to suppress spontaneous tunneling processes. In known physical realizations, the spin σ of the electrons can take only two different values, but here we shall consider here the general case, $\sigma = 1, .., f$, which allows us to perform a $1/f$ expansion for the critical exponents.

To construct the scaling equation, we proceed by representing the states of the tunneling atom by pseudofermion operators, $|i\rangle\langle j| \to b^\dagger_i b_j$, and computing the conduction electron vertex functions, and the pseudofermion's self-energy. In leading order in $1/f$ we obtain the following results for the pseudofermion propagator and the vertex function [108],

$$\begin{aligned}(\mathcal{G}^{-1})^{ij} &= \omega\,\delta^{ij} - \Delta^{ij} + f \ln\frac{D}{\omega}\,(\delta^{ij}\,\omega\,\mathrm{tr}\{v^{kl}v^{lk}\} - \mathrm{tr}\{v^{ik}\Delta^{kl}v^{lj}\}) \\ \Gamma^{ij} &= v^{ij} - \ln\frac{D}{\omega}\left([v^{ik},v^{kj}] - f\mathrm{tr}\{v^{ik}v^{lj}\}v^{kl}\right), \end{aligned} \tag{174}$$

where the matrix notations $v^{ij}_{mn} \to v^{ij}$, $\Gamma^{ij}_{mn} \to \Gamma^{ij}$, have been introduced, D is the high energy cut-off of the order of the Debye temperature, and a summation must be carried out over repeated indices.

To generate the scaling transformation, we should now determine the pseudofermion's Z-factor by substituting the above expressions into Eqs. (14) and (15) of Section 2.1.2. However, it turns out that Eqs. (14) and (15) cannot be satisfied with a constant Z-factor. Therefore we proposed the following generalized multiplicative renormalization group transformation [108]:

$$\begin{aligned}\mathcal{G}(\omega, v', \Delta', D') &= A\,\mathcal{G}(\omega, v, \Delta, D)\,A^+\,, \\ \Gamma(\omega, v', \Delta', D') &= [A^+]^{-1}\Gamma(\omega, v, \Delta, D)\,A^{-1}\,, \end{aligned} \tag{175}$$

where we introduced a matrix notation in the indices i, j too, D' stands for the rescaled cut-off and A denotes an $N \times N$ matrix acting only on the indices i, j. The matrix $A = A(v', \Delta', D'/D)$ is independent of the dynamical variable ω, and should be though of as the square root of the Z-factor. While for finite D/D' the matrix A has a rather complicated structure, for an infinitesimal change of D it can be chosen to be Hermitian and Eq. (175) can be cast in the form of a scaling equation for the

dimensionless couplings v^{ij}. Note also, that Eq. (175) has been constructed to leave the free energy invariant, and also assures that the generated Hamiltonian remains Hermitian.

From Eqs. (175) and (174) we now obtain the following scaling equations

$$\begin{aligned} \frac{dv^{ij}}{dl} &= -[v^{ik}, v^{kj}] + \frac{1}{2} f\Big(2\mathrm{tr}\{v^{ik}v^{lj}\}v^{kl} - \mathrm{tr}\{v^{ik}v^{kl}\}v^{lj} - v^{ik}\mathrm{tr}\{v^{kl}v^{lj}\}\Big) \,, \\ \frac{d\Delta^{ij}}{dl} &= -\frac{f}{2}\Big[\mathrm{tr}\{v^{ik}v^{kl}\}\Delta^{lj} + \Delta^{ik}\mathrm{tr}\{v^{kl}v^{lj}\} - 2\mathrm{tr}\{v^{ik}\Delta^{kl}v^{lj}\}\Big] \end{aligned} \tag{176}$$

with $l = \ln\ D/D'$ the scaling variable. Apart from some special cases the above differential equations can be solved only numerically. However, even for a numerical solution it is useful first to introduce some site representation in the orbital indices of the conduction electrons to exploit the symmetry properties of the system. This can be achieved most simply by taking some linear combinations of the most strongly scattered angular momentum channels and hybridize them using group theoretical methods. For a regular 3-state system in the xy plane and a free electron band, *e.g.*, one can use the three orthogonal electron states:

$$\begin{aligned} |1\rangle &= \frac{1}{\sqrt{3}}|s\rangle + \sqrt{\frac{2}{3}}|p_x\rangle \,, \\ |2,3\rangle &= \frac{1}{\sqrt{3}}|s\rangle - \frac{1}{\sqrt{6}}|p_x\rangle \pm \frac{1}{\sqrt{2}}|p_y\rangle \,, \end{aligned} \tag{177}$$

where the states $|p_x\rangle$ and $|p_y\rangle$ are defined in the usual way from the $l = 1$ angular momentum states $|m\rangle$. Working with these electron states directed towards the impurity positions, the v^{ij}'s become N^4-dimensional tensors. However, the number of independent couplings is largely reduced by symmetry. For an octahedron, *e.g.*, the $6^4 = 1296$ couplings may be replaced by 32 independent couplings making the numerical solution reasonably fast.

In Fig. 30 the dashed line shows the typical scaling of the norm of the dimensionless couplings, $u = \sum ||v^{ij}||$, for initial couplings estimated similar to Refs. [32, 111]. Clearly, the couplings gradually increase and scale to a strong coupling fixed point. While we could not find all possible fixed points of Eq. (176), based upon the results obtained for the two level system in Section 4.1.1, it quite natural to guess that the

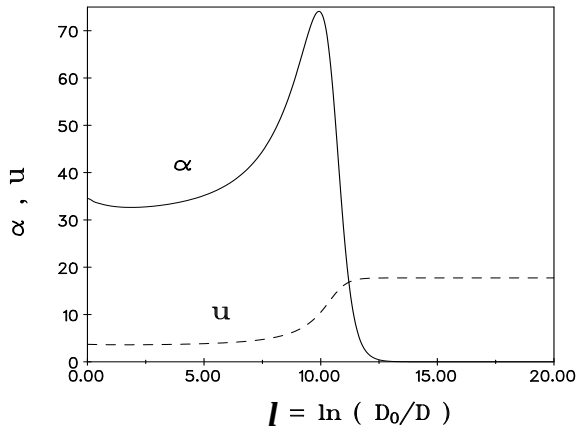

Figure 30: Scaling of the norm of the dimensionless couplings, $u = \sum ||\underline{v}^{ij}||$ (dashed line), and of the algebra coefficient α (continuous line) for a 6-state system with $f = 2$.

fixed point couplings must be unitary equivalent to the $SU(N)$ generators,

$$v_{\rm fp}^{ij} = \frac{1}{f} O^{ij} \; ; \qquad [O^{ij}, O^{kl}] = \delta^{il} O^{kj} - \delta^{kj} O^{il} \; , \tag{178}$$

where the O^{ij}'s are $N \times N$ matrices. In other words, in an appropriate basis, the effective low-temperature interaction Hamiltonian simply reads,

$$H_{\rm eff} \sim \sum_{\sigma=1,\ldots,f} \sum_{\alpha,\beta=1,\ldots,N} |\alpha\rangle\langle\beta| \psi^\dagger_{\beta\sigma} \psi_{\alpha\sigma} \; . \tag{179}$$

The model (179) is called the multichannel Coqblin-Schrieffer model [112], and is one of the models displaying non-Fermi liquid properties (see the following section). The above conjecture can be verified numerically, by computing the 'algebra coefficient' $\alpha \equiv \sum_{i,j,k,l} ||f^2 [v^{ij}, v^{kl}] - f\delta^{il} v^{kj} + f\delta^{kj} v^{il}||$, that measures in a natural way how well the fixed point algebra (178) is satisfied. As shown in Fig. 30, α indeed vanishes at the strong coupling fixed point.

One can also carry out a stability analysis of the above fixed point in the large f limit, where the multiplicative renormalization group is reliable, and show that it is indeed stable. The operator content of the N-state system's fixed point is though slightly different from that of the Coqblin-Schrieffer model [108], and the leading irrelevant operator of the N-level system is not captured by the latter. However, very likely the amplitude of this operator is quite small compared to that of the *subleading* operator, which is just the exchange operator itself, and has almost the same dimen-

sion. Therefore the f-channel Coqblin-Schrieffer model, Eq. (179) should describe the physics of the N-level system rather well in a large range of temperatures. To order $1/f$ we find that the dimension of this subleading irrelevant operator is given by $y = -N/f$, which agrees with the expansion of the exact exponent $y = -N/(f+N)$ obtained using conformal field theory and slave particle techniques [92, 113].

Let us close this subsection by shortly discussing the role of the splitting Δ^{ij}. In case of an N-state system, usually symmetry guarantees that the diagonal matrix elements Δ^{ii} are the same. However, just as for the two level system model, the tunneling between neighboring positions generates a crossover scale T^* to a Fermi-liquid state. This scale must be smaller than the Kondo scale to access the interesting non-Fermi liquid regime. Though no quantitative analysis has been carried out, we believe that the arguments of Aleiner *et al.* and those of Ref. [96] also carry over to the present model, implying that the tunneling impurity must act as a resonant scatterer for the conduction electrons to satisfy the criterion $T^* < T_K$ [124, 96].

4.2.2 Exact solution of the $SU(N) \times SU(f)$ model

In this subsection we shall construct the exact solution of the f-channel Coqblin-Schrieffer model, Eq. (179), closely following the discussion of Ref. [85]. Apart form a trivial potential scattering term, the Coqblin-Schrieffer model can well be written using the generators λ^i of $SU(N)$ as

$$H = \sum_{\sigma=1}^{N} \sum_{a=1}^{f} \int \frac{dx}{2\pi}\, \psi^\dagger_{\sigma a}(x)\, i\partial_x \psi_{\sigma a}(x) + J \sum_{i=1}^{N^2-1} \sum_{a,\sigma\sigma'} \lambda^i_{\rm imp}\, \psi^\dagger_{\sigma a}(0) \lambda^i_{\sigma\sigma'} \psi_{\sigma' a}(0)\,. \quad (180)$$

Here the exchange coupling acts on the spins σ of the electrons, which can take N different values, and correspond to orbital indices in the N-state system problem. The electron spin in the tunneling system problem, on the other hand, corresponds to the conserved channel (flavor) label a in Eq. (180).

The diagonalization procedure of this Hamiltonian is the same as the one outlined in subsection Ref. 4.1.3: One must introduce a curvature in the conduction electrons' dispersion, and also an effective exchange interaction between them both in the *spin* and in the *flavor* sectors to maintain integrability. Then the scattering matrix between the impurity and electron 'i' and conduction electrons i and j read,

respectively,

$$R_{0j} = U_{0j}(\alpha_0 - \alpha_j) \ , \qquad R_{ij} = U_{ij}(\alpha_i - \alpha_j) \otimes F_{ij}(\alpha_i - \alpha_j) \ , \tag{181}$$

where U_{ij} and F_{ij} denote the scattering matrices in the spin and flavor sectors, respectively,

$$U_{ij}(\alpha) = \frac{\alpha + icP_{ij}}{\alpha + ic} \ , \qquad F_{ij}(\alpha) = \frac{\alpha + icX_{ij}}{\alpha + ic} \ , \tag{182}$$

with P and X the exchange operators for spin and flavor. The constant c in Eq. (182) measures the strength of the exchange coupling, $c = c(J)$. The rapidities α_j are related to the momenta of the electrons, but in the limit of linear dispersion they simply become $\alpha_0 \to -1$ and $\alpha_j \to 0$.

This multichannel Coqblin-Schrieffer model is more complicated than the multichannel Kondo model studied in Section 4.1.3 in that here a nested Bethe ansatz must be made in *both* the spin and the charge sectors. As a consequence, the spin structure of the wave function is now characterized by rapidities $\{\lambda_\alpha^{(r)};\ r = 1, .., N-1,\ \alpha = 1, .., M_r\}$, while the rapidities $\{\chi_\alpha^{(b)};\ b = 1, .., f-1,\ \alpha = 1, .., N_b\}$ determine its flavor structure. The interaction introduced in the flavor sector leads to the fusion of conduction electrons when we remove the cut-off: f conduction electrons are bound to form a flavor singlet of total momentum $p = fp_\delta$ ($\delta = 1, .., N_e/f$) and we obtain a set of equations that involves only the spin sector:

$$\begin{aligned}
e^{ifp_\delta L} &= \prod_{\gamma=1}^{M_1} \frac{\lambda_\gamma^{(1)} + if/2}{\lambda_\gamma^{(1)} - if/2}, \\
-\prod_{\beta=1}^{M_r} \frac{\lambda_\gamma^{(r)} - \lambda_\beta^{(r)} + i}{\lambda_\gamma^{(r)} - \lambda_\beta^{(r)} - i} &= \prod_{t=r\pm1} \prod_{\beta=1}^{M_t} \frac{\lambda_\gamma^{(r)} - \lambda_\beta^{(t)} + i/2}{\lambda_\gamma^{(r)} - \lambda_\beta^{(t)} - i/2}; \quad (r = 2, ..., N-1), \\
-\prod_{\beta=1}^{M^1} \frac{\lambda_\gamma^{(1)} - \lambda_\beta^{(1)} + i}{\lambda_\gamma^{(1)} - \lambda_\beta^{(1)} - i} &= \frac{\lambda_\gamma^{(1)} + 1/c + i/2}{\lambda_\gamma^{(1)} + 1/c - i/2} \prod_{\delta=1}^{N^e/f} \frac{\lambda_\gamma^{(1)} + if/2}{\lambda_\gamma^{(1)} - if/2} \prod_{\beta=1}^{M^2} \frac{\lambda_\gamma^{(1)} - \lambda_\beta^{(2)} + i/2}{\lambda_\gamma^{(1)} - \lambda_\beta^{(2)} - i/2}.
\end{aligned}$$

A state is thus characterized by a set of spin rapidities $\{\lambda_\alpha^{(r)}\}$ that provide a solution for the above equations, and its energy is given by

$$E = \sum_{\delta=1}^{N^e/f} fp_\delta.$$

In the thermodynamic limit, $N_e, L \to \infty$, $D \equiv N_e/fL = cst$, the solutions

$\lambda_\alpha^{(r)}$ organize into n-strings. The thermodynamic Bethe ansatz equations can be derived for the densities $\varrho_n^{(r)}(\lambda)$ of these n-strings (and the hole-densities, $\tilde{\varrho}_n^{(r)}(\lambda)$) following the same procedure that we outlined in Section 2.2.3. In the end of this tedious procedure, we obtain the following set of integral equations for the ratios $\eta_n^{(r)}(\lambda) \equiv \tilde{\varrho}_n^{(r)}(\lambda)/\varrho_n^{(r)}(\lambda)$,

$$\begin{aligned}
\ln \eta_1^{(r)} &= -\frac{2}{f}\frac{D}{T} \arctan e^{\pi\lambda}\, \delta^{r,1}\delta_{1,f} + G * \ln(1+\eta_2^{(r)}) \\
&\quad -G * (\ln(1+(\eta_1^{(r-1)})^{-1}) + \ln(1+(\eta_1^{(r+1)})^{-1})), \qquad (183)\\
\ln \eta_n^{(r)} &= -\frac{2D}{Tf} \arctan\Big(e^{\pi\lambda}\Big)\, \delta^{r,1}\delta_{n,f} + G * (\ln(1+\eta_{n-1}^{(r)}) + \ln(1+\eta_{n+1}^{(r)})) \\
&\quad -G * (\ln(1+(\eta_n^{(r-1)})^{-1}) + \ln(1+(\eta_n^{(r+1)})^{-1})), \qquad (184)
\end{aligned}$$

with G the integral operator given by Eq. (47). These equations are, unfortunately, not well-defined in the scaling limit. The reason is that the driving term $\sim D/T$ drives the functions $\eta_f^{(r)}$ to zero in the $\lambda \to \infty$ limit (corresponding to $T \to 0$ temperatures). In this limit, the terms $\sim G * \ln(1+(\eta_1^{(r\pm1)})^{-1})$ also diverge, and an iterative solution is unstable.

With some algebraic manipulations it is therefore better rewriting these equations as [12]

$$\begin{aligned}
-\ln(1+(\eta_n^{(r)})^{-1}) &= -\frac{\Delta E_{N,r}^{fund}}{T}\delta_{n,f} \qquad (185)\\
&\quad + \sum_{q=1}^{N-1} G_N^{r,q}\Big(\ln(1+\eta_{n+1}^{(q)}) + \ln(1+\eta_{n-1}^{(q)}) - G^{-1}\ln(1+\eta_n^{(q)})\Big),
\end{aligned}$$

where $\ln(1+\eta_0^{(r)}) \equiv 0$, and the Fourier transform of the kernel of the integral operator $G_N^{r,q}$ is given by

$$\widetilde{G}_N^{r,q}(\omega) \equiv \frac{\sinh\left(\frac{\omega}{2}\ \min(r,q)\right)\ \sinh\left(\frac{\omega}{2}\ (N-\max(r,q))\right)}{\sinh(\omega/2)\sinh(N\omega/2)}. \qquad (186)$$

The right hand sides of Eqs. (185) behave already nicely in the $\lambda \to \infty$ limit. The driving term in these equations is the energy of the fundamental excitation, $\Delta E_{N,r}^{fund}$, that can be calculated explicitly as

$$\Delta E_{N,r}^{fund} = \frac{D}{f}\left\{\pi\frac{N-r}{N} - 2\arctan\Big(\tan\left(\frac{\pi}{2}\frac{N-r}{N}\right)\tanh\Big(\frac{\pi}{N}\lambda\Big)\Big)\right\}.$$

For large negative values of λ these energies scale as

$$\Delta E^{fund}_{N,r}(\lambda \to -\infty) \approx \frac{2D}{f} \sin\Big(\pi \frac{r}{N}\Big)\, e^{2\pi\lambda/N} \ . \tag{187}$$

Based on this asymptotic formula, we can now eliminate the bandwidth D from Eqs. (185) by introducing the new variables, $\xi \equiv \frac{2\pi\lambda}{N} + \ln\frac{D}{T}$. Then the $\eta_n^{(r)}$'s become universal functions of ξ, independent of the temperature, and the impurity contribution to the free energy can be expressed as

$$F^i = -\frac{T}{2\pi} \sum_{q=1}^{N-1} \int_{-\infty}^{\infty} d\xi \frac{\sin\pi\frac{N-q}{N}}{\cosh\Big(\xi - \ln(T_K/T)\Big) + \cos\pi\frac{N-q}{N}} \ln(1+\eta_1^{(q)}(\xi)) \ , \tag{188}$$

where the Kondo temperature is defined as

$$T_K = D\, e^{-2\pi/Nc} \ . \tag{189}$$

Clearly, the free energy is determined by the distributions of one-strings only (but in all spin sectors), and is a universal function of T/T_K and H/T. The magnetic field-dependence only appears implicitly in Eqs. (185) through the boundary conditions for the functions $\eta_n^{(q)}$.

The asymptotic analysis of Eqs. (185) can be carried out similar to Section 4.1.3. The residual entropy is determined by the limiting value of the functions $\eta_n^{(r)}(\lambda \to \infty)$, and is given by

$$S^i_{T=0} = \ln \frac{\sin\frac{\pi N}{f+N}}{\sin\frac{\pi}{f+N}} \ . \tag{190}$$

The behavior of the susceptibility and the specific heat depend on the ratio N/f. For $f > N$ the thermodynamics is singular, and the susceptibility and the linear specific heat coefficients diverge as

$$\chi^{\rm imp}_{f>N} \sim c^{\rm imp}_{f>N}/T \propto \frac{1}{T_K}\left(\frac{T}{T_K}\right)^{\frac{N-f}{N+f}} \ . \tag{191}$$

The power law divergences are reduced to logarithmic singularities for the marginal case, $f = N$,

$$\chi^{\rm imp}_{f=N} \sim c^{\rm imp}_{f=N}/T \propto \frac{1}{T_K} \ln\frac{T_K}{T} \ . \tag{192}$$

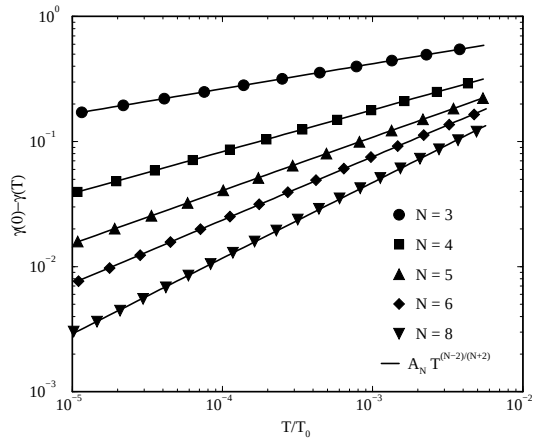

Figure 31: Subleading contribution to $\gamma(T) = C_V^i/T$, for $f = 2$, and $N > f$ vs. T, in a Log-Log graph. The symbols correspond to the numerical calculation. The lines correspond to power-law fits with exponents $(N-2)/(N+2)$.

Finally, in the case $1 < f < N$, also relevant for the N-state tunneling system problem, $\chi^{\rm imp}$ and $c^{\rm imp}/T$ display cusp-like singularities:

$$\chi^{\rm imp}_{f<N} \sim c^{\rm imp}_{f<N}/T \propto \frac{1}{T_K} - B\left(\frac{T}{T_K}\right)^{\frac{N-f}{N+f}} \quad . \tag{193}$$

The above results are only valid for $f > 1$. For $f = 1$ channels, on the other hand, the ground state is always simply that of a Fermi liquid, and $\chi^{\rm imp}$ and $c^{\rm imp}/T$ are analytical functions of T/T_K

The above results can be also verified through the numerical solution of the Bethe ansatz integral equations. As an example, in Fig. 31 we present the scaling of the leading singularity of the linear specific heat coefficient for $f = 2$. The numerical data are in full agreement with Eq. (193).

Let us close this subsection by mentioning that the Bethe ansatz solution can be easily generalized to the case of 'higher' impurity spin representations, which are analogues of an impurity spin $S > 1/2$ in the multichannel Kondo problem. Similar to the multichannel Kondo problem, the low temperature thermodynamics depends then on the details of this representation, which can give rise to new interesting underscreened $SU(N)$ fixed points [85]. Unfortunately, the discussion of these fixed points exceeds already the page limits of the present dissertation.

5 Correlations in mesoscopic devices

Although no rigorous definition exists, we usually call a device 'mesoscopic' if its characteristic size is in the range of $\sim 100 - 10000\mathring{A}$. In these small devices electrons can move coherently, and physical properties of the system usually depend on microscopic details. Moreover, since electrons are confined to a small region, electron-electron interactions start to become very important in these structures.

In most of the present chapter, we shall focus our attention on the physics of mesoscopic grains, metallic islands and quantum dots. All these mesoscopic devices consist of a tiny island weakly connected to various leads that are used to send current through them or control their charge state through the application of gate voltages. While these structures can be prepared using a variety of techniques, they have the common feature that Coulomb interaction-induced electronic correlations play a dominant role in them, and that quantum impurity models are of great value to understand these correlation effects and the physical properties of these systems.

While most of the present chapter deals with grains and quantum dots, at the end of this chapter, we shall also discuss the physics of point contacts. These mesoscopic structures turn out to be ideal tools to study small grains and also to measure the properties of individual atomic defects in detail and test quantum impurities.

5.1 Coulomb blockade and Kondo effect in quantum dots

Although no rigorous definition exists, we typically call a 'quantum dot' a small artificial structure containing conduction electrons, and weakly coupled to the rest of the world. There is a variety of ways to produce these structures: Maybe the most common technique to do this is by defining a typically μ-size region by shaping a two-dimensional electron gas using gate electrodes placed on the top of a semiconductor heterostructure or by etching (see, *e.g.*, Refs. [47, 114, 115]). In Fig. 32 we show the top view of such a single electron transistor (SET) that has been first used to detect the Kondo effect in such a structure [114, 130]. Beside semiconductor technologies, quantum dots can also be built from metallic grains [116, 117], and more recently it became possible to integrate even real molecules into electronic circuits[118]. The common feature of all these devices is that Coulomb correlations play an essential role in them, and induce Coulomb blockade [119] and Kondo effect [114, 120, 121].

There is two essential energy scales that characterize an isolated quantum dot:

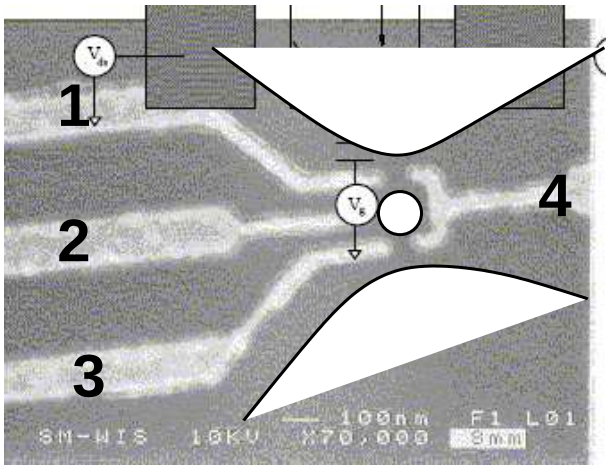

Figure 32: Top view of the SET used by David Goldhaber-Gordon and his collaborators to first observe the Kondo effect in a quantum dot, from Ref. [114]: The white areas indicate regions where conduction electrons are present. The quantum dot is at the central region (white circle). The various electrodes (1-4) have been used to define the dot and the junctions.

One of them is the *charging energy*, E_C, the typical cost of putting an extra electron on the device. The other is the typical separation of single particle energies, also called level spacing, Δ. Typically $\Delta \ll E_C$, but for very small structures (*e.g.* in the extreme case of a molecule) these two energy scales can be of the same order of magnitude. While the charging energy E_C is usually of the order of e^2/L with L the characteristic size of the device, the level spacing Δ depends very much on the material and dimensionality of the dot: it is typically very small in mesoscopic metallic grains, where it roughly scales as $\Delta \sim E_F/(k_F L)^3$, and becomes of the order of one Kelvin only for nanoscale structures with $L \sim 20\mathring{A}$. For two-dimensional semiconductor structures, on the other hand, both k_F and the Fermi energy are much smaller and since Δ scales as $\Delta \sim E_F/(k_F L)^2$, in these structures, Δ becomes of the order of a Kelvin typically for $L \sim 0.1\mu$.

Coulomb correlations may become only important if the measurement temperature is less than the charging energy, $T < E_C$. Clearly, this criterion can be only satisfied with our current cooling technology if E_C is in the range of a few Kelvins, *i.e.* the size of the system is in the μ range or below. The behavior of a quantum dot is also very different in the regimes $T > \Delta$ and $T < \Delta$: while in the former regime electron-hole excitations on the dot are important, for $T < \Delta$ these excitations do not play an essential role.

Beside the difference in the typical energy scales E_C and Δ, there is also a difference in the way semiconducting and metallic devices are usually connected. Although metallic particles can be also contacted through single or few mode contacts using *e.g.* STM tips, these grains are typically connected through multichannel leads with contact sizes much larger than the Fermi wavelength λ_F. Lateral semiconducting devices are, on the other hand, usually contacted through few or single mode contacts (though *e.g.* vertical dots are connected through a large contact area). While these details can be important for some phenomena [122, 123], the behavior of all these devices is very similar in many respects. In the following, we shall therefore mainly focus on lateral quantum dots with single mode contacts.

5.1.1 Coulomb blockade

In almost all systems discussed in the introduction we can describe the isolated dot by the following second quantized Hamiltonian

$$H_{\rm dot} = \sum_{j,\sigma} \epsilon_j \; d^\dagger_{j\sigma} d_{j\sigma} + H_{\rm int} + H_{\rm gate} \; , \tag{194}$$

where the second term describes interactions between the conduction electrons on the island, and the effects of various gate voltages are accounted for by the last term. The operator $d^\dagger_{j\sigma}$ creates a conduction electron in a single particle state φ_j with spin σ on the dot.

Fortunately, the terms $H_C = H_{\rm int} + H_{\rm gate}$ can be replaced in most cases with a very good accuracy by a simple classical interaction term [124]

$$H_C = \frac{e^2}{2C} \left(n_{\rm dot} - \frac{V_g C_g}{e} \right)^2 \; , \tag{195}$$

where C denotes the total capacitance of the dot, C_g is the gate capacitance, e is the electron's charge, V_g stands for the gate voltage (roughly proportional to the voltage on electrode '2' in Fig. 32), and $n_{\rm dot} = \sum_{j,\sigma} : d^\dagger_{j\sigma} d_{j\sigma}$ is the number of extra electrons on the dot. This simple form can be derived by estimating the Coulomb integrals for a chaotic dot [124], however, it also follows from the phenomenon of *screening* in a metallic particle. We outline this rather instructive derivation of Eq. (195) within the Hartree approximation in Appendix B. Clearly, the dimensionless gate voltage $N_g = V_g C_g / e$ sets the number of electrons on the dot, $\langle n_{\rm dot} \rangle \approx N_g$.

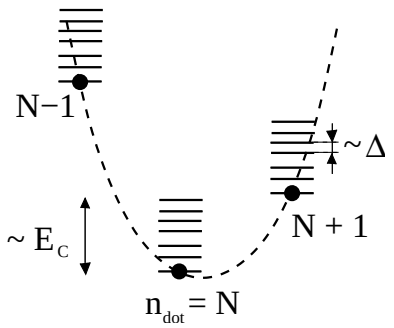

Figure 33: Excitation spectrum of an island. Lines represent eigenenergies of the island. Charging excitations typically need an energy $\sim E_C$ while internal electron-hole and spin excitations cost an energy $\Delta \ll E_C$.

The single particle levels ϵ_j above are random but correlated: The distribution of these levels for typical (*i.e.* large and chaotic) islands is given with a good accuracy by random matrix theory [125], which predicts among others that the separation s between two neighboring states displays a universal distribution,

$$P(s) = \frac{1}{\Delta} p\left(s/\Delta\right) \ , \tag{196}$$

with Δ the average level spacing between two neighboring levels. For small separations, energy levels repel each-other and p vanishes as $p\left(\frac{s}{\Delta}\right) \sim \left(\frac{s}{\Delta}\right)^{\beta}$, where the exponent is $\beta = 1, 2$ or 4, depending on the symmetry of the Hamiltonian (orthogonal, unitary, and symplectic, respectively). In some special cases cross-overs between various universality classes can also occur,and in some cases level repulsion may be even absent for dots with special symmetry properties.

The spectrum of an isolated dot described by Eqs. (194) and (195) is sketched in Fig. 33. As we already mentioned, for typical parameters and relatively large lateral dots or metallic islands, the charging energy is much larger than the level spacing, $E_C \gg \Delta$. Accordingly, internal electron-hole excitations cost much smaller energy than charge excitations of the dot. For dot sizes in the 0.1μm range the capacitance C can be small enough so that the charging energy $E_C = e^2/2C$ associated with putting an extra electron on the dot can safely be in the meV range. Therefore, unless $N_g = \frac{V_g C_g}{e}$ is a half-integer, it costs a finite energy to charge the device, and therefore the number of electrons on the dot becomes quantized at low enough temperatures, $T \ll E_C$, and a Coulomb blockade develops - provided that quantum fluctuations induced by coupling the dot to leads are not very strong.

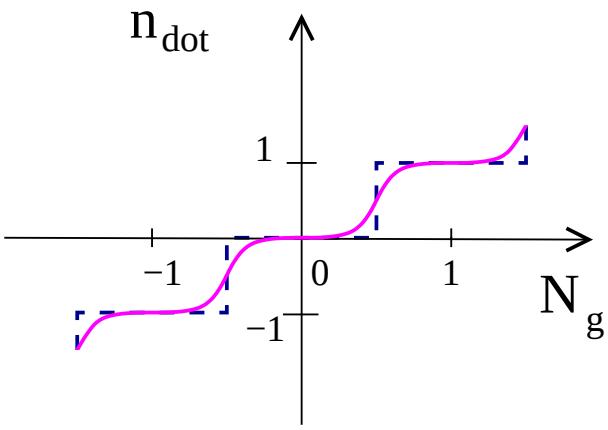

Figure 34: The number of electrons on a quantum dot as a function of the dimensionless gate voltage. The sudden jumps of an isolated dot become smeared out due to quantum fluctuation as soon as we couple the dot to leads.

Let us now consider a quantum dot that is weakly tunnel-coupled to leads, 'weak coupling' in this context meaning that the conductance between the island and the leads is less than the quantum conductance, $G_Q \equiv 2e^2/h$. In the particular case of a lateral quantum dot this condition is satisfied when the last conduction electron channel is being pinched off. If the lead-dot conductance is much larger than G_Q then the Coulomb blockade is lifted by quantum fluctuations. In the absence of tunneling processes, the charge on the dot would change in sudden steps at $T = 0$ temperature (see Fig. 34). However, in the vicinity of the jumps, where $N_g = \frac{V_g C_g}{e}$ is a half-integer, two charging states of the island become almost degenerate. Therefore quantum tunneling to the leads induces quantum fluctuations between these two charging states, smears out the steps, and eventually completely suppresses the steps only leaving some small oscillations on the top of a linear $\langle n_{\rm dot}\rangle(V_g)$ dependence [126]. At a finite temperature $T \neq 0$, thermal fluctuation play a similar role, and the charging steps are also washed out if $T \gg E_C$.

Charge quantization is also reflected in the transport properties of the dot. To study transport through a quantum dot, one typically builds a single electron transistor (SET) by attaching it to two leads, as shown in Figs. 32 and 35. Let us first assume that the conductances G_L and G_R between the dot and the lead on the left / right are small compared to G_Q and that quantum fluctuations are small. In this limit we can describe charge fluctuations on the dot by the following simple tunneling

Hamiltonian:

$$\hat{V} = \sum_j \sum_\epsilon \Big\{ t_j^L \; d_{j\sigma}^\dagger \psi_{L,\epsilon\sigma} + \text{h.c.} \Big\} + \text{“}L \leftrightarrow R\text{''} \; , \tag{197}$$

where we assumed single mode contacts. The fields $\psi_{L,\epsilon\sigma}^\dagger$ and $\psi_{R,\epsilon\sigma}^\dagger$ denote the creation operators of conduction electrons of energy ϵ and spin σ in the left and right leads, respectively, and are normalized to satisfy the anticommutation relations $\{\psi_{L/R,\epsilon\sigma}^\dagger, \psi_{L/R,\epsilon'\sigma'}\} = \delta_{\sigma\sigma'}\delta_{\epsilon\epsilon'}$. Note that the tunneling matrix elements t_j^L and t_j^R fluctuate from level to level since they depend on the amplitude of the wave function φ_j at the tunneling position. Using a simple Boltzmann equation approach one then finds that for $T < E_C$ the linear conductance of the SET has peaks whenever two charge states of the dot are degenerate and N_g is a half-integer. In the regime, $\Delta \ll T \ll E_C$, in particular, one finds that [127]

$$G(T) \approx \frac{1}{2} \frac{G_L G_R}{G_L + G_R} \frac{\Delta E/T}{\sinh(\Delta E/T)} \; , \tag{198}$$

where ΔE is the energy difference between the two charging states of the dot, and $G_{L/R} = (8\pi^2 e^2/h) \; \varrho_{\rm dot} \; \varrho_{L/R} \; \langle |t_j^{L/R}|^2 \rangle_j$ is the tunnel conductance of the two junctions, with $\varrho_{\rm dot}$ and $\varrho_{L/R}$ the density of states on the dot and the leads. Note that even for perfect degeneracy, $\Delta E = 0$, the resistance of the SET is twice as large as the sum of the two junction resistances due to Coulomb correlations. As we decrease the temperature, the conductance peaks become sharper and sharper, while the conductance between the peaks decreases exponentially, and the Coulomb blockade develops. This simple Boltzmann equation picture, however, breaks down at somewhat lower temperatures, where higher order processes and quantum fluctuations become important. These quantum fluctuations may even completely lift the Coulomb blockade and result in a perfect conductance at low temperatures as we shall explain in the next section.

Let us first study the conductance of the SET in the regime where the difference ΔE between the energy of the two charging states considered is much larger than the temperature. It turns out that the range of validity of Eq. (198) describing an activated behavior is rather small for typical parameters, and the conductance is dominated by second order virtual processes as soon as we lower the temperature much below ΔE. From the point of view of these second order processes two regimes must be distinguished: In the regime $\Delta \ll T \ll E_C$ the leading term to the conduc-

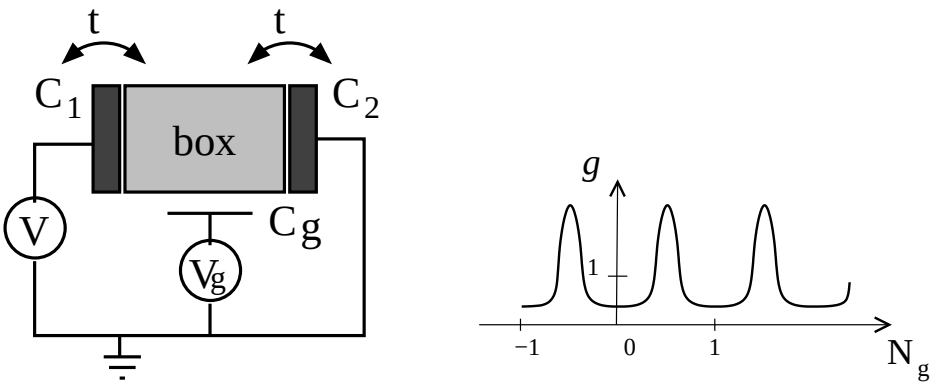

Fig.a Fig.b

Figure 35: (a) Sketch of a single electron transistor. (b) Conductance of the SET as a function of gate voltage for $E_C \ll T \ll \Delta$. At the degeneracy points Coulomb blockade is lifted and transport is allowed through the single electron transistor.

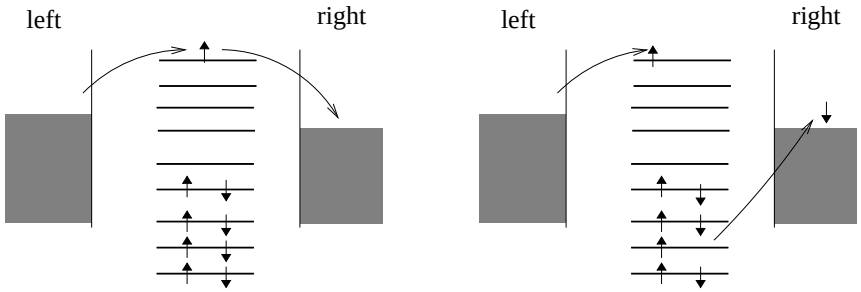

Fig.a Fig.b

Figure 36: Elastic (a) and inelastic (b) co-tunneling processes. Inelastic co-tunneling processes give a conductance $\sim T^2$ while elastic co-tunneling gives a finite conductance as $T \to 0$.

tance comes from elastic and inelastic *co-tunneling* processes shown in Fig. 36 [128]: In the inelastic co-tunneling process a conduction electron jumps into the dot from one lead and another electron jumps out of the dot to the other lead in a second order virtual process, leaving behind (or absorbing) an electron-hole excitation on the dot, while in an elastic co-tunneling it is the same electron that jumps out. Inelastic co-tunneling gives a conductance $G_{\rm inel} \sim G_L G_R (T/E_C)^2/(e^2/h)$, and is thus clearly suppressed as the temperature decreases [128], while elastic co-tunneling results in a small temperature independent residual conductance, $G_{\rm el} \sim G_L G_R (\Delta/E_C)/(e^2/h)$ even at $T = 0$ temperature [128].

5.1.2 Kondo effect

For $T \ll \Delta \ll E_C$ inelastic co-tunneling processes are not allowed, and the properties of the SET depend essentially on the *number of electrons* on the dot. The ground state of the isolated dot must be spin degenerate if there is an *odd number of electrons* on the dot, while it is usually non-degenerate, if the number of electrons on the dot is even. In the latter case nothing special happens: quantum fluctuations due to coupling to the leads produce just a residual conductance as $T \to 0$. If, however, the number of the electrons on the dot is *odd*, then the ground state has a *spin degeneracy*, which can give rise to the Kondo effect discussed below. In this case, exchange processes shown in Fig. 37 give a contribution to the conductance. As we lower the temperature, the effective amplitude of these processes increases due to the Kondo effect, and ultimately gives a conductance that can be as large as the quantum conductance $G_Q = 2e^2/h$ at $T = 0$ temperature [120]. This strong enhancement is due to strong quantum fluctuations of the spin of the dot, and the formation of a strongly correlated Kondo state. The typical temperature-dependence of the conductance for N_g odd is shown in Fig. 38.

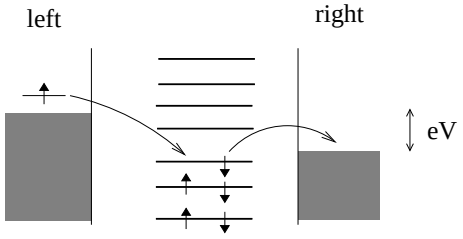

Figure 37: Exchange process leading to the enhancement of the conductance as $T \to 0$.

To understand why the conductance of the dot becomes large, let us keep only the last, singly occupied level that gives rise to the Kondo effect, $d_{j\sigma} \to d_\sigma$, $\epsilon_j \to \epsilon_d$, and write the Hamiltonian of the dot as

$$\begin{aligned} H &= \sum_\sigma \epsilon_d \, d_\sigma^\dagger d_\sigma + H_C \\ &+ \sum_\sigma \sum_{\mu=L,R} \int d\epsilon \, \epsilon \, \psi_{\mu,\sigma}^\dagger(\epsilon)\psi_{\mu,\sigma}(\epsilon) \\ &+ \int d\epsilon \left\{ t^L \varrho_L^{1/2} \, (d_\sigma^\dagger \psi_{L,\sigma}(\epsilon) + \text{h.c.}) + \text{“}L \leftrightarrow R''\right\}, \end{aligned} \tag{199}$$

where we introduced the fields, $\psi_{L,\sigma}(\epsilon) \equiv \varrho_{L/R}^{1/2} \, \psi_{L/R,\epsilon\sigma}$. For the sake of simplicity,

let us assume that $t^R \varrho_L^{1/2} = t^L \varrho_R^{1/2}$. If we then make a unitary transformation and introduce the even and odd field operators,

$$\psi_\pm \equiv \frac{\psi_R \pm \psi_L}{\sqrt{2}} \,, \tag{200}$$

then obviously the odd combination ψ_- fully decouples from the dot, and the tunneling part of the Hamiltonian can be written as

$$\hat{V} = \tilde{t} \int d\epsilon \, (d_\sigma^\dagger \psi_{+,\sigma}(\epsilon) + \text{h.c.}) \,, \tag{201}$$

where $\tilde{t} = \sqrt{2}\; t^R \varrho_R^{1/2}$. One can now perform second order degenerate perturbation theory in $\hat{V}$ in the subspace $\sum_\sigma d_\sigma^\dagger d_\sigma = 1$ to obtain the following effective exchange Hamiltonian:

$$\begin{aligned} H_{\text{eff}} &= \sum_\sigma \sum_\epsilon \, \epsilon \, \psi_{+,\sigma}^\dagger(\epsilon) \psi_{+,\sigma}(\epsilon) \\ &+ \frac{j}{2} \vec{S} \sum_{\sigma,\sigma'} \int\int d\epsilon \, d\epsilon' \psi_{+\sigma}^\dagger(\epsilon) \vec{\sigma}_{\sigma\sigma'} \psi_{+\sigma'}(\epsilon') \,, \end{aligned} \tag{202}$$

where $\vec{S} = \frac{1}{2}(d^\dagger \vec{\sigma} d)$ is the spin of the dot, and $j \sim \tilde{t}^2/E_C$ is a dimensionless antiferromagnetic exchange coupling. Thus electrons in the even channel ψ_+ couple antiferromagnetically to the spin on the partially occupied d-level, and try to screen it to get rid of the residual entropy associated with it.

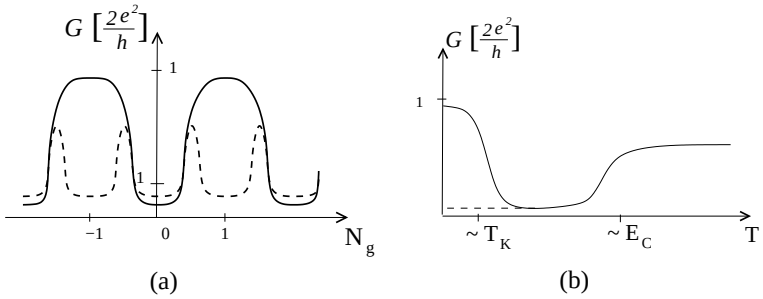

Figure 38: (a) Linear conductance of the SET for $T_K \ll T \ll E_C$ (dashed line) and $T \to 0$ (solid line). (b) Temperature-dependence of the conductance of a SET for an odd number of electrons on the dot (continuous line) and for an even number of electrons with non-degenerate ground state (dashed line).

Written in the original basis, Eq. (202) contains terms $\sim j\vec{S}\psi_R^\dagger(\epsilon)\vec{\sigma}\psi_L(\epsilon')$, which allow for charge transfer from one side of the dot to the other side, and in leading

order these terms give a conductance $\sim j^2$. However, higher order terms in j turn out to give logarithmically divergent contributions,

$$G \sim \frac{e^2}{h}\Big(j^2 + 2\, j^3 \ln(\Delta/T) + \ldots\Big) \,. \tag{203}$$

As a result, the conductance of the device increases as we decrease the temperature and our perturbative approach breaks down at the so-called Kondo temperature,

$$T_K \approx \Delta e^{-1/j} \,. \tag{204}$$

One can try to get rid of the logarithmic singularity in Eq. (203) by summing up the most singular contributions in each order in j. This can be most easily done by performing a renormalization group calculation and replacing j by its renormalized value in the perturbative expression, $G \sim \frac{e^2}{h} j^2$ [4, 7, 8]. However, this procedure does not cure the problem and gives a conductance that still diverges at $T = T_K$,

$$G \sim \frac{e^2}{h} \frac{1}{\ln^2(T/T_K)} \,. \tag{205}$$

It is not difficult to show that then for $t^L \varrho_L^{1/2} = t^R \varrho_R^{1/2}$ the SET must have perfect conductance at $T = 0$ temperature. To show this, let us apply the Friedel sum rule [2, 129]. that relates the number $N_{\rm bound}$ of electrons bound to the impurity and the phase shifts δ of the electrons ψ_+, as

$$N_{\rm bound} = 2\frac{\delta}{\pi} \,, \tag{206}$$

where the factor 2 is due to the spin. This relation implies that in the even channel conduction electrons acquire a phase shift $\delta = \pi/2$, and correspondingly, $\psi_+ \to e^{2i\delta}\psi_+ = -\psi_+$ in course of a scattering process at $T = 0$ temperature. Going back to the original left-right basis, this implies that left and right electrons scatter as

$$\psi_L \to -\psi_R \,, \qquad \psi_R \to -\psi_L \,. \tag{207}$$

In other words, an electron coming from the left is transmitted to the right *without any backscattering*, and thus the quantum dot has a perfect conductance, $2e^2/h$.

We remark here that only a symmetrical device can have a perfect transmission,

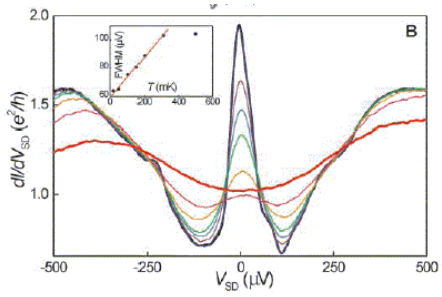

Figure 39: The Kondo resonance appears as a peak in the differential conductance of the SET (figure taken from Ref. [130]). At $T = 0$ temperature the conductance approaches the quantum limit of the conductance, $2e^2/h$.

and only if the the number of electrons on the d-level is approximately one, $\langle n_d \rangle \approx 1$. All the considerations above can be easily generalized to the case $t^L \varrho_L^{1/2} \neq t^R \varrho_R^{1/2}$, and one obtains for the zero temperature conductance in the Kondo limit,

$$G(T \to 0) = \frac{2e^2}{h} \frac{4\varrho_L t_L^2 \, \varrho_R t_R^2}{(\varrho_L t_L^2 + \varrho_R t_R^2)^2} \, , \tag{208}$$

which is clearly less than $2e^2/h$ for non-symmetrical dots.

The phase shift $\delta = \pi/2$ also implies that there must be a *resonance* at the Fermi energy. In fact, this resonance is called the Kondo resonance, and can be directly seen in the differential conductance (related to the density of states as usual) of the single electron transistor shown in Fig. 39. This is a many-body resonance that develops at the Fermi energy (zero bias) as the temperature is cooled down below the Kondo temperature T_K.

The basic transport properties of the SET have been summarized in Fig. 38. Although we could get a fairly good analytical understanding of behavior of a SET, based on the simple considerations outlined above, it is rather difficult to obtain a *quantitative* description. In fact, even to obtain a quantitative description extensive computations such as numerical renormalization group calculations are needed [15]. A valid and complete description of the out of equilibrium physics of a SET is still missing [54, 55, 56].

5.1.3 Orbital degeneracy and correlations in quantum dots

In the previous section we sketched the generic behavior of a quantum dot, and assumed that the separation of the last, partially occupied level is by an energy

distance $\sim \Delta \gg T$ separated from all other single particle levels of the dot. This is, however, not always true. In the case of a symmetrical arrangement like the one shown in Fig. 40, *e.g.*, some of the states of the dot are orbitally degenerate by *symmetry* [132, 133], while in some other cases almost degenerate orbitals may show up just by accident [48, 49]. This orbital degeneracy can play a very important role when we fill up these degenerate (or almost degenerate) levels, and leads to such phenomena as the SU(4) Kondo state [133, 50] or eventually the singlet-triplet transition [48, 49, 132].

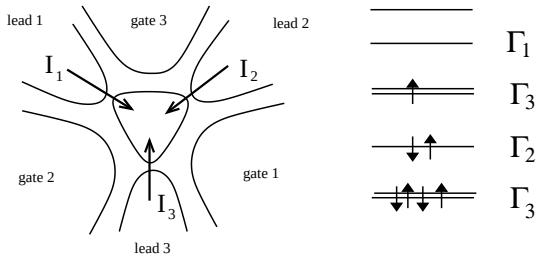

Figure 40: Arrangement with triangular symmetry and the structure of the four-fold degenerate ground state of the isolated triangular dot.

SU(4) physics and triangular dots

Let us first discuss what happens if we have just a single electron on an orbitally degenerate level. As first shown in Ref. [133], the presence of the orbital degeneracy leads to an unusual state of (approximate) SU(4) symmetry in this case, where spin and charge degrees of freedom are entangled. This SU(4) state has been proposed first theoretically to appear in double dot systems and quantum dots with triangular symmetry in Refs. [50] and [133]. However, while there is no unambiguous experimental evidence of an SU(4) Kondo effect in double dot devices [134], the SU(4) state has been recently observed in vertical dots of cylindrical symmetry [51] as well as in carbon nanotube single electron transistors [135]. In both chases the degeneracy index is due to a chiral symmetry just as in Ref. [133]. Other realizations of states with SU(4) symmetry have been also proposed later in more complicated systems [136, 137], and also in the context of heavy fermions [138].

For the sake of concreteness, we shall focus here to the case of the triangular dot shown in Fig. 40. However, our discussions carry over with trivial modifications to the previously mentioned experimental systems in Refs. [51] and [135]. Let us first assume that we have two orbitally degenerate levels $|\pm\rangle$ that can be labeled by some

chirality index $\tau = \pm$, and let us focus on the charging of this multiplet only. At the Hartree-Fock level, these levels of the isolated dot can be described by:

$$H_{\rm dot} = \sum_{\tau,\tau',\sigma} d^\dagger_{\tau\sigma}(E_{\tau\tau'} + \Delta E\ \delta_{\tau\tau'})d_{\tau'\sigma} - \frac{J_H}{2}\vec{S}^{\,2} + \frac{E_C}{2}(n_+ + n_-)^2 + \frac{\tilde{E}_C}{2}(n_+ - n_-)^2\ , \tag{209}$$

where $d^\dagger_{\tau\sigma}$ creates an electron on the dot within the degenerate multiplet with spin σ and orbital label τ. The energy shift ΔE above is proportional to the (symmetrically-applied) gate voltage and controls the charge on the dot, while $E_{\tau\tau'}$ accounts for the splitting generated by deviations from perfect triangular symmetry ($\sum_\tau E_{\tau\tau} = 0$). We denote the total number of electrons in state $\tau = \pm$ by $n_\tau \equiv \sum_\sigma d^\dagger_{\tau\sigma}d_{\tau\sigma}$, and $\vec{S} = \frac{1}{2}\sum_{\tau,\sigma,\sigma'} d^\dagger_{\tau\sigma}\vec{\sigma}_{\sigma\sigma'}d_{\tau\sigma'}$ is the total spin of the dot. The terms proportional to E_C and $\tilde{E}_C$ are generated by the Hartree interaction, while that proportional to J_H in Eq. (209) is the Hund's rule coupling, generated by exchange. This term has no importance if there is only a single electron on the dot.

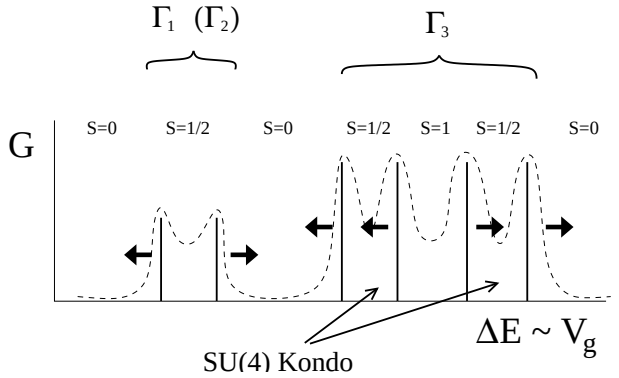

Figure 41: Structure of the Coulomb blockade peaks of the triangular dot. The multiplets are labeled by the corresponding irreducible representations. The arrows indicate the direction the peaks move when applying a Zeeman field.

Let us first consider the linear conductance. The currents I_j between leads j and the dot are related to the voltages V_j applied on them by the conductance tensor,

$$I_j = \sum_{j'} G_{jj'}V_{j'}\ , \tag{210}$$

which further simplifies to $G_{jj'} = \frac{3}{2}G\delta_{jj'} - G/2$ for a symmetrical system. A schematic plot of the conductance G as a function of ΔE is shown in Fig. 41.

The arrangement of the four Coulomb blockade peaks associated to the Γ_3 state is symmetrical, and the height of the four peaks turns out to be numerically almost identical at high temperatures [133].

The most interesting regime in Fig. 41 appears between the first two peaks. Here there is one electron on the dot, and correspondingly the ground state of the isolated dot is fourfold degenerate. Let us now tunnel couple the dots to conduction electrons in the three leads, ψ_j ($j = 1, 2, 3$). To simplify the Hamiltonian we first introduce new fields that transform with the same symmetry as the states $|\tau\rangle$,

$$\psi_j \to \psi_\pm \equiv \frac{1}{\sqrt{3}} \sum_j e^{\pm i\, 2\pi j/3} \psi_j \ . \tag{211}$$

With this notation the tunneling Hamiltonian of a perfectly symmetrical dot becomes

$$\hat{V} = t \sum_{\sigma,\tau} \int d\epsilon \left(d^\dagger_{\tau\sigma} \psi_{\tau\sigma}(\epsilon) + h.c. \right) . \tag{212}$$

To describe the fourfold degenerate ground state of the dot, we can introduce the spin and and orbital spin operators $\vec{S}$ and $\vec{T}$, with $S_z = \pm 1/2$ and $T_z = \pm 1/2$ corresponding to the states $\sigma = \pm$ and $\tau = \pm$. Likewise, we can introduce spin and orbital spin operators $\vec{\sigma}$ and $\vec{\tau}$ also for the conduction electrons, and then proceed as in the previous section to generate an effective Hamiltonian by performing second order perturbation theory in the tunneling $\hat{V}$, Eq. (212). The resulting interaction Hamiltonian is rather complex, and contains all kinds of orbital and spin couplings of the type $\sim T^+\tau^- \vec{S}\vec{\sigma}$ or $\sim T^z\tau^z$ [50, 133]. These terms are generated by processes like the one shown in Fig. 42, and clearly couple spin and orbital fluctuations to each-other.

Fortunately, a renormalization group analysis reveals that at low temperatures the various couplings become equal, and the Hamiltonian can be simply replaced by the following, remarkably simple SU(4) symmetrical effective Hamiltonian (Coqblin-Schrieffer model),

$$H_{\rm eff}(T \to 0) = \tilde{J} \sum_{\alpha,\beta=1,..,4} \psi^\dagger_\alpha \psi_\beta \, |\beta\rangle\langle\alpha| \ , \tag{213}$$

where the index α labels the four combinations of possible spin and pseudospin indices, and the $|\alpha\rangle$'s denote the four states of the dot. This can be also verified by solving the original complicated Hamiltonian by the powerful machinery of numerical renormalization group [10, 50]. The numerical renormalization group spectrum of

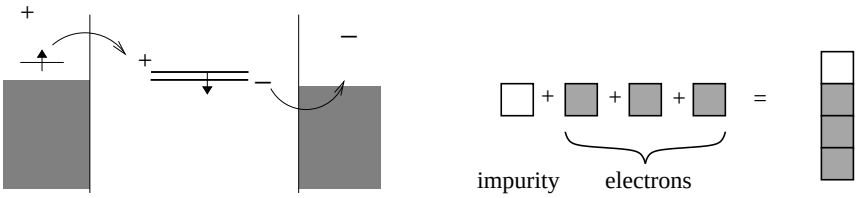

Fig. a Fig. b

Figure 42: (a) Example of a virtual process generating a coupling between the spin and the orbital spin. (b) To screen the SU(4) spin of a triangular dot one needs three conduction electrons. The singlet formed corresponds to the Young tableau on the right, while the defining four-dimensional SU(4) representations are denoted by squares.

the strongly anisotropic model is shown in Fig. 43, and exhibits a beautiful structure, characteristic of the SU(4) Coqblin-Schrieffer model.

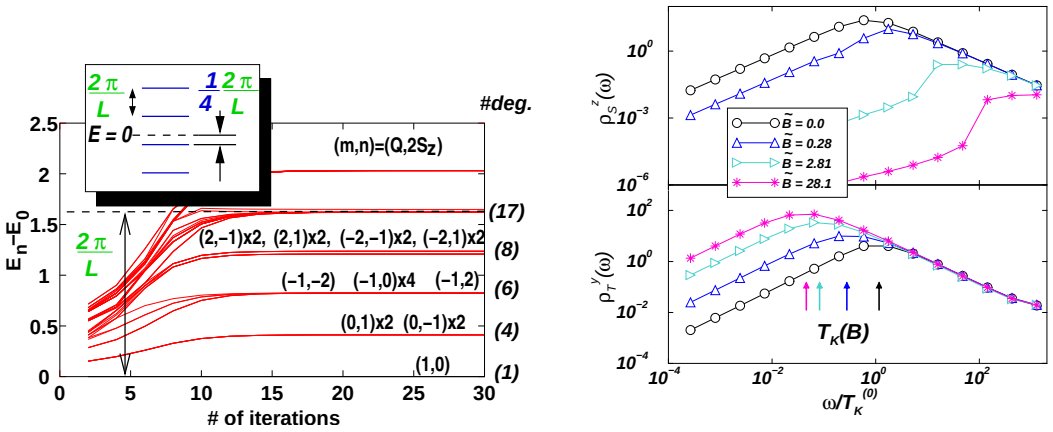

Fig. a Fig. b

Figure 43: (a) Finite size spectrum of the double dot system. The regular pattern is characteristic of the SU(4) fixed point. (b) Spin and orbital spin spectral functions as a function of an external field.

We remark here that the structure of the fixed point Hamiltonian, Eq. (213) is rather robust. Even if the system does not have a perfect triangular symmetry, the exchange part of the effective Hamiltonian at low temperatures will take the form Eq. (213), and the effect of imperfect symmetry only generates some splitting $E_{\tau\tau'}$ for the orbitally degenerate levels and some small potential scattering [108]. These terms, of course, break the SU(4) symmetry of Eq. (213), but represent only marginal perturbations, and do not influence the physical properties of the system if they are small. In a similar way, the SU(4) symmetric fixed point discussed here may be

relevant even for systems with (approximate) accidental degeneracy even if they do not have a perfect SU(4) symmetry. Spin and orbital entangled states apparently also show up in molecular clusters, but there they may lead to the appearance of unusual non-Fermi liquid states [139, 140, 141].

The Hamiltonian Eq. (213) is one of the exactly solvable models [13], and has been studied thoroughly before [24, 112]. Just as in the Kondo problem, the SU(4) spin of the dot is screened below the 'SU(4)' Kondo temperature, $T_K^{(0)}$. However, to screen an SU(4) spin, one needs *three* conduction electrons, as shown in Fig. 42. As a result, the Friedel sum rule in the present case is modified to

$$3 = \sum_{\sigma,\tau} \frac{\delta_{\sigma\tau}}{\pi} = 4\frac{\delta}{\pi} \,, \tag{214}$$

corresponding to a phase shift $\delta = 3\pi/4$ for the electrons $\psi_{\pm,\sigma}$.

The application of a magnetic field on the dot, $H \to H - B\, S^z$ clearly suppresses spin fluctuations.[3] However, it does not suppress orbital fluctuations, which still lead to a more conventional SU(2) Kondo effect, by replacing the spin in the original Kondo problem. The Kondo temperature of this orbital Kondo effect is, however, somewhat reduced compared to the SU(4) Kondo temperature [133],

$$T_K^{\rm orb} \sim \frac{(T_K^{(0)})^2}{\Delta} \,. \tag{215}$$

The emergence of this new scale and the suppression of the spin Kondo effect can be nicely seen in the numerically computed spin and pseudospin spectral functions of Fig. 43. The phase shifts in this case are simply $\delta_{\pm,\uparrow} \approx \pi/2$, while $\delta_{\pm,\downarrow} \approx 0$, just as for the original Kondo problem. The splitting of the two levels $\tau = \pm$ has a similar effect and drives the dot to a simple spin SU(2) state.

The zero-temperature phase shifts can be related to the transport properties of the device: From the $T = 0$ phase shifts $\delta_{\tau\sigma}$ one can construct the conduction electrons' scattering matrix in the original basis ψ_j and compute all transport coefficients using the Landauer-Buttiker formula [142, 133, 143]. The $T = 0$ conductance G turns out to be independent of the magnetic field, and both for the SU(4) and

[3] A Zeeman field B corresponds to a field applied parallel to the surface in a lateral quantum dot experiment.

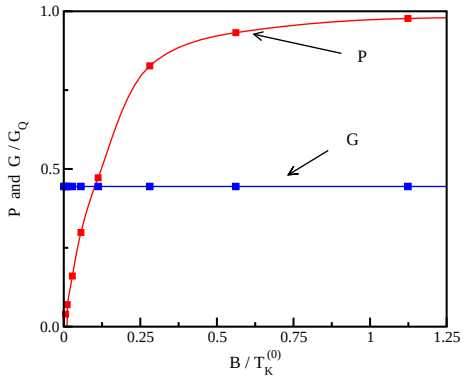

Figure 44: Spin polarization of the current through the triangular dot as a function of magnetic field.

orbital Kondo states one finds the same value,

$$G(B) = \frac{8e^2}{9h} \sum_\sigma \sin^2(\delta_\sigma(B)) = \frac{8e^2}{9h} \ .$$

The *polarization* of the current,

$$P = \frac{\sin^2(\delta_\uparrow) - \sin^2(\delta_\downarrow)}{\sin^2(\delta_\uparrow) + \sin^2(\delta_\downarrow)} \ , \tag{216}$$

however, *does* depend on the magnetic field and takes the values $P = 0$ and $P = 1$ in the SU(4) and orbital Kondo states, respectively. The phase shifts in Eq. (216) can be extracted with very high accuracy from the finite size spectrum computed via the numerical renormalization group procedure [10, 50, 61], and the results (originally computed for the double dot system in Ref. [50]) are shown in Fig. 44. Clearly, this device can be used as a spin filter: Applying a Zeeman field one can induce a large spin polarization at low temperatures while having a large $\sim e^2/h$ conductance through the device. A slightly modified version of this spin filter has indeed been realized in Ref. [135], where two orbital states originating from different multiplets have been used to generate the orbital Kondo effect.

To close the analysis of the SU(4) Kondo effect, let us shortly discuss how the SU(4) state emerges in capacitively coupled quantum dots, where it actually has been identified first. In this device, shown in Fig. 45, the capacitively coupled dots

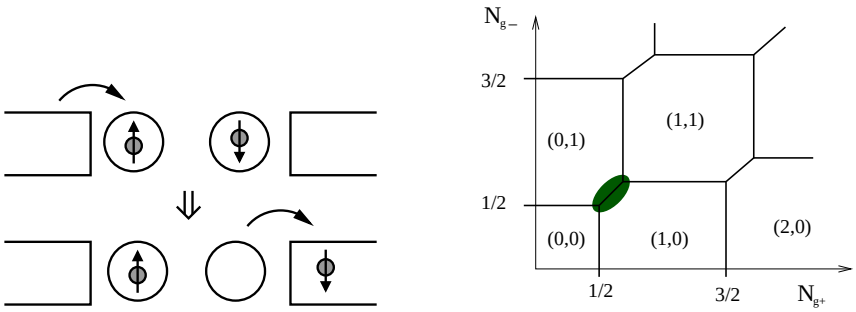

Fig.a Fig.b

Figure 45: (a) A virtual process leading to entanglement between charge and spin fluctuations and the SU(4) Kondo state in the double dot device. (b) Charging states of the double dot device as a function of the dimensionless gate voltages $N_{g\pm}$. The colored region indicates the regime where the two states $(1,0)$ and $(0,1)$ are almost degenerate.

can be described by the following simple Hamiltonian

$$H_{\rm dot} = \frac{E_{C+}}{2}(n_+ - N_{g+})^2 + \frac{E_{C-}}{2}(n_- - N_{g-})^2 + \tilde{E}_C n_+ n_- \ , \qquad (217)$$

where the dimensionless gate voltages $N_{g\pm}$ set the number n_+ and n_- of the electrons on the left and right dots, respectively. The last term is due to the capacitive coupling between the two dots, and it is essentially this term which is responsible for the SU(4) physics discussed. As shown in Fig. 45.b, in the parameter space of the two-dot regions appear, where the two states $(n_+, n_-) = (1,0)$ and $(n_+, n_-) = (0,1)$ are almost degenerate, while the states $(n_+, n_-) = (0,0)$ and $(n_+, n_-) = (1,1)$ are pushed to higher energies of order $\sim \tilde{E}_C$. In the simplest, however, most frequent case the states $(1,0)$ and $(0,1)$ have both spin $S = 1/2$, associated with the extra electron on the dots. Therefore, in the regime above for temperatures below the charging energy $\tilde{E}_C$ and the level spacing Δ of the dots, the dynamics of the double dot is restricted to the subspace $\{S^z = \pm 1/2;\ n_+ + n_- = 1\}$, and we can describe its charge fluctuations in terms of the *orbital pseudospin* $T^z \equiv (n_+ - n_-)/2 = \pm\frac{1}{2}$. Coupling the two dot system to leads, we arrive at the very same Hamiltonian as for the triangular dots, although with very different parameters. Much of the previous discussions apply to this system as well which, in addition to being a good spin-filter, also exhibits a giant magneto-resistance [50].

Singlet-triplet transition

So far we discussed the case where there is a single conduction electron on the degenerate levels. The regime between the two middle peaks in Fig. 41 where there is two electrons on the (almost) degenerate multiplet is, however, also extremely interesting.

In this regime the Hund's rule coupling J_H in Eq. (209) is very important. This coupling is usually smaller than the typical level spacing Δ. If, however, it is larger than the separation between the last occupied and first empty levels, $\delta\epsilon$, then it gives rise to a triplet ground state with $S = 1$. Since in many cases one can shift the levels and actually tune $\delta\epsilon$ by an external magnetic field [48, 135] or simply by changing the shape of the dot by gate electrodes [49], one can actually drive the a quantum dot from a triplet to a singlet state as illustrated in Fig. 46. Although in the case of a triangular dot or a nanotube $\delta\epsilon \approx 0$ are guaranteed by symmetry [133, 135], almost degenerate states may also occur in usual single electron transistors just by accident [48].

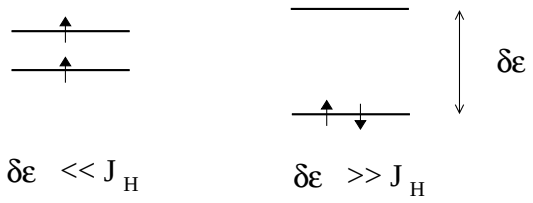

Figure 46: The state of a quantum dot changes from a triplet to a singlet as the separation $\delta\epsilon$ between the last occupied and first empty level increases.

While this transition has been first studied in vertical dots [132, 143, 144], here we shall focus on the usual lateral arrangement of Fig. 46 which has very different transport properties [48, 61, 145]. For the sake of simplicity let us assume that we have a completely symmetrical device and that the two levels $|\pm\rangle$ participating in the formation of the triplet state are even and odd. In this case we can introduce the even and odd fields $\psi_\pm \equiv (\psi_R \pm \psi_L)/\sqrt{2}$ by Eq. (200), which by symmetry only couple to the even and odd states, $|+\rangle$ and $|-\rangle$, respectively. The hybridization term in this case simply reads

$$\hat{V} = t_+ \sum_\sigma \int d\epsilon \left(d^\dagger_{+\sigma} \psi_{+\sigma}(\epsilon) + h.c. \right) + t_- \sum_\sigma \int d\epsilon \left(d^\dagger_{-\sigma} \psi_{-\sigma}(\epsilon) + h.c. \right) . \qquad (218)$$

To describe the isolated dot we can use the following simplified version of Eq. (209),

$$H_{\rm dot} = \sum_\sigma \Big(\epsilon_+ d^\dagger_{+\sigma} d_{+\sigma} + \epsilon_- d^\dagger_{-\sigma} d_{-\sigma} \Big) - \frac{J_H}{2} \vec{S}^{\,2} + \frac{E_C}{2} (n_+ + n_-)^2 \; . \tag{219}$$

It is instructive to study the triplet state of the dot first, $\delta\epsilon \ll J_H$. Second order perturbation theory in Eq. (218) in this regime gives the following Hamiltonian replacing (202)

$$\begin{aligned} H_{\rm eff} \;\; &= \;\; \sum_{\tau=\pm} \sum_\sigma \sum_\epsilon \; \epsilon \; \psi^\dagger_{\tau,\sigma}(\epsilon) \psi_{\tau,\sigma}(\epsilon) + \frac{j_+}{2} \vec{S} \sum_{\sigma,\sigma'} \int\int d\epsilon \; d\epsilon' \psi^\dagger_{+\sigma}(\epsilon) \vec{\sigma}_{\sigma\sigma'} \psi_{+\sigma'}(\epsilon') \\ &+ \;\; \frac{j_-}{2} \vec{S} \sum_{\sigma,\sigma'} \int\int d\epsilon \; d\epsilon' \psi^\dagger_{-\sigma}(\epsilon) \vec{\sigma}_{\sigma\sigma'} \psi_{-\sigma'}(\epsilon') \; . \end{aligned} \tag{220}$$

Clearly, the even and odd electrons couple with different dimensionless exchange couplings $j_\pm$ to the spin. However, now $\vec{S}$ is a spin $S = 1$ operator, and to screen it completely, one needs to bind *two* conduction electrons to it. This implies that an electron from both the even and the odd channels will be bound to the spin, and correspondingly two consecutive Kondo effects will take place at temperatures

$$T_+ \approx \Delta \; e^{-1/j_+} \;\; \gg \;\; T_- \approx \Delta \; e^{-1/j_-} \; . \tag{221}$$

This also implies that the conductance at $T = 0$ temperature must vanish in the Kondo limit by the following simple argument [145]: Again, we can use the Friedel sum rule to obtain the $T = 0$ temperature phase shifts $\delta_\pm = \pi/2$ in both the even and odd channels. In the original left-right basis this implies that the lead electrons scatter as $\psi_{L/R} \to -\psi_{L/R}$, *i.e.*, their wave function vanishes at the dot position (by Pauli principle), and $\psi_{L/R}$ are completely reflected.

It is a simple matter to express the $T = 0$ temperature conductance in terms of the $T = 0$ temperature phase shifts using the Landauer-Buttiker formula as [142]

$$G = \frac{e^2}{h} \sum_\sigma \sin^2(\delta_{+,\sigma} - \delta_{-,\sigma}) \; . \tag{222}$$

This formula immediately implies that the conductance as a function of a Zeeman field B must be non-monotonic [145]: for $T_- \ll B \ll T_+$ the Kondo effect in the odd channel is suppressed and correspondingly the phase shifts in this channel are approximately given by $\delta_{-\uparrow} \approx \pi$ and $\delta_{-\downarrow} \approx 0$, and by Eq. (222) the conductance must

be close to $2e^2/h$. The magnetic field-dependence of the phase shifts obtained from a numerical renormalization group calculation and the corresponding conductance are shown in Fig. 47 [61]. By general arguments, similar non-monotonic behavior must occur in the temperature- and bias-dependence of the conductance, as it has indeed been observed experimentally [145, 48].

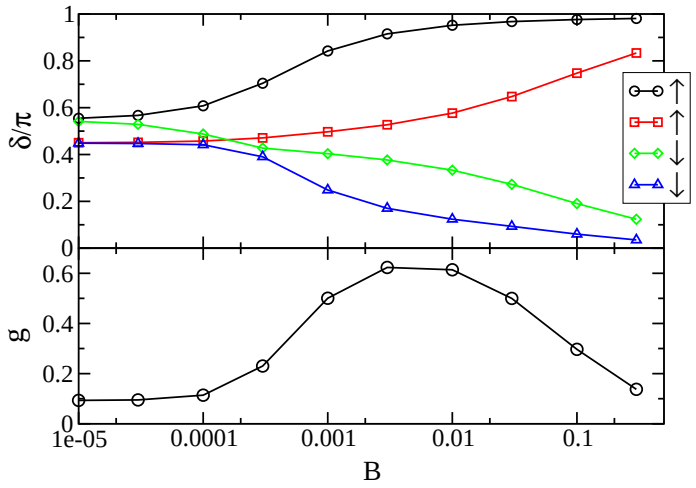

Figure 47: Phase shifts (top) and dip structure in the conductance as a function of Zeeman field B on the triplet side of the transition at zero temperature.

Clearly, the $T = 0$ temperature conductance must be also small on the singlet side of the transition, $\delta\epsilon \gg J_H$, where the dot is in a singlet state and no Kondo effect occurs. However, in the vicinity of the degeneracy point, $\delta\epsilon \approx J_H$, the triplet and the singlet states of the dot are almost degenerate, and quantum fluctuations between these four states generate another type of strongly correlated state with an increased Kondo temperature and a large conductance [48, 61, 145].

To compute the full $T = 0$ conductance as a function of $\delta\epsilon$, non-perturbative methods such as numerical renormalization group are needed [61]. In the vicinity of the transition point the conductance goes up to $2e^2/h$, in perfect agreement with the experimental observations. While the non-monotonic behavior characteristic of the triplet disappears in the vicinity of the transition, it reappears on the singlet side. However, there the size of the dip is not determined by the smaller Kondo scale, T_-, but rather by the excitation energy of the triplet, $\sim \delta\epsilon - J_H$ [48, 61]. Note that the transition between the triplet and singlet states is smooth and the singlet-triplet transition is rather a cross-over than a phase transition in the above scenario.

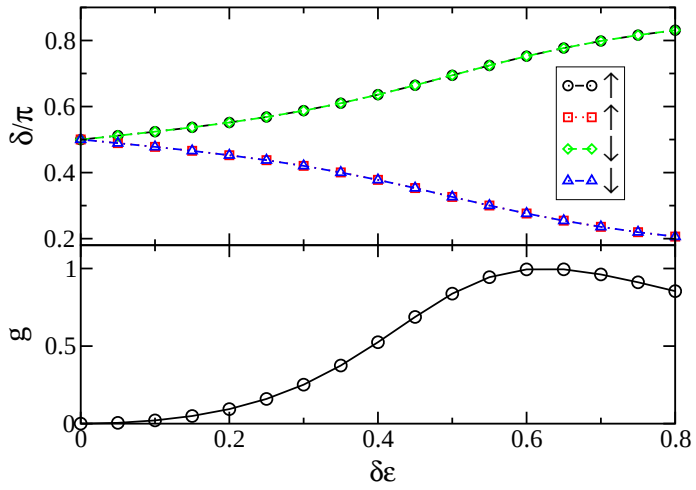

Figure 48: Phase shifts (top) and corresponding conductance (bottom) as a function of orbital splitting $\delta\epsilon$ at temperature $T = 0$.

Also, the picture outlined above changes substantially if both states $|\pm\rangle$ happen to have the same symmetry, and couple only to one of the fields, say ψ_+. In this case the spin of the dot cannot be screened on the triplet side even at $T = 0$ temperature, and a real Kosterlitz-Thouless type quantum phase transition occurs, where the $T = 0$ temperature conductance has a jump at the transition point [146]. The triplet phase in this case is also anomalous, and in fact is of a 'marginal Fermi liquid type' [104, 147], since the spin is *underscreened*. Correspondingly, the conductance saturates very slowly, and behaves asymptotically as $G \sim cst - 1/\ln^2(T_+/T)$. Similar behavior is expected to occur if the smaller Kondo temperature T_- is much below the measurement temperature, and indeed a behavior in agreement with the Kosterlitz-Thouless scenario of Ref. [146] has been observed in some experiments [49].

5.1.4 Kondo effect from ferromagnetic grains

In quantum dots the Hund's rule coupling is small, and the formation of the triplet state is a consequence of 'accidental degeneracy'. This must be contrasted to ferromagnetic grains, where the Hund's rule coupling plays an an essential role and the magnetic moment of the cluster is typically large.

One expects that for a large ferromagnetic cluster the spin of the cluster should behave as a classical object and no Kondo effect should be found. Experiments of Odom *et al.* have found, however, that small ferromagnetic grains can display zero-

bias anomalies clearly indicating the formation of a correlated Kondo state [148]. In these experiments small clusters of Co have been deposited on carbon nanotubes and transport through these clusters has been measured by means of an STM tip directly positioned above the cluster. The clusters consisted of 10 up to 50 atoms, but only the small clusters exhibited a clear zero bias anomaly with an experimentally observed Kondo temperature as large as $T_K \sim 80$ K.

Motivated by these experiments, in this section we shall attempt to understand how the strongly correlated Kondo state disappears as we increase the size of a ferromagnetic cluster.

Itinerant model

First we shall analyze a cluster described by the mean field Hamiltonian,

$$H_{\rm cluster} = \sum_{j,\sigma} \epsilon_j d^\dagger_{j\sigma} d_{j\sigma} - \frac{J_H}{2}\vec{S}^2 + \frac{E_C}{2}(\hat{N} - n_g)^2 \,, \tag{223}$$

which is a simplified version of Eq. (209). Throughout this section we shall denote the number of electrons on the dot by $\hat{N}$. This Hamiltonian has been successfully used earlier to study the transport properties of itinerant ferromagnetic grains within a master equation approach [149, 150]. In the end of this section we shall also construct and analyze another mean field model of local moment ferromagnetism, where local moments couple to conduction electrons antiferromagnetically to form a ferromagnetic state.

In order to have a cluster spin that increases linearly with the number of atoms N_A on the cluster, J_H in Eq. (195) must clearly scale as $J_H \sim 1/N_A$. We therefore introduce the energy scale $U \equiv J_H N_A > 0$, which is roughly independent of the size of the cluster. In the present context the first term in Eq. (223) represents the kinetic energy of the hybridized s, p and d-band electrons on the cluster The second term in Eq. (223) gives rise to a spontaneous polarization of the cluster by making spin alignment of different levels energetically favorable, while the last term describes the charging energy of the cluster with N_g the dimensionless gate voltage. In the more general situation a magnetic anisotropy term should be added to the Hamiltonian. Nevertheless, for the experimentally investigated clusters this anisotropy is much less then the width of the Kondo resonance observed, and we shall therefore neglect it.

The Hamiltonian in Eq. (223) can be diagonalized exactly and the ground state

can be explicitly constructed as

$$|S_0, S^z = S_0\rangle_G^N = \prod_{j=1}^{n_\uparrow} d_{j\uparrow}^\dagger \prod_{j=1}^{n_\downarrow} d_{j\downarrow}^\dagger |vac\rangle \tag{224}$$

with S_0 and N the spin and particle number in the ground state. The remaining states within the ground state multiplet can be generated by applying the operator $S^- = \sum_j d_{j\downarrow}^\dagger d_{j\uparrow}$ to this state. In itinerant ferromagnets there is an approximate rigid band splitting between spin up and spin down electron density of states [151]. In the mean field model, this band splitting energy can be defined as the energy difference between the highest occupied spin up level, ϵ_A, and the highest occupied spin down level, ϵ_I:

$$\Delta_s \equiv \epsilon_A - \epsilon_I \ ,$$

and is typically of the order of a few electron volts [151]. The value of Δ_s is determined by demanding that the ground state of the ferromagnetic cluster be stable to fluctuations of energy level occupations with constant particle number, and is related to the interaction parameter U as [149]

$$U = \frac{N_A}{S_0}\Delta_s + d_0 \ , \tag{225}$$

where d_0 is a mesoscopic sample-dependent scale, $d_0 \sim 1/N_A$.

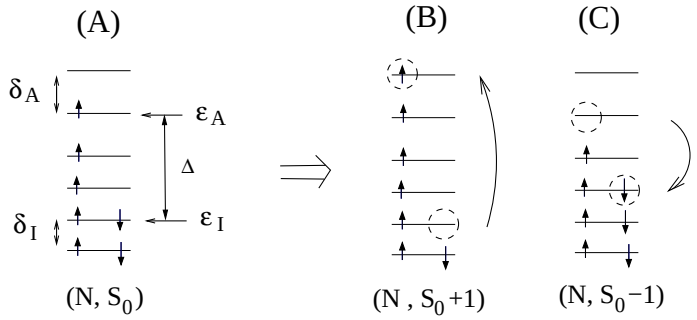

Figure 49: Spin excitations of a ferromagnetic nanoparticle. For the precise definition of $\epsilon_{A/I}$, $\delta_{A/I}$, and Δ_s see text. Fig. A: The fully polarized ground state. Figs. B and C: Lowest lying particle-hole excitations having energy $\sim \delta_{A/I}$.

For later purposes we also determine the energy of various excitations of the cluster. The lowest energy particle-hole excitations turn out to be the ones shown

in Fig. 49, and have energies

$$\delta E(S_0 \pm 1, N) \equiv \min\{E_{\rm excited}(S_0 \pm 1, N) - E_G\} \sim \delta_A, \delta_I \ . \tag{226}$$

where E_G denotes the ground state energy, and δ_A (δ_I) is the level spacing near ϵ_A (ϵ_I). The minimum cost of adding a particle or a hole to the cluster so that the total spin changes as $S_0 \to S_0 + \sigma/2$ is given by $\delta E_{\pm,\sigma}$. These energies can also be estimated by carrying out a stability analysis similar to the previous one to find that typically

$$\delta E_{\pm,\sigma} \equiv \min\{E(N \pm 1, S_0 + \sigma/2) - E_G\} \sim E_C \ . \tag{227}$$

Let us now couple our cluster to a lead through a tunnel coupling.While the theory has been worked out for the general case in Ref. [153], for the sake of simplicity we shall assume here that there is only a single point of contact. Then the tunneling Hamiltonian can be written as

$$\hat{V} = \sum_{\sigma,j,\epsilon} (t^j_\epsilon d^\dagger_{j\sigma} a_{\epsilon\sigma} + h.c.) \ , \tag{228}$$

where $a_{\epsilon\sigma}$ denotes the creation operator of a conduction electron of energy ϵ in the lead. The tunneling coefficients above are proportional to the product of the wave functions ψ_ϵ and φ_j of the electrons in the lead and at the dot at the tunneling position $\vec{R}$. These amplitudes have therefore random phases and amplitudes and scale as $t^j_\epsilon \sim \varphi_j(\vec{R})^* \psi_\epsilon(\vec{R}) 1/\sqrt{N_A}$.

Let us first compute the tunneling spectrum of the cluster through an attached STM tip at position $\vec{r}$. This is approximately given by

$$\frac{dI}{dV}(\vec{r}, V) \propto \varrho(\vec{r}, eV) = -\frac{1}{\pi} {\rm Im}[G^R(\vec{r}, \omega = eV)], \tag{229}$$

where G^R denotes the retarded Green's function and V is the voltage drop between the STM tip and the cluster. Though it is not very simple, one can carry out perturbation theory up to second order in the t^j-s to compute the tunneling spectrum. To lowest order, the STM spectrum of the cluster can then be approximated as [153]

$$\frac{dI}{dV} \propto \sum_{j,\sigma,\pm} |\varphi_j(\vec{r})|^2 \frac{\Gamma^j_{\pm,\sigma}}{(\omega \mp \delta E^j_{\pm,\sigma})^2 + (\Gamma^j_{\pm,\sigma}/2)^2} \tag{230}$$

where $\delta E^j_{\pm,\sigma}$ denotes the energy cost of adding a particle or hole to *any* level j in the ground state, $\delta E^j_{\pm,\sigma}(N \pm 1, S_0 + \sigma/2)$, and $\Gamma^j_{\pm,\sigma}$ is the total decay rate of this excited state. It must be emphasized that $\Gamma^j_{\pm,\sigma}$ incorporates all possible decay processes generated by the couplings t^j to the lead, and these processes leave the cluster in general in some excited state with some particle-hole excitations. As a result, $\Gamma^j_{\pm,\sigma}$ is *not* simply the broadening of the j's single particle level, $\Gamma^j_0 \approx 2\pi\varrho(\epsilon = \pm\delta E^j_{\pm,\sigma})\langle|t^j_\epsilon|^2\rangle_\epsilon$, with $\varrho(\epsilon)$ the density of states of the electrons in the lead.

Typical tunneling spectra computed in this way are shown in Fig. 50 for a cluster of $N_A = 32$ atoms. For the sake of simplicity, we neglected the fluctuations of the single particle decay rates, $\Gamma^j_0 = \Gamma_0 = .02$eV, and those of the amplitudes $\varphi_j(\vec{r})$. We also fixed the charging energies $E^+_C = .01$eV, $E^-_C = .08$eV, and took level spacings δ_A and δ_I, that correspond to a Co cluster of this size. Remarkably, the only difference between the two spectra in Fig. 50 is just a small change in the value of the unknown mesoscopic energy d_0 that appears in Eq. (225). The small difference in d_0 completely changes the structure of the STM spectrum by opening up more decay channels on the electron or hole side of the STM spectrum, and makes the spectrum very asymmetrical, thereby reproducing this characteristic feature of the experimental spectra [148]. The dip in the middle of the spectrum is just the Coulomb gap, while the many small peaks correspond to single particle excitations of the cluster.

The above perturbative approach is, of course, unable to account for the Kondo anomaly observed in small clusters. Therefore we followed the strategy of [154] of simply estimating the Kondo temperature and then adding the corresponding resonance to the STM spectrum by hand. To obtain the Kondo temperature, we first have to compute the effective exchange coupling between the cluster spin and the spin of the electrons. A relatively straightforward second order calculation yields in this case that the Kondo coupling is given as a some of three terms,

$$J = J_d + J_s + J_e \; . \tag{231}$$

The couplings J_d and J_e are generated by virtual tunneling processes to empty and doubly occupied states on the cluster and are *ferromagnetic*, while J_s comes from the singly occupied states and is therefore antiferromagnetic. Instead of giving the full and rather lengthy expression of these terms, let us consider the limit where the level spacings are small. Then the dimensionless coupling $j = J\varrho_0$ can be expressed

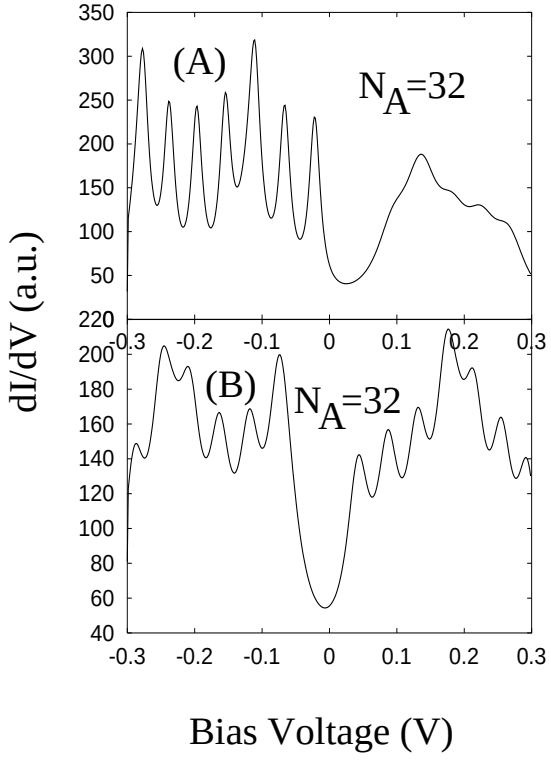

Figure 50: Calculated STM spectra of nanometer-size ferromagnetic clusters with parameters $N_A = 32$, $E_C^+ = .01$eV, $E_C^- = .08$eV, $\Gamma_0^j = \Gamma_0 = .02$eV, and $|\varphi(\vec{r})|^2 = const.$ In Fig. A we set $d_0 = .07$eV while in Fig. B $d_0 = -.05$eV. The difference between the two cases demonstrates the sensitivity to mesoscopic parameters.

as

$$j \approx \frac{\Gamma_0}{2\pi S_0 N_A}\left[\int_{-\infty}^{\infty}\frac{\Delta_s \varrho(\xi)d\xi}{(\xi-\epsilon_I)(\epsilon_A-\xi)} - \varrho(\epsilon_I)\,\ln\frac{\delta E_{+,\downarrow}}{\delta E_{-,\uparrow}} + \varrho(\epsilon_A)\,\ln\frac{\delta E_{+,\uparrow}}{\delta E_{-,\downarrow}}\right], \quad (232)$$

where ϱ is the (unshifted) bulk density of states per atom of the cluster (Cobalt in our case). The second two terms are *mesoscopic fluctuations* that depend on the specific charging energy of the nanocluster and the density of states at the top of the minority and majority bands. These mesoscopic corrections become more and more pronounced for smaller cluster sizes and lead to strong fluctuations around the average coupling j. Remarkably, the effective coupling is inversely proportional to the cluster size, implying that the Kondo effect must be indeed suppressed for larger clusters, in agreement with the experimental findings.

The Kondo temperature of the cluster can then be estimated as

$$T_K \sim \min\{E_C, \delta_{A,I}\}\ \sqrt{j}\ e^{-1/j}\ , \tag{233}$$

where the prefactor is just the energy cut-off given by the typical energy of inelastic excitations of the grain. To have an estimate for T_K, we extracted the parameters Γ_0 and the level spacings from the experimental data and plugged them into Eq. (232). Unfortunately, even with the optimistic assumptions of a single point of contact and the coincidence of the single particle decay rate Γ_0 and the full decay rate Γ^j, we find a T_K which is more than two orders of magnitude smaller than the experimentally observed T_K. On the other hand, this discrepancy is largely due to the fact that the Kondo scale is exponentially sensitive to the specific value of j and already a factor of two increase of j could account for the experimentally observed T_K. Just for curiosity we mention here that, had we neglected the ferromagnetic contribution to the Kondo couplings, we would have obtained perfect agreement with the experiments. However, in view of this large ferromagnetic contribution to the effective exchange coupling j, the experimentally observed anomalously large Kondo scale still remains a puzzle.

Local moment model

Let us briefly discuss the results obtained by using an alternative mean field model before closing this subsection. This simple mean field model has been proposed in Ref. [153] to describe local moment ferromagnetism on a cluster, and reads

$$\hat{H}_{\text{cluster}} = \sum_{j,\sigma} \epsilon_j d^\dagger_{j\sigma} d_{j\sigma} + \frac{J_{s-d}}{N_A} \hat{S} \cdot \hat{S}_{\text{loc}} + \frac{E_C}{2} (\hat{N} - n_g)^2. \tag{234}$$

Here $\hat{S}$ and $\hat{S}_{\text{loc}}$ denote the total spin of the extended states on the cluster and of the local moments, respectively. Similar to the itinerant model, the first term describes the kinetic energy of the extended electron states, and the third term accounts for the finite charging energy of the cluster. The second term of Eq. (234) describes the exchange interaction between the local moments and the extended states and tends to polarize the latter. We assume in what follows that the total spin of the conduction electrons is much smaller than that of the localized electrons. The exchange J_{s-d} is typically antiferromagnetic, $J_{s-d} > 0$, and the conduction

electrons are thus polarized opposite to d-electrons [155].

Similar to Eq. (223), the Hamiltonian Eq. (234) can also be exactly diagonalized. Though the calculations are somewhat more involved in this case, essentially all previously obtained results carry over to this local moment model (see Ref. [153] for details). The only difference is that S_0 in Eq. (232) is replaced by the *total* spin of the cluster, $S_T = S - S_{\rm loc}$. This result has a deep physical meaning. Though both the local moment's spin $S_{\rm loc}$ and the electron's polarization S can be large, what really matters from the point of view of quantum fluctuations (and thus that of the Kondo effect), is the total spin of the cluster: the smaller S_T the larger is the effective coupling. This observation also provides a possible explanation for the discrepancy between the experimentally observed and estimated Kondo temperatures: It is quite possible that the interaction between spins in these small clusters is partially frustrated. As a consequence, the total spin of the cluster may be reduced compared to our previous estimates, which could lead to a substantial increase in T_K.

5.2 Quantum impurities in point contacts

In the last section of this chapter we shall discuss slightly different mesoscopic structures called point contacts (PCs), where quantum impurities can be studied. These structures consist of two typically metallic pieces that are attached to each-other at a small area of diameter d (see Fig. 51). There is a number of techniques that are used to prepare these tiny structures: One can fabricate atomic scale break junctions by simply breaking a thin mesoscopic wire and then re-attaching the two pieces [156], or just plugging an STM tip into a piece of metal and then slowly removing it. It is also possible to construct very stable point contacts by means of chemical etching techniques [33, 71], but semiconductor technologies can be also used to produce such contacts by gating a two-dimensional electron gas [157].

While all these structures have slightly different characteristics, they have the common feature that they are inherently *out of equilibrium*. In fact, the transport properties of these contacts have features somewhat similar to tunnel junctions, and their differential conductance provides detailed information on inelastic scattering processes that take place in the contact region [158]. The big advantage of these structures is that they test *local properties*, unlike tunnel junctions which average over the whole surface of the junction.

To understand how such a point contact works, let us first assume that the

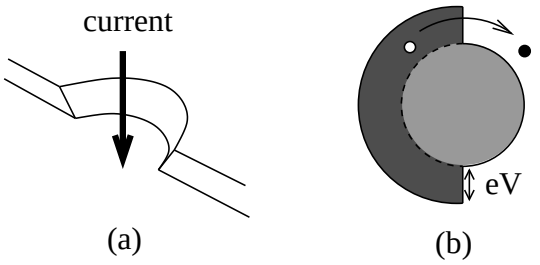

Figure 51: (a) Schematic cross section of a point contact. (b) Semiclassical momentum distribution of the electrons in the middle of the point contact. Electrons coming from the right have a larger chemical potential, and elastic scattering scatters these electrons always backwards thus reducing the current.

temperature is very small ($T = 0$) and that the contact is ballistic, *i.e.*, the electron's elastic mean free path is larger than the diameter of the contact. The distribution of the conduction electrons can then be determined in a semiclassical approach, and in leading order one obtains that the chemical potential of electrons coming from the right is shifted with respect that of electrons coming from the left, resulting in the intrinsically out of equilibrium distribution sketched in Fig. 51 [159].

Suppose now that an electron is subject to an inelastic scattering process and gives an energy ω to its environment. Clearly, because of the Pauli principle this electron can be scattered only *backwards* and furthermore this process is only possible if the voltage drop is large enough, $eV > \omega$. A simple calculation then shows that the differential conductance at bias V is proportional to the inelastic cross section $\sigma(\omega)$ at the corresponding energy [158, 159],

$$\frac{dI}{dV} \approx G_0 - B\,\sigma(\omega = eV)\ , \tag{235}$$

where the conductance G_0 is roughly the geometrical conductance of the ballistic junction, the so-called Sharvin's conductance, and is proportional to $N_c\ e^2/h$ with $N_c \sim k_F^2 A$ the number of conductance channels through the contact and $A \sim d^2$ the junction area. The constant B is proportional to the volume of the junction and the concentration c of scattering centers producing the inelastic process, $B \sim c\,d^3$.

Since the inelastic scattering length of the electrons is very large compared to the diameter d, G_0 depends on the microscopic details of the junction geometry and even the move of a single atom changes its value by an amount $\sim e^2/h$. This property enables one to use quantum point contacts to detect the time-dependent motion of

individual atoms [71]. The most interesting information is, however, buried in the second, inelastic piece of Eq. (235): This makes it possible to detect the phonon spectrum (weighted by the electron-phonon coupling) of a metal and also various inelastic processes in the contact region [158], to study inelastic scattering properties of magnetic impurities [160, 161], or the transprot properties of small grains [117].

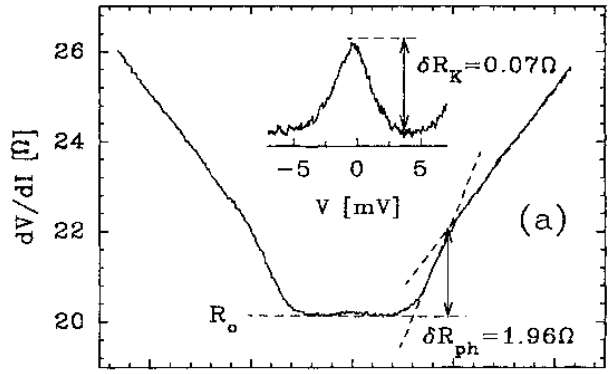

Figure 52: Experimental point contact spectra obtained by Yanson *et al.* for a CuMn break junctions.

As an example, in Fig. 52 we show the point contact spectrum obtained by Yanson *et al.* for small Mn doped Cu break junctions [162]. One can see a nice zero-bias anomaly that develops due to the resonant Kondo scattering at the Fermi energy. This zero bias disappears at large energies (voltages) and is also suppressed with increasing temperature. There is only one strange thing about these experimental data: Yanson *et al.* used a number of methods to determine the Kondo temperature, T_K, but all of them gave consistently orders of magnitude larger Kondo temperatures than observed in bulk CuMn alloys. Moreover, the extracted T_K strongly depended on the diameter of the junction. In the rest of this subsection, we shall give an explanation to these experiments.

In the present subsection we show that the increase of the Kondo temperature observed by Yanson *et al.* can be understood as a consequence of mesoscopic fluctuations. We show that in a small point contact the electronic local density of states, $\varrho(\mathbf{r}, \epsilon)$ strongly fluctuates both as a function of energy and position. As a result, magnetic impurities in the contact region experience very different environment depending on their specific position, and their Kondo temperarures have a broad distribution. Transport properties of the contact at some finite temperature turn out to be dominated by impurities having large Kondo temperatures, leading

to a an increase in the experimentally measured Kondo temperature. Similar ideas emerged in the context of disordered magnetic alloys, where the vicinity to a localization transition produces large fluctuations in the local density of states, and may eventually generate a non-Fermi liquid behavior [163].

The local density of states is defined as

$$\varrho(\mathbf{r},\epsilon) = \sum_n \delta(\epsilon - \epsilon_n)\ |\varphi_n(\mathbf{r})|^2\ , \tag{236}$$

where the summation is over all eigenstates with wave function $\varphi_n(\mathbf{r})$ and energy ϵ_n. For an open system as a point contact, the summation in Eq. (236) must be done over all scattering states [164, 165].

To gain some insight to the structure of $\varrho(\mathbf{r},\epsilon)$ we studied a simple free electron model where the point contact consists simply of two infinite half-spaces connected by a cylinder of radius R and length L [165]. In this case one can make use of the symmetry and write the electron's wave function in cylindrical coordinates as

$$\varphi_{\pm,\epsilon\lambda m}(r,z,\varphi) = e^{i\varphi m} J_m(\lambda r) e^{\pm i k_z(\lambda)\ z}\ , \tag{237}$$

where m is the angular momentum around the axis z and electrons propagate along the axis z of the PC. The signs $\pm$ correspond to right- and left-going states, respectively, ϵ denotes the energy of the conduction electron, and J_m stands for the m'th Bessel function. The z component of the momentum in Eq.(237), k_z, is related to the energy ϵ and the radial momentum λ of the electron as $k_z = (2m_e\epsilon - \lambda^2)^{1/2}$ and $k_z = i(\lambda^2 - 2m_e\epsilon)^{1/2}$ for $\sqrt{2m_e\epsilon}\lambda$ and $\sqrt{2m_e\epsilon} < \lambda$, respectively. (To avoid confusion, we denoted the electron mass by m_e). The radial momentum λ is a continuous parameter in the infinite half-spaces while it must take discrete values inside the tube. We were able to solve the above scattering problem numerically by performing a Bessel-Fourier transform, and matching the wave functions and their derivatives at the two ends of the cylinder [165, 166]. In Fig. 53 we show the local density of states obtained in this way at a fixed position as a function of energy and at the Fermi energy as a function of position inside the tube for a point contact with diameter $d = 2R = 30\mathring{A}$ and $L = 15\mathring{A}$.

Clearly, the local density of states shows huge fluctuations as a function of energy. These fluctuations have a simple origin: as we mentioned before, inside the tube the radial momentum is quantized and takes discrete values $\lambda \to \lambda_{n,m}$. Correspondingly,

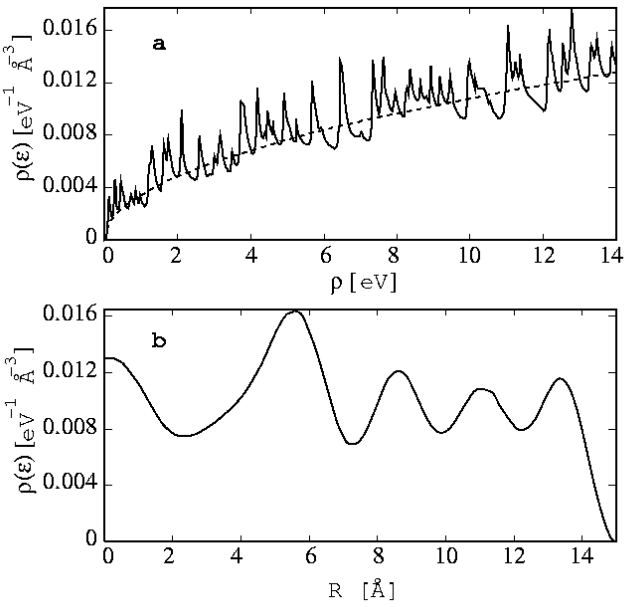

Figure 53: (a): Fluctuations of the local density of states (LDOS) $\varrho(\epsilon, z, r)$ inside the tube for a PC with $R = 15\mathring{A}$ and $L = 15\mathring{A}$ at the point $r = 7\mathring{A}$ and $z = 7\mathring{A}$. The fluctuating LDOS does not integrate exactly to its bulk value (dashed line) because the hard wall of the PC pushes the conduction electrons in the inside region of the tube. (b): $\varrho(\epsilon, z, r)$ for the same PC at $z = 7\mathring{A}$ and energy $\epsilon = 7eV$ as a function of the radius r.

the spectrum of an infinite cylinder would consist of one-dimensional subbands of energies dispersion

$$\epsilon_{n,m}(k_z) = \frac{\lambda_{n,m}^2 + k_z^2}{2m_e} \; . \tag{238}$$

The density of states and thus the local density of states have therefore a $\sim 1/\sqrt{\epsilon}$ singularity at every energy, $E_{n,m}^0 = \lambda_{n,m}^2/2m_e$. When we connect a finite segment of the cylinder to two infinite half-planes then these singularities evolve into large peaks/fluctuations in the local density of states. Of course, for large diameters these fluctuations become less and less pronounced and they are only important in the vicinity of the boundaries defining the point contact.

Let us consider now a magnetic impurity in the contact region. The interaction of this Kondo impurity with its environment can be expressed as

$$H_{\rm int} = \frac{J}{2} \sum_{n,n',\sigma,\sigma',i} \varphi_n^*(\mathbf{r})\varphi_{n'}(\mathbf{r}) \; a_{n\sigma}^+ \sigma_{\sigma\sigma'}^i a_{n'\sigma'} S^{\,i} \; , \tag{239}$$

where we assumed that the impurity is at the position $\mathbf{r}$, and the $a^\dagger_{n\sigma}$'s create conduction electrons in a scattering state φ_n with spin σ. In this basis the conduction electron's Green function and self energies as well as the vertex function defined in Section 2.1.2 become matrices,

$$G_e,\ \Sigma_e,\ \Gamma \to G_{nn'},\ \ \Sigma_{nn'},\ \ \Gamma_{nn'}\ . \tag{240}$$

Fortunately, as one can easily see by a direct evaluation of Feynman diagrams, due to the local character of the exchange interaction, all the above matrices can be factorized. The vertex function reads, in particular, as

$$\Gamma_{nn'}(\omega_i) = \varphi^*_n(\mathbf{r})\ \Gamma(\omega_i)\ \varphi_{n'}(\mathbf{r})\ , \tag{241}$$

where $\Gamma(\omega_i)$ depends only on the local density of states at the position of the impurity [165]. This also holds for the pseudofermion's self energy, Σ and their Green's function $\mathcal{G}$, which all depend solely on the local density of states [165]. The usual multiplicative renormalization group equations discussed in Section 2.1.2 can then be easily generalized to the quantities Σ, Γ, and $\mathcal{G}$ to give

$$\begin{aligned} \frac{dj}{dl} &= \frac{1}{2}j^2(R(D)+R(-D)) \\ &- \frac{1}{2}j^3\ \int_0^D \frac{d\xi}{D}\frac{1}{(1+\xi/D)^2}\left(R(\xi)R(-D)+R(-\xi)R(D)\right)\ , \end{aligned} \tag{242}$$

where $l = \ln(D_0/D)$ is the scaling variable, and $R(\xi) = \varrho(\xi)/\varrho_{\rm bulk}(\epsilon_F)$, with ξ the energy of an electron measured from the Fermi level. The dimensionless coupling in this equation is defined in terms of the bulk density of states at the Fermi energy, $j = J\varrho_{\rm bulk}(\epsilon_F)$. Sufficiently far from the contact region the function R approaches one, and we recover the usual scaling equations.

It is instructive to solve these equations in the leading logarithmic order, *i.e.* by dropping the $\sim j^3$ term in Eq. (242). In this limit we can obtain a simple expression for the ratio of the Kondo temperature in the bulk, T_K^*, and in the local environment, T_K,

$$\frac{T_K}{T_K^*} = \exp\left\{\int_{T_K^*}^D \frac{d\xi}{2\xi}(\delta R(\xi)+\delta R(-\xi))\right\}\ . \tag{243}$$

Here $\delta R(\xi) = R(\xi) - R_{\rm bulk}(\xi)$ is just the relative change in the local density of states compared to the bulk at energy ξ, and T_K^* denotes the Kondo temperature in the

bulk. The important feature of this formula is the appearance of the weight $1/\xi$ in the exponent: the physical meaning of this factor is that, while the contribution of high-energy electron-hole excitations is also significant, the Kondo resonance is mainly formed by low-energy electron-hole excitations. Therefore, in a very crude estimate, T_K is increased at sites with $\delta\varrho(\epsilon_F) > 0$, while positions with $\delta\varrho(\epsilon_F) < 0$ will tend to have a smaller T_K. Since T_K is exponentially sensitive to the local density of states, even relatively small $\sim 20\%$ fluctuations in the density of states may lead to huge fluctuations in the Kondo scale depending on the impurity position.

Having established how to determine the Kondo temperature in an environment with an arbitrary local density of states, we can now proceed to estimate the Kondo temperature in a small point contact by just substituting the ratio $\delta R(\xi)$ of the free electron model calculations into Eq.(243) and then averaging over the contact region. The result is shown in Fig. 54.(a). We indeed find an average Kondo temperature which is orders of magnitude larger than the bulk Kondo temperature of CuMn, $T_K^* \sim 0.01$ K. Although mesoscopic fluctuations are large, a rough fitting of the diameter-dependence of our data gives $\langle T_K \rangle \sim d^{-\alpha}$ with an exponent $\alpha = 2.2 \pm 0.5$, which agrees quite reasonably with the experimentally found exponent, $\alpha = 2$.

We can also estimate the change in the conductance of the point contact due to backscattering from these magnetic impurities as

$$\Delta G(eV) \approx -\frac{e^2}{h}\Omega\, c\varrho^2(\epsilon_F)\, \langle J^2(\max\{eV, T\})\rangle\ , \tag{244}$$

where c is the concentration of the impurities, $\langle \ldots \rangle$ denotes the average over the contact region, and $\Omega = d^3/3$ is the effective volume of the point contact [162].

From Eq. (244) we can compute the size-dependence of the zero bias anomaly at the measurement temperature and compare it to the experimental data (see Fig. 54.b). Both the amplitude of $\Delta G(R)$ and its sample to sample fluctuations are in very good agreement with the experiments. We have to emphasize at this point that *there is no free parameter* in Eq. (244) except for the length of the PC which hardly influenced our results. To show that there is a striking size effect in Fig. 2(b) we also plotted the theoretically computed amplitude of the Kondo signal with impurities having the bulk Kondo temperature T_K^*. Clearly, both the overall amplitude and the size-dependence ($\Delta G \sim d^{2.2}$) of the experimental and the computed Kondo conductances are quite different from the one we obtained by assuming the bulk Kondo temperature for each impurity in the contact region ($\Delta G \sim d^3$).

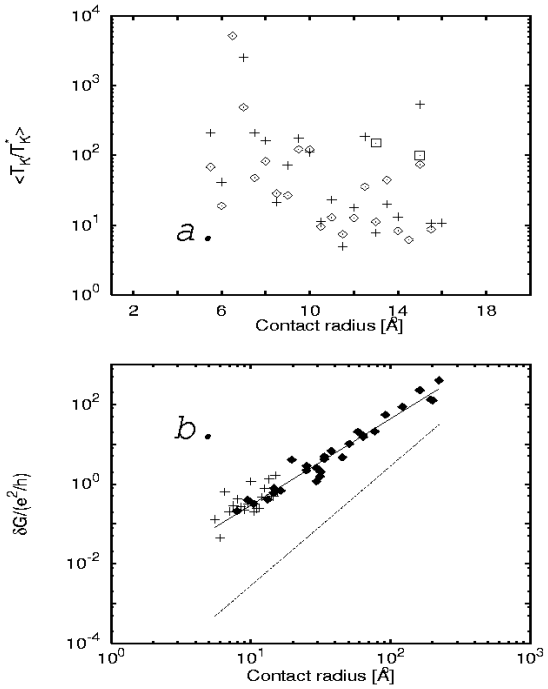

Figure 54: (a) $\langle T_K/T_K^* \rangle$ as a function of the radius R of a CuMn point contact with $L = 5\mathring{A}$. Crosses and diamonds denote the results obtained in the leading and in the next to leading logarithmic orders, while boxes indicate the experimental results of Ref. [162]. The large fluctuations are due to the sensitivity of the interference pattern to the geometry of the PC. (b) Size-dependence of the amplitude of the dimensionless Kondo conductance $\Delta g = \Delta G\ h/e^2$ for impurity concentration $c = 0.1\%$ at $T = 0.05$ K. Diamonds denote experimental data from Ref. [162] while our results are indicated by crosses. The dashed line shows the results without any local density of states fluctuations. ($g \sim R^3$) while the continuous line is the best fit $g \sim R^{2.17}$.

Although the results of this subsection were obtained for the rather special case of a point contact, the phenomenon we discussed here is rather general: In a mesoscopic wires and films or disordered alloys local density of states fluctuations will always have a large influence on physical quantities that depend on the local density of states at the Fermi energy. Note that local density of states fluctuations propagate deep inside the bulk, much farther than Friedel oscillations in the charge density. In mesoscopic wires, however, other phenomena like surface-induced anisotropy may also be important [167, 168], and therefore the interplay of local density of states fluctuations and spin-orbit coupling can give rise to rather rich physics.

6 Conclusion

In the present thesis, I tried to review some recent results within the field of quantum impurity problems, with a special emphasis on a few topics covered by my research in the past ten years.

After introducing in Chapter 2 the basic notions related to quantum impurity models and giving an introduction to the most important techniques used to investigate them in this thesis, I studied various aspects of dissipative quantum impurity problems in Chapter 3. First, in Section 3.1, I showed how one can obtain an exact solution for the dissipative two state system model using the Bethe ansatz method and utilizing an exact mapping between the dissipative two state system model and the anisotropic Kondo problem, and determined the full thermodynamic behavior of the dissipative two state system model by solving the Bethe ansatz equations numerically for all magnetic fields.

Then, in Section 3.2, I studied the problem of a tunneling particle with spin using numerical renormalization group methods. In this case exchange coupling to the conduction electrons generated dissipation. I found that the spin of the particle induced a Kondo effect at a temperature T_K, below which the particle acted as a maximally strong potential scatterer. Thus the Kondo effect gave rise to a large increase in the dissipative coupling in this case, and resulted in the suppression of the coherent motion of the particle. I determined the corresponding effective dissipation $\alpha_{\rm eff}(T/T_K, F)$ numerically, with F a dimensionless overlap parameter characterizing the separation between the two tunneling positions.

In Section 3.3, I studied the so-called anisotropic Bose-Fermi Kondo model where, beside the conduction electrons' spin, a dissipative bosonic field is also coupled to the impurity spin. The bosonic field in this model usually represents some collective degrees of freedom. In this model several quantum-phase transitions take place between a fermion-dominated Kondo fixed point and various dissipation-dominated (bosonic) fixed points. I classified the non-trivial fixed points of this model by performing an ϵ expansion up to second order in ϵ, and showed that at the $SU(2)$ symmetric and XY symmetric critical points anisotropy is relevant and drives the system to a critical point of Ising symmetry. This latter Ising critical point is probably relevant for most applications (*e.g.*, magnetic quantum phase transitions, dissipative phase transitions in quantum dots). I also obtained an exact expression for the impurity susceptibility at these quantum critical points using a Ward identity and a conformal mapping. I

showed that the exponent of the local susceptibility is simply related to the spectral function of the dissipative field coupled to the spin. This result has important implications on the so-called locally quantum critical theory.

In Chapter 4, I studied exotic quantum impurity models that display non-Fermi liquid behavior. First, in Section 4.1.1, I investigated the problem of a tunneling two state system in a metal by performing a $1/f$ expansion up to second order in $1/f$, with f the spin degeneracy of the conduction electrons. These calculations allowed me to prove in the large f limit even below the Kondo temperature the conjectures of Vladár and Zawadowski, that only two orbital channels dominate the low temperature physics of the tunneling systems, which therefore maps on the two-channel Kondo problem. I could also identify the leading irrelevant operators and determine their scaling dimension.

Then, in Section 4.1.2, I showed how one can solve by the simple Abelian bosonization and refermionization technique of Emery and Kivelson the two-channel Kondo problem and obtain an almost complete understanding of this model. I generalized the method of Emery and Kivelson to the case of a finite system sizes, and derived the famous non-Fermi liquid spectrum by straightforward diagonalization. I also determined the scattering states and showed how the unitarity paradox appears in this approach.

In Section 4.1.3, I constructed the thermodynamic Bethe ansatz equations for the anisotropic f-channel Kondo problem. I showed that while at high temperatures the susceptibility $\chi^{\rm imp}$ and the specific heat $c^{\rm imp}$ display non-universal power law behavior, at low temperatures the properties of this model become universal and are characterized by the exponents characteristic of the isotropic two-channel Kondo problem. I determined the complete thermodynamics of this model by numerically solving the Bethe ansatz integral equations.

In Section 4.2.1, I carried out a $1/f$ expansion for an atom that tunnels between N different positions. For this purpose, I introduced a new version of the multiplicative renormalization group, where the square roots of the Z-factors are replaced by matrices to handle anisotropic mass generation. Performing a stability analysis and solving numerically the scaling equations I showed that in the large f limit this model maps to the $SU(N) \times SU(f)$ Coqblin-Schrieffer model. In Section 4.2.2 I derived the Bethe ansatz equations for the latter model, and discussed its singular low temperature thermodynamic behavior.

In the last chapter of this thesis I presented some applications of quantum impurity models in mesoscopic and nanoscale systems. In Section 5.1.3, I studied capacitively coupled quantum dots and symmetrical quantum dots with orbitally degenerate ground states using renormalization group methods, and showed that in both systems an SU(4)-symmetrical correlated state develops where spin and charge degrees of freedom are entangled. I also determined the transport properties of these devices using numerical renormalization group methods and showed that, in a relatively small magnetic field, these devices can be used as efficient spin filters. This theoretically predicted SU(4) state has been observed in several systems since then.

In Section 5.1.3, I introduced a new method to determine the $T = 0$ temperature transport properties of quantum dot systems by a direct use of the finite size spectrum obtained from a numerical renormalization group calculation. I applied this technique first for the so-called singlet-triplet transition and I was able to reproduce all important features of the experimental data with this method.

Motivated by the experiments of [148], in Section 5.1.4 I studied theoretically the tunneling spectrum of a ferromagnetic nanocluster coupled to leads using a simple mean field Hamiltonian. I showed that for a ferromagnetic cluster the effective exchange coupling contains large ferromagnetic contributions that depend on specific details of the band structure. I also computed the STM spectrum of this cluster and showed that, in agreement with the experimental data, it displays rather asymmetrical features that have mesoscopic origin.

As a last application in mesoscopic physics, in Section 5.2, I showed that in a mesoscopic point contact very strong local density of states fluctuations show up. I showed that these fluctuations can lead to a broad distribution of the Kondo temperatures of magnetic impurities in the contact region, and gave a consistent explanation of some experimentally observed anomalies.

7 Acknowledgement

I would like to thank all my collaborators, especially Lászó Borda, Jan von Delft, Greg Fiete, Walter Hofstetter, László Udvardi, and Károly Vladár for the stimulating discussions that led to the results presented in this thesis. I am also deeply indebted to Fred Zawadowski, who introduced me into the physics of quantum impurities and stimulated me to put research aside for a while and prepare this work, and to

all members of the Theoretical Physics Department of the Budapest University of Technology for their helpfulness and the friendly atmosphere. I am also very thankful to László Borda for the careful reading of this dissertation.

Special thanks should go to my wife for her patience and love, and to our parents, who helped us so much and so generously without the least hesitation.

The preparation of this work has been supported by OTKA grants No. T038162, T046267, and T046303.

A Bosonization techniques

A.1 Basic bosonization identities

In this appendix we shall review the Abelien bosonization technique. This method - which is a powerful tool to study (1+1)-dimensional relativistic quantum field theories - relies on the observation that for a one-dimensional relativistic fermion field almost all excitations can be constructed in terms of bosonic denisty waves.

To start width, we shall consider a spinless left-moving fermion field $\psi(x)$ on a string of length L, satisfying the anticommutation relations $\{\psi(x), \psi^\dagger(x')\} = \delta(x - x')$. For the sake of simplicity, we shall assume here that ψ satisfies antiperiodic boundary conditions. The field ψ can, of course, be expanded in Fourier basis as

$$\psi(x) \equiv \sqrt{\tfrac{2\pi}{L}} \sum_k e^{-ikx} c_k \ , \tag{245}$$

where $k = \frac{2\pi}{L}(n_k - 1/2)$ with n_k an integer. The Hamiltonian is defined as

$$H_0 = \int_{-L/2}^{L/2} \frac{dx}{2\pi} \psi^\dagger(x)\ i\partial_x \psi(x) = \sum_k k\ :c_k^\dagger c_k: \ , \tag{246}$$

where the symbol $:\ldots:$ denotes normal ordering with respect to the free Fermi sea or "vacuum state" $|0\rangle_0$, defined by

$$c_k|0\rangle_0 \equiv 0 \quad \text{for} \quad k > 0, \qquad c_k^\dagger|0\rangle_0 \equiv 0 \quad \text{for} \quad k < 0. \tag{247}$$

Next, we define bosonic electron-hole creators by

$$b_q^\dagger \equiv i\sqrt{\frac{2\pi}{qL}} \sum_k c_{k+q}^\dagger c_k \ , \tag{248}$$

where $q = \frac{2\pi}{L} n_q > 0$ is the momentum of the electron-hole excitation with n_q a positive integer. Very importantly, these operators can be shown to satisfy canonical commutation relations. They also commute with the total fermion number, $\hat{N} \equiv \sum_k :c_k^\dagger c_k:$, the latter being a conserved quantity. The Hilbert space can be devided onto subspaces characterized by given values of $\hat{N} = N$, and within each subspace there is a unique state $|N\rangle_0$ which contains no electron-hole excitations. One can show that one can build up each subspace of (and thus the whole) Hilbert space from

these states using just the operators $b_q^\dagger$ and that H_0 can be simply expressed as

$$H_0 = \frac{2\pi}{L}\frac{1}{2}\hat{N}^2 + \sum_{q>0} q\, b_q^\dagger b_q \,. \tag{249}$$

To compute ferionic correlation functions, however, it is not sufficient to bosonize the Hamiltonain, we need to construct the *fermionic field* ψ in terms of the b_q's. To this end, we define bosonic fields by

$$\phi(x) \equiv \sum_{q>0} -\sqrt{\frac{2\pi}{qL}} \left(e^{-iqx} b_q + e^{iqx} b_q^\dagger\right) e^{-aq/2} \,. \tag{250}$$

Here $a \sim 1/p_F$ is a short-distance cutoff; it is introduced to cure any ultraviolet divergences. It is easy to prove that the field $\partial_x\phi(x)$ is canonically conjugate to $\phi(x)$, in that

$$[\phi(x), \partial_{x'}\phi_(x')] = 2\pi i(\delta_a(x-x') - 1/L) \,, \tag{251}$$

where $\delta_a(x-x')$ is a smeared delta function, $\delta_a(x-x') = \frac{a/\pi}{(x-x')^2+a^2}$. With this definition, H_0 can be also written in a somewhat simpler form:

$$H_0 = \frac{2\pi}{L}\frac{1}{2}\hat{N}^2 + \int_{-L/2}^{L/2} \frac{dx}{4\pi} : \left(\frac{\partial\phi}{\partial x}\right)^2 : \,, \tag{252}$$

which is more frequently used in the literature.

The field ϕ is, however, obviously not enough to represent fermion operators since it does not change the value of N while fermionic fields do so. Therefore, we need to define another operator, F, the so-called co-cycle or Klein factor, which does this job

$$[F, \hat{N}] = F \,, \qquad [F, b_q] = 0 \,, \qquad FF^\dagger = F^\dagger F = 1 \,. \tag{253}$$

The Klein factor can be constructed explicitely in terms of the original fermionic operators.

Now we are ready to present the most important identities relating the field ϕ to the fermionic operator ψ and the density operator $\varrho \sim :\psi^\dagger\psi:$,

$$\psi(x) = F\frac{1}{\sqrt{a}} e^{-i(\hat{N}-1/2)2\pi x/L}\, e^{-i\phi(x)} \,, \qquad \frac{1}{2\pi} :\psi^\dagger(x)\psi(x): = \frac{1}{2\pi}\partial_x\phi(x) + \frac{\hat{N}}{L}. \tag{254}$$

The last equation is particularily transparent: The field ϕ can be interpreted as a

displacement field, the divergence of which gives the changes in the density. However, it contains only excitations which reorder the spatial charge distribution along the line without changing the total fermion number; the last term is needed to take into account changes in the latter.

In many cases, one can take the $L \to \infty$ limit. Then the bosonization identities simplify,

$$H_0 = \int \frac{dx}{4\pi} : \left(\frac{\partial \phi}{\partial x}\right)^2 : , \qquad [\phi(x), \partial_{x'}\phi(x')] = 2\pi i \delta_a(x - x') \; , \tag{255}$$

$$\psi(x) = F \frac{1}{\sqrt{a}} e^{-i\phi(x)} \; , \qquad \frac{1}{2\pi} :\psi^\dagger(x)\psi(x): = \frac{1}{2\pi}\partial_x \phi(x) \; . \tag{256}$$

The above procedure can be readily generalized to the case of several Fermi fields. The only important difference is, that in this case Klein factors belonging to different fermionic field must *anticommute* to insure the anticommutation relations of the Fermi fields. In the $L \to \infty$ limit these operators can usually be replaced by Majorana fermions, but sometimes it is important to keep track of the time-dependence of these fields.

A.2 Mapping between the spin-boson model and the dissipative two state system model

To establish the mapping, we bosonize the Hamiltonian (69) using the bosonization rules of the previous subsection as

$$\begin{aligned} H_{\rm AK} &= \sum_{\sigma=\pm} \int \frac{dx}{4\pi} \left(\frac{\partial \phi_\sigma}{\partial x}\right)^2 + \frac{1}{2}\tilde{j}_z S_z \left(\frac{\partial \phi_\uparrow(0)}{\partial x} - \frac{\partial \phi_\downarrow(0)}{\partial x}\right) \\ &+ \frac{1}{2}\frac{j_\perp}{a}\Big(e^{i(\phi_\uparrow(0) - \phi_\downarrow(0))} F_\uparrow^\dagger F_\downarrow \, S^- + \text{h.c.}\Big) \; . \end{aligned} \tag{257}$$

We have to remark that the bosonization cut-off scheme defined by the length scale a changes the meaning of the original couplings, $j_z \to \tilde{j}_z$, and the new coupling is simply related to the phase shift of the fermions as [88]

$$\tilde{j}_z = 4\delta_z = 4 \, \text{atan}(\pi \, j_z/4) \; . \tag{258}$$

Next we introduce charge and spin fields, as

$$\phi_c = \frac{1}{\sqrt{2}}\left(\phi_\uparrow + \phi_\downarrow\right) \ , \qquad \phi_s = \frac{1}{\sqrt{2}}\left(\phi_\uparrow - \phi_\downarrow\right), \tag{259}$$

and realize that only the spin part couples to the spin operator. Thus the spin dynamics is fully captured by the Hamiltonian:

$$H^{\rm spin}_{\rm AK} = \int \frac{dx}{4\pi}\ \left(\frac{\partial\phi_s}{\partial x}\right)^2 + \frac{1}{\sqrt{2}}\tilde{j}_z S_z \frac{\partial\phi_s(0)}{\partial x} + \frac{1}{2}\frac{j_\perp}{a}\left(e^{i\sqrt{2}\phi_s(0)}F^\dagger_\uparrow F_\downarrow\, S^- + \text{h.c.}\right). \tag{260}$$

Finally, we show that the unitary transformation $U = \exp(i\sqrt{2}S_z\phi_S(0))$ applied to $H^{\rm spin}_{AK}$ gives the spin-boson Hamiltonian, H_{SB}, for Ohmic dissipation. Using the commutation relation of the fields ϕ_s and $\partial\phi_s$ we find

$$U\left[\int \frac{dx}{4\pi}\ \left(\frac{\partial\phi_s}{\partial x}\right)^2\right]U^\dagger = \int \frac{dx}{4\pi}\ \left(\frac{\partial\phi_s}{\partial x}\right)^2 - \sqrt{2}S_z\frac{\partial\phi_s(0)}{\partial x}\ ,$$
$$US^-U^\dagger = e^{-i\sqrt{2}\phi_S(0)}S^-, \qquad US^+U^\dagger = e^{i\sqrt{2}\phi_S(0)}S^+,$$

implying that under this unitary transformation $\tilde{j}_z \to \tilde{j}_z - 2$, and that ϕ_s is completely transformed out of the term $\sim j_\perp$. Finally, we notice that the operators $\tau^- \equiv F_\downarrow F^\dagger_\uparrow\, S^+$, $\tau^+ \equiv (\tau^-)^\dagger$ and $\tau_z \equiv -2S_z$, satisfy the usual algebra of Pauli matrices and rewrite $H^{\rm spin}_{AK}$ as

$$UH^{\rm spin}_{AK}U^\dagger = H^{\rm spin}_{\rm AK} = \int \frac{dx}{4\pi}\ \left(\frac{\partial\phi_s}{\partial x}\right)^2 + \frac{1}{\sqrt{2}}(1 - \frac{\tilde{j}_z}{\sqrt{2}})\tau_z\frac{\partial\phi_s(0)}{\partial x} - \frac{j_\perp}{2a}\tau_x\ , \tag{261}$$

which is just the spin-boson model with

$$\sqrt{\alpha} = 1 - \frac{\tilde{j}_z}{2} = 1 - \frac{2\delta_z}{\pi}\ . \tag{262}$$

To clarify the meaning of this uitary transformation we notice that the spin density, given by $\varrho_s = \frac{1}{2\pi}(\partial_x\phi_\uparrow - \partial_x\phi_\downarrow) = \frac{1}{\pi\sqrt{2}}\partial_x\phi_s$, transforms under the unitary transformation as

$$\varrho_s \to \varrho_s - S_z\delta(x)\ , \tag{263}$$

implying that we indeed bind a conduction electron to the impurity spin antiferromagnetically at the origin, $x = 0$, as stated in the main text.

B Hartree approximation for a quantum dot

To derive Eq. (195), let us consider a metallic grain within the Hartree approximation. Then the wave functions φ_j must be determined self-consistently by solving the following equations:

$$\begin{aligned} \Big(-\frac{\Delta}{2m} + V_H(\vec{r})\Big)\varphi_j &= E_j\ \varphi_j\ , \\ V_H(\vec{r}) &= V(\vec{r}) + \int d\vec{r}' U(\vec{r}-\vec{r}')\varrho(\vec{r}')\ , \end{aligned} \tag{264}$$

where V is the confining potential generated by the positively charged ions, U is the electron-electron interaction, and V_H is the Hartree potential. The electronic density $\varrho(\vec{r})$ in Eq. (264) must be computed as $\varrho(\vec{r}) = \sum_{j,\sigma} n_{j,\sigma}\ |\varphi_j|^2$, with $n_{j,\sigma}$ the occupation number of the levels.

The total energy of the system with $N = \sum_{j,\sigma} n_{j,\sigma}$ electrons is

$$E_H^N = \sum_{j,\sigma} E_j\ n_{j,\sigma} - \frac{1}{2}\int d\vec{r}\, d\vec{r}'\, \varrho(\vec{r}) V(\vec{r}-\vec{r}')\varrho(\vec{r}')\ , \tag{265}$$

where the second term compensates for overcounting the electron-electron interaction. In order to compute the energy cost of adding another electron to the grain, we should solve selfconsistently Eqs. (264) for $\sum_{j,\sigma} n_{j,\sigma} = N+1$, compute E_H^{N+1} and then determine the difference between these two energies, $E_H^{N+1} - E_H^N$. However, one can approximately compute this energy by just noticing that the charge of the extra electron in state $N+1$ must go to the *surface* of the grain to produce an approximately constant potential inside the grain, and is screened within a layer of the Fermi wavelength $\sim \lambda_F$. The change in the Hartree potential is simply given as

$$\delta V_H = \int d\vec{r}' U(\vec{r}-\vec{r}')\ \delta\varrho(\vec{r}')\ . \tag{266}$$

But since the change of the electronic density can be very well approximated by a classical *surface charge* for a grain size $L \gg \lambda_F$, δV_H is just the classical potential of the charged grain. Consequently, $\delta V_H \approx e^2/C$ inside the metallic grain. Using this simple fact we find that adding an extra electron to the grain shifts all Hartree energies as $E_j \to E_j + e^2/C$ and requires an energy

$$E^+ \approx E_f + \frac{e^2}{2C}\ , \tag{267}$$

with E_f the Hartree energy of the first unoccupied level, and C the classical capacitance of the grain. Defining the chemical potential as the Hartree energy of the last occupied level, $\mu \equiv \epsilon_l$ and defining the quasiparticle energies as $\epsilon_j \equiv E_j - \mu$ we find by extending the above analysis to the excited states as well that the energy of the dot is approximately described by Eqs. (194) and (195). Note that for an isolated dot this analysis gives $N_g = -\mu C/e^2$, which is usually not equal to zero, so adding and removing an electron requires different energies, just as in case of an atom.

References

[1] J. Kondo, Prog. Theor. Phys. **32**, 37 (1964).

[2] For a review on Kondo effect and heavy fermions, see A.C. Hewson, *The Kondo Problem to Heavy Fermions* (Cambridge University Press, Cambridge, 1993).

[3] P.W. Anderson and G. Yuval, Phys. Rev. Lett. **23**, 1522 (1969); G. Yuval an P.W. Anderson, Phys. Rev. B **1**, 1522, 4464 (1970); P.W. Anderson, G. Yuval, and D.R. Hamann, Phys. Rev. B **1**, 4464 (1970).

[4] P.W. Anderson, J. Phys. C **3**, 2436 (1970).

[5] A.A. Abrikosov, Physics **2**, 5 (1965).

[6] Sólyom J. and Zawadowski A., J. Phys. F **4**, 2269 (1974).

[7] Abrikosov A.A. and Migdal A.A., J. Low Temp. Phys. **3** 519 (1970)

[8] Fowler M. and Zawadowski A., Solid State Commun. **9**, 471 (1971)

[9] Nozières P., J. Low Temp. Phys. **17**, 232 (1974)

[10] Wilson K.G., Rev. Mod. Phys. **47**, 773 (1975); Wilson K.G. and Kogut J., Phys. Rep. C **12**, 75 (1974).

[11] Andrei N., Phys. Rev. Lett.**45**, 379 (1980);

[12] N. Andrei, K. Furuya and J. H. Lowenstein, Rev. Mod. Phys. **55**, 331 (1983).

[13] P. B. Wiegmann, Sov. Phys. JETP. Lett. **31**, 364 (1980); A. M. Tsvelick and P. B. Wiegmann, *Adv. Phys.* **32**, 453 (1983).

[14] P. B. Wiegmann, Sov. Phys. JETP. Lett. **31**, 364 (1980).

[15] T. A. Costi, Phys. Rev. Lett. **85**, 1504-1507 (2000).

[16] Anderson P.W. Phys. Rev. **124**, 41 (1961).

[17] J.R. Schrieffer and P.A. Wolff, Phys. Rev. **149**, 491 (1966).

[18] K. Yamada, Prog. Theor. Phys. **53**, 970 (1975); K. Yosida and K. Yamada, Prog. Theor. Phys. **53**, 1286 (1975); K. Yamada, Prog. Theor. Phys. **54**, 316 (1975); K. Yamada, Prog. Theor. Phys. **55**, 1345 (1976).

[19] Luttinger J.M. Phys. Rev. **119**, 1153 (1960).

[20] Luttinger J.M. Phys. Rev. **121**, 942 (1961).

[21] A. J. Leggett, in *Percolation, Localization and Superconductivity*, NATO ASI Series: Physics Vol. **109**, edited by M. Goldman and S. A. Wolf.

[22] For a review see A. J. Leggett, S. Chakravarty, A. T. Dorsey, M. P. A. Fisher, A. Garg and W. Zwerger, Rev. Mod. Phys. **59**,1 (1987); **67**, 725 (1995).

[23] U. Weiss, Series in Modern Condensed Matter Physics, Vol. 2, World Scientific, Singapore (1993).

[24] P. Nozières and A. Blandin, Journal de Physique **41**, 193 (1980).

[25] N. Andrei and C. Destri, Phys. Rev. Lett.**52**, 364 (1984)

[26] Teor. Fiz. **38**, 489 (1983) [JETP Lett. **38**, 591 (1983)].

[27] I. Affleck and A.W.W. Ludwig, Nucl. Phys. B **352**, 849 (1991); *ibid.* **360**, 641 (1991); Phys. Rev. Lett. **67**, 161 (1991); Phys. Rev. Lett. **68** 1046 (1992); Phys. Rev. B **48** 7297 (1993).

[28] M. Maldacena and A.W.W. Ludwig, Nucl. Phys. B **506**, 565 (1997).

[29] A. W. Mirtschin and P. Lloyd, J. Phys C **17**, 5399 (1984); D. M. Cragg, P. Lloyd and P. Nozières, J. Phys C **13**, 803 (1980).

[30] Cox D.L, Phys. Rev. B **35** 4561 (1987); Phys. Rev. Lett.**59**, 1240 (1987); Phys. Rev. Lett.**58**, 2730 (1987).

[31] D.L. Cox, Physica C **153** 1642 (1988); J. Magn. Mater. **76-77** 53 (1988)

[32] A. Zawadowski. Phys. Rev. Lett. 45, 211-214 (1980); K. Vladár and A. Zawadowski, Phys. Rev. B **28**, 1564 (1983); *ibid* **28**, 1582 (1983).

[33] D.C. Ralph, A.W.W. Ludwig, Jan von Delft, and R.A. Buhrman, Phys. Rev. Lett. **72**, 1064 (1994);D.C. Ralph and R.A. Buhrman, Phys. Rev. Lett. **69**, 2118 (1992).

[34] For a review on the two-channel Kondo problem see D.L. Cox and A. Zawadowski, Adv. Phys. **47**, 599 (1998).

[35] K.A. Matveev, Zh. Eksp. Teor. Fiz. **98**, 1598 (1990) [Sov. Phys. JETP 72, 892 (1991)]; Phys. Rev. B **51**, 1743 (1995).

[36] Y. Oreg and D. Goldhaber-Gordon, Phys. Rev. Lett. **90**, 136602 (2003)

[37] W. Metzner and D. Vollhardt, Phys. Rev. Lett. **62**, 324 (1989).

[38] For reviews see A. Georges, G. Kotliar, W. Krauth, and M. Rozenberg, Rev. Mod. Phys. **68**, 13 (1996).

[39] B. Andraka and A.M. Tsvelick, Phys. Rev. Lett. **67**, 2886 (1991).

[40] L. Forró, R. Gaál, H. Berger, P. Fazekas, K. Penc, I. Kézsmárki, and G. Mihály, Phys. Rev. Lett. **85**, 1938 (2000)

[41] Schröder A., Aeppli G., Coldea R., Adams M., Stockert O., von Lohneysen H., Bucher E., Ramazashvili R., and Coleman P., Nature **407**, 351 (2000); H. von Löhneysen, J. Phys. Cond. Mat. **8** (1996) 9689.

[42] N. D. Mathur et al., Nature, 394, **39** (1998).

[43] M. Grosche et al., J. Phys. Cond. Mat. **12** (2000) 533.

[44] P. Gegenwart et al., Phys. Rev. Lett. **82** (1999) 1293; P. Gegenwart et al., Phys. Rev. Lett. **89** (2002) 56402.

[45] R. A. Fisher et al., Phys. Rev. B **65**, 224509 (2002); A. Sidorov et al., Phys. Rev. Lett. **89** (2002) 157004; S. Nakatsuji et al.,n Phys. Rev. Lett. **89**, 106402 (2002).

[46] Subir Sachdev, *Quantum phase transitions* (Cambridge Univ. Press, 2001).

[47] L.P. Kouwenhoven, D.G. Austing, S. Tarucha, Rep. Prog. Phys. **64**, 701 (2001).

[48] W.G. van der Wiel *et al.*, Phys. Rev. Lett. **88**, 126803 (2002).

[49] A. Kogan *et al.*, Phys. Rev. B **67**, 113309 (2003).

[50] L. Borda, G. Zaránd, W. Hofstetter, B. I. Halperin, and Jan von Delft, Phys. Rev. Lett. **90**, 026602 (2003).

[51] S. Sasaki, S. Amaha, N. Asakawa, M. Eto and S. Tarucha, Phys. Rev. Lett. **93**, 17205 (2004).

[52] P. Jarillo-Herrero *et al.*, to appear in Nature.

[53] J. Park et al., Nature (London) 417, 722 (2002); W. J. Liang et al., Nature (London) 417, 725 (2002).

[54] Y. Meir, N. S. Wingreen, and P. A. Lee, Phys. Rev. Lett. **70**, 2601 (1993).

[55] A. Rosch, J. Paaske, J. Kroha, and P. Wölfle, Phys. Rev. Lett. 90, 076804 (2003).

[56] P. Coleman, C. Hooley, and O. Parcollet, Phys. Rev. Lett. 86, 4088-4091 (2001).

[57] C. Itzikson and J.B. Zuber, *Quantum Field Theory* (McGraw-Hill, 1985).

[58] For a pedagogical introduction, see N. Andrei, Integrable Models in Condensed Matter Physics, in *Series on Modern Codensed Matter Physics - Vol. 6*, 458 - 551, World Scientific, Lecture Notes of ICTP Summer Course 1992. Editors: S. Lundquist, G. Morandi and Yu Lu. cond-mat/9408101.

[59] H. Bethe, Z. Phys. **71** 205 (1931).

[60] H.R. Krishnamurthy, J. W. Wilkins, and K.G. Wilson, Phys. Rev. B **21**, 1003; *ibid.* 1044.

[61] W. Hofstetter and G. Zarand, Phys. Rev. B **69**, 235301 (2004).

[62] T. A. Costi and C. Kieffer, Phys. Rev. Lett. **76**, 1683 (1996).

[63] E. Melnikov and A.M. Tsvelick, unpublished.

[64] T. A. Costi and G. Zaránd, Phys. Rev. B **59**, 12398 (1999).

[65] M. Takahashi and M. Suzuki, Prog. Theor. Phys. **48**, 2187 (1972); M. Takahashi, Prog. Theor. Phys. **50**, 1519 (1973).

[66] P. B. Vigmann and A. M. Finkel'steĭn, Sov. Phys. JETP **48**,102 (1978).

[67] M. Yoshida, Phys. Rev. B **41**, 9403 (1990).

[68] B. A. Jones *et al.*, Phys. Rev. Lett. 61, 125 (1988).

[69] L. Borda and G. Zaránd, Phys. Rev. Lett. **88**, 247203 (2002).

[70] I.L. Aleiner, B.L. Altshuler, Y.M. Galperin, and T.A. Shutenko, Phys. Rev. Lett. **86**, 2629 (2001); I.L. Aleiner and D. Controzzi, Phys. Rev. B **66**, 045107 (2002).

[71] K.S. Ralls and R. A. Buhrman, Phys. Rev. Lett. **60**, 998 (1988); B. Golding,*et al.*, **68**, 998 (1992); D. H. Cobden *et al.*, Phys. Rev. Lett. **71**, 4230 (1993).

[72] A.H. Castro Neto, E. Novais, L. Borda, G. Zaránd, and I. Affleck, Phys. Rev. Lett. **91**, 096401 (2003).

[73] A. Georges, O. Parcollet, and S. Sachdev, Physical Review B 63, 134406 (2001).

[74] S. Sachdev and J. Ye, Phys. Rev. Lett. **70**, 3339 (1993).

[75] M. Vojta, C. Buragohain, S. Sachdev, Phys. Rev. B **61**, 15152 (2000); S. Sachdev, M. Troyer, and M. Vojta, Phys. Rev. Lett. **86**, 2617 (2001); S. Sachdev, Physica C **357-360**, 78 (2001).

[76] P. Coleman, C. Pepin, Q. Si, and R. Ramazashvili, Journal of Physics (Condensed Matter) **13**, 723 (2001).

[77] Q. Si, S. Rabello, K. Ingersent, and L. Smith, Nature **413**, 804 (2001); for details see Q. Si, S. Rabello, K. Ingersent, and L. Smith, cond-mat/0202414.

[78] Sengupta A.M., Phys. Rev. B **61**, 4041 (2000).

[79] Smith J.L. and Si Q., Europhys. Lett. **45**, 228 (1999).

[80] Zaránd G. and Demler E., Phys. Rev. B **66**, 024427 (2002).

[81] Cardy J., *Scaling and renormalization in Statistical Physics* (Cambridge University Press, 1997).

[82] M.C. Aronson, M.B. Maple, P. De Sa, A.M. Tsvelick, R. Osborn, Europhys. Lett. **40**, 245 (1997).

[83] J.L. Cardy, Nucl. Phys. **B324**, 581 (1989).

[84] H. B. Pang and D. L. Cox, Phys. Rev. B **44**, 9454 (1991); I. Affleck, A. W. W. Ludwig, H. B. Pang, and D. L. Cox, Phys. Rev. B **45**, 7918 (1992); H. Pang, Phys. Rev. Lett. **73**, 2736 (1994).

[85] Andrés Jerez, Natan Andrei, and G. Zaránd, Phys. Rev. B **58**, 3814 (1998).

[86] V. J. Emery and S. Kivelson, Phys. Rev. B **47**, 10812 (1992).

[87] J. W. Ye, Phys. Rev. Lett. **77**, 3224 (1996); J. W. Ye, Phys. Rev. Lett. **79**, 1385 (1997).

[88] Jan von Delft, G. Zaránd, and M. Fabrizio, Phys. Rev. Lett. **81**, 196 (1998); G. Zaránd and J. von Delft, Phys. Rev. B **61**, 6918 (2000).

[89] A. Muramatsu and F. Guinea, Phys. Rev. Lett. **57**, 2337 (1986).

[90] J. Gan, N. Andrei, and P. Coleman, Phys. Rev. Lett. **70**, 686 (1993).

[91] G. Zaránd, Phys. Rev. B **51**, 273 (1995); G. Zaránd and K. Vladár, Phys. Rev. Lett. **76**, 2133 (1996).

[92] D.L. Cox and A. E. Ruckenstein, Phys. Rev. Lett. **71**, 1613 (1993).

[93] G.Zaránd, T.Costi, A.Jerez, N.Andrei, Phys. Rev. B **65**, 134416 (2002).

[94] J. Kondo, Physica (Amsterdam) **84B** 207 (1976).

[95] H. Shiba, Prog. Theor. Phys. **43**, 601 (1970).

[96] G. Zaránd, cond-mat/0411348 (unpublished).

[97] For an elementary introduction into Abelian bosonization see Jan von Delft and H. Schoeller, Annalen der Physik (Leipzig), **7**, 225-306 (1998).

[98] G. Toulouse, C. R. Acad. Sci. **268**, 1200 (1969).

[99] A. Zawadowski, J. von Delft, and D. C. Ralph, Phys. Rev. Lett. **83**, 2632-2635 (1999).

[100] G. Zaránd, L. Borda, J. von Delft, and N. Andrei, Phys. Rev. Lett. **93**, 107204 (2004).

[101] P. B. Vigmann and A. M. Finkel'steĭn, Sov. Phys. JETP **48**,102 (1978).

[102] K. Vladár, A. Zawadowski and G. T. Zimànyi, Phys. Rev. B **37**, 2001, 2015 (1988).

[103] K. Furuya and J. H. Lowenstein, Phys. Rev. B 25, 5935 (1982).

[104] P. Mehta, L. Borda, G. Zaránd, N. Andrei, P. Coleman, cond-mat/0404122.

[105] M. Fabrizio and G. Zaránd, Phys. Rev. B **54**, 10008 (1996).

[106] P. Coleman, Phys. Rev. B **29**, 3035 (1984).

[107] O. Parcollet, A. Georges, G. Kotliar, and A. Sengupta Phys. Rev. B **58**, 3794 (1998).

[108] G. Zaránd, Phys. Rev. Lett. **77**, 3609 (1996).

[109] S. Katayama, S. Maekawa, and H. Fukuyama, J. Phys. Soc. Jpn. **50**, 694 (1987).

[110] M. Tornow *et al.*, Physica B **194-196**, 1063 (1994).

[111] G. Zaránd, Solid State Comm. **86**, 413 (1993).

[112] B. Coqblin and J. R. Schrieffer, Phys. Rev. **185**, 847 (1969).

[113] I. Affleck and A. W. W. Ludwig, Nucl. Phys. B **428**, 545 (1994).

[114] D. Goldhaber-Gordon *et al.*, Nature (London), **391**, 156 (1998); D. Goldhaber-Gordon *et al.*, Phys. Rev. Lett. **81**, 5225 (1998).

[115] S. Tarucha D.G. Austing, Y. Tokura, W.G. van der Wiel, and L.P. Kouwenhoven, Phys. Rev. Lett. **84**, 2485 (2000);

[116] P. Joyez *et al.*, Phys. Rev. Lett. **79**, 1349 (1997).

[117] Ralph DC, Black CT, Tinkham M Phys. Rev. Lett. **78**, 4087 (1997).

[118] J. Park et al., Nature (London) 417, 722 (2002); W. J. Liang et al., Nature (London) 417, 725 (2002).

[119] R. Wilkins, E. Ben-Jacob, and R. C. Jaklevic, Phys. Rev. Lett. **63**, 801 (1989).

[120] S.M. Cronenwett, T.H. Oosterkamp, and L.P. Kouwenhoven, Science **281**, 540 (1998).

[121] L. I. Glazman and M. E. Raikh, JETP Lett. **47**, 452 (1988); T. K. Ng and P. A. Lee, Phys. Rev. Lett. **61**, 1768 (1988).

[122] N. Andrei, G.T. Zimanyi and G. Schön, Phys. Rev. B **60**, 5125 (R) (1999).

[123] G. Zaránd, G.T. Zimányi, and F. Wilhelm, Phys. Rev. B **62**, 8137 (2000).

[124] I.L. Aleiner, P.W. Brouwer, and L.I. Glazman, Physics Reports **358**, 309 (2002).

[125] M. L. Mehta, Random Matrices (Academic Press, New York, 1991).

[126] D. S. Golubev, J. König, H. Schoeller, G. Schön, and A. D. Zaikin, Phys. Rev. B **56**, 15782 (1997); J. König and H. Schoeller, Phys. Rev. Lett. **81**, 3511 (1998);

[127] I.O. Kulik and R.I. Shekhter, Zh. Eksp. Teor. Fiz. **62** (1975) 623 [Sov. Phys. JETP **41** (1975) 308]; L.I. Glazman and R.I. Shekhter, Journ. of Phys.: Condens. Matter **1** (1989) 5811.

[128] D.V. Averin and Yu.V. Nazarov, Phys. Rev. Lett. **65** (1990) 2446.

[129] The Friedel sum rule can be only applied in our case at $T = 0$ temperature, where the impurity spin is screened and disappears from the problem, and conduction electrons at the Fermi surface experience only some residual scattering. The Friedel sum rule has rigorously been derived only for the Anderson Hamiltonian, where it relates the number of electrons on the dot to the phase shifts. [See D.C. Langreth, Phys. Rev. **150**, 516 (1966)]. In case of the Kondo problem, there seems to be an ambiguity modulo π in the phase shift's definition.

[130] W.G. van der Wiel *et al.*, Science **289**, 2105 (2000).

[131] T. A. Costi Phys. Rev. B **64**, 241310 (2001).

[132] S. Sasaki *et al.*, Nature **405**, 764 (2000).

[133] G. Zaránd, A. Brataas, and D. Goldhaber-Gordon, Solid State Commun. **126**, 463-466 (2003).

[134] Wilhelm U, Weis J Physica E **6**, 668 (2000).

[135] P. Jarillo-Herrero *et al.*, to appear in Nature.

[136] K. Le Hur and P. Simon, Phys. Rev. B **67**, 201308 (2003).

[137] K. Le Hur, P. Simon, and L. Borda, Phys. Rev. B **69**, 045326 (2004)

[138] L. D. Leo and M. Fabrizio, Phys. Rev. B **69**, 245114 (2004).

[139] T. Jamnaela *et al.*, Phys. Rev. Lett. **87**, 256804 (2001).

[140] B. Lazarovits *et al*, cond-mat/0407399.

[141] B. C. Paul and K. Ingersent, cond-mat/9607190.

[142] R. Landauer, IBM J. Res. Dev. **1**, 223 (1957); D.S. Fisher and P.A. Lee, Phys. Rev. B **23**, 6851 (1981); M. Büttiker, Phys. Rev. Lett. **57**, 1761 (1986).

[143] M. Pustilnik and L. I. Glazman, Phys. Rev. Lett. **85**, 2993 (2000); Phys. Rev. B **64**, 045328 (2001).

[144] M. Eto and Yu.V. Nazarov, Phys. Rev. Lett. **85**, 1306 (2000); Phys. Rev. B **66**, 153319 (2002).

[145] M. Pustilnik and L.I. Glazman, Phys. Rev. Lett. **87**, 216601 (2001); M. Pustilnik, L. I. Glazman and W. Hofstetter: Phys. Rev. B **68** (2003) 161303(R).

[146] M. Vojta, R. Bulla, and W. Hofstetter, Phys. Rev. B **65**, 140405 (2002).

[147] A. Posazhennikova and P. Coleman, cond-mat/0410001 (accepted for publication in Phys. Rev. Lett.).

[148] T.W. Odom, J-L. Huang, C.L. Cheung and C.M. Lieber, Science **290**, 1549 (2000)

[149] C. M. Canali and A. H. MacDonald, Phys. Rev. Lett. **85**, 5623 (2000).

[150] S. Kleff and J. von Delft Phys. Rev. B **65**, 214421 (2002); S. Kleff, J. v. Delft, M. M. Deshmukh, and D. C. Ralph Phys. Rev. B 64, 220401 (2001).

[151] D.A. Papaconstantopoloulos, *Handbook of the Band Structure of Elemental Solids* (Plenum, New York, 1986).

[152] In the experiments of [148] the role of the lead is played by the nanotube itself.

[153] G. A. Fiete, G. Zaránd, B. I. Halperin, Y. Oreg, Phys. Rev. B **66**, 024431 (2002).

[154] O. Újsághy, J. Kroha, L. Szunyogh and A. Zawadowski, Phys. Rev. Lett. **85**, 2557 (2000).

[155] F.J. Himpsel *et al.*, Adv. Phys. **47**, 511 (1998).

[156] Sz. Csonka, A. Halbritter, G. Mihály, O. I. Shklyarevskii, S. Speller, and H. van Kempen Phys. Rev. Lett. **93**, 016802 (2004); R. J. P. Keijsers, O. I. Shklyarevskii, and H. van Kempen Phys. Rev. Lett. **77**, 3411 (1996).

[157] B. J. van Wees et al., Phys. Rev. Lett. 60, 848 (1988); D. A. Wharam et al., J. Phys. C 21, L209 (1988); S. M. Cronenwett et al., Phys. Rev. Lett. **88**, 226805 (2002).

[158] I.K. Yanson and O. I. Shklyarevskii, Fiz. Nizk. Temp. **12**, 899 (1986) [Sov. J. Low Temp. Phys. **12**, 509 (1986); A. G. Jansen, A. P. van Gelder and P. Wyder, J. Phys. C **13**, 6073 (1980).

[159] A. Halbritter, L. Borda, and A. Zawadowski, Adv. Phys. **53**, 939 (2004).

[160] A. A. Lysykh, I. K. Yanson, O. I. Shklyarevskii, and Yu. G. Naidyuk, Solid State Commun. **35**, 987 (1980).

[161] A. G. M. Jansen, A. P. van Gelder, P. Wyder and S. Strässler, J. Phys. F: Metal Phys. **11**, L15 (1981).

[162] I.K. Yanson *et al.*, Phys. Rev. Lett. **74**, 302 (1995); I.K. Yanson *et al.*, Low Temp. Phys. **20**, 836 (1994).

[163] V. Dobrosavljević, T.R. Kirkpatrick, and G. Kotliar, Phys. Rev. Lett. **69**, 1113 (1992).

[164] G. Zaránd and L. Udvardi, Physica B **218**, 68 (1996).

[165] G. Zaránd and L. Udvardi, Phys. Rev. B **54**, 7606 (1996).

[166] E. Tekman and S. Ciraci, Phys. Rev. B **39**, 8772 (1989).

[167] O. Újsághy, A. Zawadowski, and B. L. Gyorffy Phys. Rev. Lett. 76, 2378-2381 (1996).

[168] G. Chen and N. Giordano, Phys. Rev. Lett. **66**, 209 (1991); J. F. DiTusa *et al.*, Phys. Rev. Lett. **68**, 678 (1992).